UNIVERSITÉ DE SHERBROOKE
Faculté de génie
Département de génie mécanique

ANALYSE DES INTERACTIONS ÉNERGÉTIQUES ENTRE UN ARÉNA ET SON SYSTÈME DE RÉFRIGÉRATION

Thèse de Doctorat
Spécialité : génie mécanique

Lotfi SEGHOUANI

Jury: Nicolas GALANIS (directeur)
Roberto SUNYÉ (codirecteur)
Yves MERCADIER
Mohamed OUZZANE
Radu ZMEUREANU

Sherbrooke (Québec), CANADA Juin 2009

Your file Votre référence
ISBN: 978-0-494-52858-7
Our file Notre référence
ISBN: 978-0-494-52858-7

RÉSUMÉ

La présente thèse s'inscrit dans le cadre d'un projet stratégique sur les arénas financé par le CRSNG (Conseil de Recherche en Sciences Naturelles et en Génie du Canada) qui a pour but principal le développement d'un outil numérique capable d'estimer et d'optimiser la consommation d'énergie dans les arénas et curlings.

Notre travail s'inscrit comme une suite à un travail déjà réalisé par DAOUD et coll. (2006, 2007) qui a développé un modèle 3D (AIM) en régime transitoire de l'aréna Camilien Houde à Montréal et qui calcule les flux de chaleur à travers l'enveloppe du bâtiment ainsi que les distributions de températures et d'humidité durant une année météorologique typique. En particulier, il calcule les flux de chaleur à travers la couche de glace dus à la convection, la radiation et la condensation.

Dans un premier temps nous avons développé un modèle de la structure sous la glace (BIM) qui tient compte de sa géométrie 3D, des différentes couches, de l'effet transitoire, des gains de chaleur du sol en dessous et autour de l'aréna étudié ainsi que de la température d'entrée de la saumure dans la dalle de béton. Par la suite le BIM à été couplé le AIM.

Dans la deuxième étape, nous avons développé un modèle du système de réfrigération (REFSYS) en régime quasi-permanent pour l'aréna étudié sur la base d'une combinaison de relations thermodynamiques, de corrélations de transfert de chaleur et de relations élaborées à partir de données disponibles dans le catalogue du manufacturier. Enfin le couplage final entre l'AIM +BIM et le REFSYS a été effectué sous l'interface du logiciel TRNSYS.

Plusieurs études paramétriques on été entreprises pour évaluer les effets du climat, de la température de la saumure, de l'épaisseur de la glace, etc. sur la consommation énergétique de l'aréna. Aussi, quelques stratégies pour diminuer cette consommation ont été étudiées. Le considérable potentiel de récupération de chaleur au niveau des condenseurs qui peut réduire l'énergie requise par le système de ventilation de l'aréna à été mis en évidence.

Mots clés: Aréna, Système de réfrigération, Consommation d'énergie, Efficacité énergétique, Conduction au sol, Performance annuelle.

REMERCIEMENTS

La réalisation de cette thèse fut une occasion merveilleuse de rencontrer et d'échanger avec de nombreuses personnes. Je ne saurais pas les citer toutes sans dépasser le nombre de pages raisonnablement admis dans ce genre de travail. Je reconnais que chacune a, à des degrés divers, mais avec une égale bienveillance, apporté une contribution positive à sa finalisation. Mes dettes de reconnaissance sont, à ce point de vue, énormes à leur égard.

Je pense particulièrement à mes parents pour leur long sacrifice qui m'a permis d'atteindre ce niveau d'étude et de consécration, mon épouse et mes enfants pour leurs encouragements, leur soutien et leur patience.

Je tiens à remercier sincèrement le Professeur Nicolas GALANIS, mon directeur de recherche, pour son attitude très positive aussi bien sur le plan humain que scientifique. Ses remarques successives ont permis d'améliorer les différentes versions de ce travail. Il a toujours trouvé, comme directeur, le juste équilibre entre la liberté qu'il m'a laissé dans le choix des grandes orientations et dans la détermination des pistes à suivre, d'une part, et un soutien total et sans faille dans les moments délicats, d'autre part. De lui, j'ai toujours reçu non seulement les encouragements dont le doctorant a tant besoin, mais aussi les précieux conseils techniques et pratiques. Grâce à son approche respectueuse de la personne humaine, je me suis continuellement senti à l'aise. Je lui suis infiniment reconnaissant.

J'exprime ma gratitude également à tous ses collaborateurs notamment Roberto SUNYÉ (mon codirecteur), Omar BELLACHE et Mohamed OUZZANE pour m'avoir continuellement fourni la documentation actualisée sur la question de ma recherche. Et aussi aux autres membres du jury pour avoir accepté de lire cette thèse et de m'avoir fait l'honneur d'assister à la soutenance.

Enfin, j'adresse mes plus sincères remerciements à tous mes proches et collègues, qui m'ont toujours soutenu, aidé et encouragé au cours de la réalisation de cette thèse.

Merci à toutes et à tous !

TABLE DES MATIÈRES

LISTE DES FIGURES :

LISTE DES TABLEAUX :

CHAPITRE 1

INTRODUCTION GÉNÉRALE ET REVUE BIBLIOGRAPHIQUE

1.1 Introduction

L'efficacité énergétique est un objectif primordial des gestionnaires de bâtiments. Au Canada, les deux gouvernements, fédéral et provincial, incitent par de nombreux moyens à en favoriser l'application car elle constitue un moyen sûr de réduire leur consommation d'énergie et leurs effets environnementaux et de ce fait, contribuer à concrétiser l'engagement canadien au protocole de Kyoto.

Vu sous cet aspect, les arénas et curlings constituent une cible de choix car ce sont des structures extrêmement énergivores. Ainsi, les systèmes de réfrigération utilisés dans les arénas offrent des possibilités d'économie énergétique et de réduction de gaz à effet de serre à la fois par l'amélioration de l'efficacité énergétique des systèmes de réfrigération, la réduction des fuites de réfrigérant synthétique ainsi que par l'optimisation de leur intégration aux systèmes CVC-R.

Une étude du Centre de la Technologie de l'Énergie de CanmetÉNERGIE de Ressources Naturelles Canada (Varennes) a révélé que les arénas et curlings au Québec présentent un potentiel d'efficacité énergétique inexploité d'environ 620 MWh/an et un potentiel de réduction des gaz à effet de serre d'environ 146 tonnes-eq CO_2/an (**Lavoie** et coll. (2000)). Au vu de ces chiffres pour le moins impressionnants et sachant qu'il existe environ 435 arénas au Québec et plusieurs milliers en Amérique du Nord, moderniser est devenu indispensable compte tenu que la plupart des arénas et curlings au Québec ont été construits dans les années 70 où les connaissances sur l'efficacité énergétique étaient encore balbutiantes. De nos jours de nouvelles technologies ont déjà fait leurs preuves notamment aux États Unis, il serait donc intéressant d'étudier la possibilité de les intégrer dans les installations au Canada en tenant compte du climat local, afin de réduire et optimiser au maximum la consommation d'énergie.

Dans le but de réaliser ces objectifs, il est nécessaire de recourir à des méthodes de calcul précises des différentes charges qui opèrent sur la glace, dues entre autres aux phénomènes de convection, de rayonnement et des fréquentes opérations de resurfaçage de la

glace, tout en tenant compte de la conduction dans le sol en dessous et autour de l'aréna. La consommation énergétique du système de réfrigération et l'interaction de ce dernier avec l'aréna doivent être analysés afin de quantifier la quantité de chaleur rejetée par les condenseurs qui peut potentiellement couvrir totalement ou partiellement les besoins de chauffage de l'aréna et ainsi réduire la facture de consommation énergétique de ces bâtiments tout en assurant une bonne qualité de glace et un bon confort aux usagers et spectateurs.

Dans les sections suivantes de ce chapitre d'introduction, on présente une brève description des parties de l'aréna qui seront étudiées dans cette thèse:

- La dalle de béton avec échangeur de chaleur
- Le système de réfrigération

Une revue bibliographique fait suite à chacune de ces deux sections avant de présenter les objectifs de ce projet et les différents travaux de notre groupe de recherche.

1.2 Dalle de béton avec échangeur de chaleur:

L'échangeur de chaleur dans la dalle de béton sous la glace constitue l'élément essentiel dans les arénas et curlings car c'est à lui qu'incombe la tâche d'absorber les charges dues aux phénomènes de convection et de rayonnement qui opèrent au dessus de la surface de la glace. Il doit aussi absorber les importantes charges thermiques que génèrent les fréquentes et courtes opérations de resurfaçage de la surface de la glace. Ces charges sont alors transportées par la saumure circulant dans la tuyauterie contenue dans la dalle de béton et sont évacuées par le système de réfrigération, permettant ainsi de contrôler la température de glace et sa qualité. Aussi, pour une modélisation plus complète, les charges provenant du sol en dessous de la dalle et du sol environnant doivent être à leurs tours prises en considération.

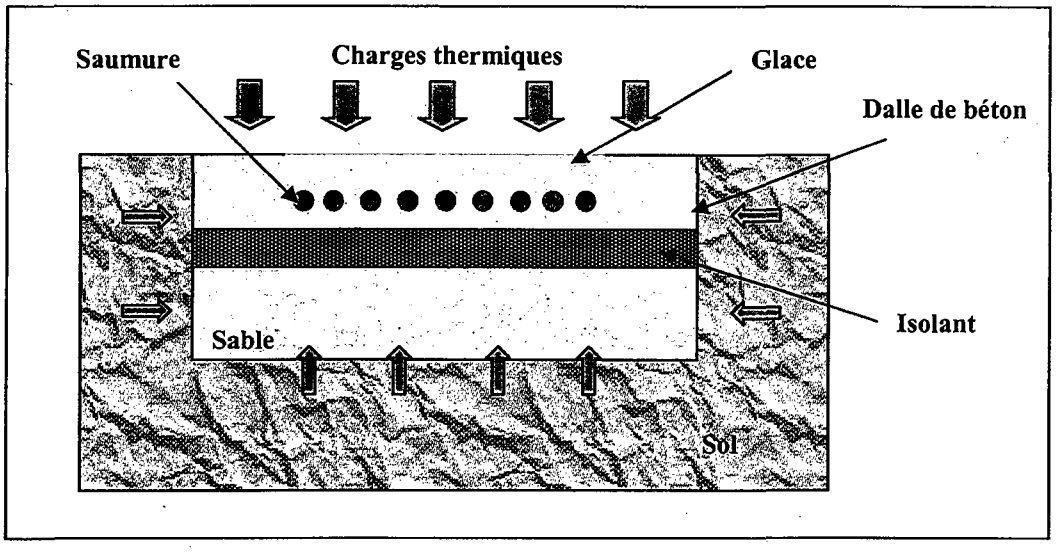

Figure 1.1 Description schématique générale de la structure sous la glace d'un aréna

À cet effet, la modélisation de cette partie de l'aréna est très délicate et complexe, car non seulement il faut tenir compte de la répartition des tuyaux dans la dalle de béton et la circulation de la saumure mais il faut tenir compte de toute la structure (voir figure 1.1) qui est constituée de plusieurs couches différentes aussi bien au niveau de leurs dimensions qu'au niveau de leurs propriétés thermiques; sol, sable, isolant thermique, dalle de béton, tuyaux de saumure et glace.

Très peu d'études ont été effectuées par le passé dans le but de modéliser des échangeurs sous-terrains couplés au sol et au bâtiment; les rares travaux qu'on trouve dans la littérature concernent surtout les planchers chauffés. Parmi ceux-là on peut citer les travaux réalisés par :

El-Biyaali et coll. (1996) qui ont mis en œuvre une méthode de réduction des modèles basée sur la sous-structuration du système thermique étudié. L'application sur l'évaluation des transferts thermiques entre un bâtiment et le sol a montré que cette méthode donne des résultats très satisfaisants, aussi bien vis à vis de la méthode détaillée qui consiste à traiter le problème par agrégation directe que pour la méthode de couplage. Pour cette dernière, ils se sont limités à un découpage en deux éléments avec un couplage dit "bord-à-bord". Ainsi, les perspectives d'utilisation, dans les codes de calcul dédiés à des non experts, de la sous-structuration et de la réduction des bases locales de transferts d'une structure complexe

apparaissent grandes. Ces modèles réduits ont pour vocation essentielle d'alimenter des codes de simulation, plus globaux, du comportement thermo-aéraulique des bâtiments. Dans ce contexte la constitution de bibliothèques de modèles réduits devrait rendre de grands services à leurs utilisateurs. Par ailleurs, le prix à payer, en termes de temps de calcul, pour l'obtention du modèle réduit est largement compensé par les gains de temps obtenus lors de la simulation d'un cas.

Roux et coll.(1997) ont publié un article dans lequel ils présentent les techniques utilisées pour réaliser un modèle d'état réduit, pour un plancher à chauffage à eau, et son couplage avec un modèle de bâtiment, réalisé à l'aide du logiciel TRNSYS.

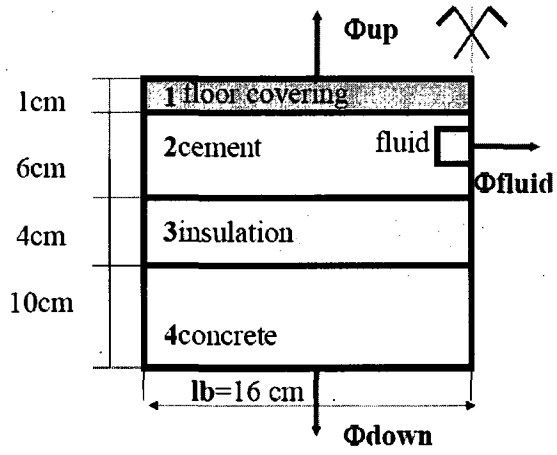

Table 1.

N° layer	thermal conductivity (W/mK)	thermal capacity (10^6 J/m^{3}K)
1	1.04	1.05
2	1.15	1.64
3	0.04	0.05
4	1.50	2.21

Figure 1.2 Description schématique du système radiant [Roux et coll. (1997)]

Le comportement thermique dynamique du plancher a été modélisé, en intégrant l'équation de la chaleur en deux étapes. Premièrement, ils ont procédé par la discrétisation de l'espace en utilisant une méthode aux volumes finis. Les différentes matrices (état, commande, etc.) sont ainsi calculées pour le modèle de référence qui est de l'ordre 215 volumes de contrôle pour l'exemple traité (Figure 1.2). Par agrégation linéaire, une technique utilisée pour la réduction du modèle, ils ont obtenus un modèle réduit de l'ordre de 13 volumes de contrôle. Deuxièmement, une fois le modèle réduit réalisé, il est ensuite inclus comme nouveau type (sous-programme) dans TRNSYS, le logiciel qui intègre numériquement les équations, et il est couplé à d'autres composants du modèle thermique, particulièrement le modèle de bâtiment.

Par ailleurs, de nombreux auteurs se sont intéressés aux pertes thermiques des bâtiments vers le sol par l'intermédiaire de leurs fondations en béton :

Une technique analytique appelée : *Interzone Température Profile Estimation* (ITPE) *method* développée par **Krarti** et coll. (1988) a été appliquée à plusieurs problèmes de transfert thermique de couplage avec le sol. En particulier, des solutions d'ITPE ont été développées pour calculer le transfert thermique à partir des planchers de dalle en béton, sous-sols, utilisées généralement avec des configurations d'isolation (**Krarti**, 1990, 1993, et 1994).

La méthode d'ITPE combine à la fois les techniques analytiques et numériques pour obtenir les solutions bidimensionnelles et tridimensionnelles de l'équation de conduction de la chaleur. Puisqu'elle est basée sur une solution analytique, la méthode d'ITPE peut tenir compte de n'importe quelle valeur d'isolation thermique, profondeur de la table d'eau (water table), et propriétés thermiques du sol. Dans une formalisation typique d'ITPE, le sol (ou tout milieu conducteur) est premièrement divisé en plusieurs zones de formes régulières par des surfaces « imaginaires ». La géométrie et les conditions aux frontières, déterminent ces surfaces imaginaires qui divisent le milieu du sol. Puis, la distribution de la température est déterminée dans chaque zone en résolvant l'équation de conduction de la chaleur par une technique analytique. Le long des surfaces imaginaires, les profils de température ne sont pas connus. Cependant, ces profils de température sont déterminés en utilisant la continuité de flux de la chaleur entre les zones.

Laouadi (2004)**:** a développé un modèle détaillé pour le chauffage radiant et les systèmes de refroidissement (Figure 1.3), dans le but de l'intégrer dans le logiciel de simulation d'énergie. Le modèle vise les logiciels de simulation d'énergie qui emploient la modélisation numérique unidimensionnelle pour calculer le transfert thermique dans des bâtiments.

Le modèle développé comporte deux ensembles: un ensemble emploie la méthode de source de chaleur pour calculer le transfert thermique dans le milieu radiant tandis que l'autre calcule le transfert thermique dans la tuyauterie du circuit. Le transfert thermique dans le milieu radiant est résolu en utilisant la modélisation numérique unidimensionnelle, déjà établi dans le logiciel de simulation d'énergie, et une solution analytique bidimensionnelle est apposée à elle. Le transfert thermique à partir de la tuyauterie de circuit au milieu adjacent est résolu en utilisant un modèle analytique.

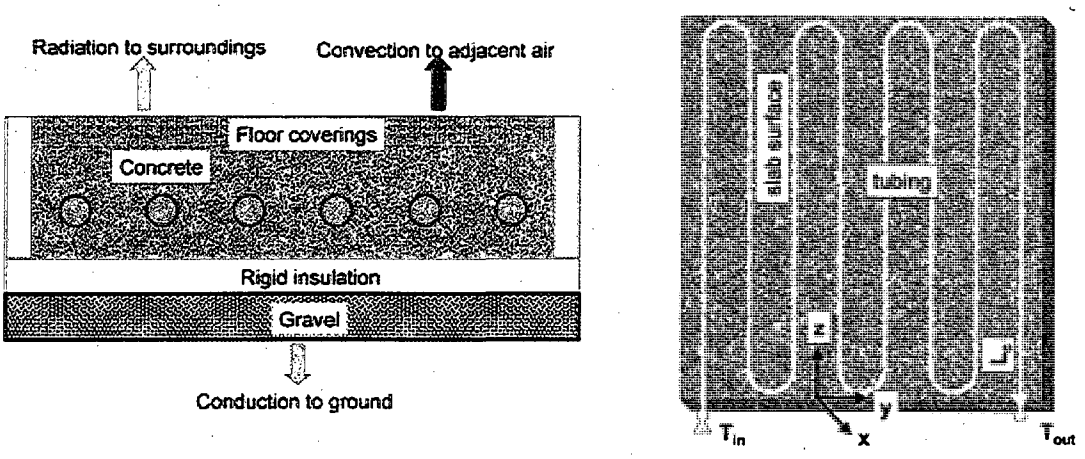

Figure 1.3 Description schématique du système radiant à dalle de béton avec tuyauterie en serpentin

Les deux ensembles sont couplés par l'intermédiaire de la température du nœud de source de chaleur, c.-à-d., la température du nœud de source de chaleur est égale à celle de la surface extérieure de la tuyauterie du circuit. L'avantage de ce modèle par rapport au modèle unidimensionnel, est qu'il prévoit avec plus de précision la température de contact tuyauterie de circuit-dalle de béton.

Somrani et coll. (2007) : ont présenté deux modèles dans le but de calculer les gains de chaleur du sol vers la saumure pour des applications sur les arénas. Le premier modèle est basé sur la méthode d'analyse (ITPE) décrite précédemment, tandis que le second utilise un schéma implicite aux différences finies. Les prédictions des deux modèles ont été comparées et un bon rapprochement des résultats à été constaté. Aussi, les résultats du modèle numérique transitoire sont comparés à des mesures obtenues pour une petit aréna exploité dans des conditions de laboratoire. Les mesures prévoient la période de temps nécessaire pour faire geler la surface de glace ainsi que la température à différents endroits du sol de l'aréna. Les résultats du modèle numérique ont été ensuite utilisés pour étudier l'impact des différentes conditions d'opération et aussi du design de ce type de bâtiment. Les auteurs stipulent que la température de la glace et le temps nécessaire pour faire geler l'eau peuvent être influencés à long terme par l'épaisseur de l'isolant thermique sous la dalle de béton, l'épaisseur de la couche de glace, la température de consigne de la saumure, la température de l'air intérieur et le transfert de chaleur par convection au dessus de la surface de la glace.

1.3 Système de réfrigération :

Les systèmes de réfrigération des arénas et curling sont considérés comme faisant partie des larges systèmes de réfrigération, car ils sont constitués de plusieurs évaporateurs, compresseurs, vannes de détentes, condenseurs...etc. Ils constituent le cœur de l'aréna et c'est la partie qui consomme le plus d'énergie avec le système de ventilation

La modélisation et la simulation numérique des systèmes de réfrigération de tout genre ont fait l'objet de nombreuses études. Les modèles existants peuvent être classés généralement selon leur degré de complexité. Mais, un examen plus approfondi de la littérature indique cependant, que la modélisation des systèmes de réfrigération au complet ou par composante peut être répartie en deux principaux types :

- Les modèles « Curve fitting»
- Les modèles fondamentaux

Dans le premier type, le modèle utilise des données fournies dans le catalogue du manufacturier pour chaque composante du système de réfrigération afin de générer une corrélation. L'application valide est limitée à la plage des données et aux conditions fournies par les fabricants.

Dans le deuxième type, le modèle repose sur des équations de transfert de chaleur et sur les lois thermodynamiques qui sont une description exhaustive des phénomènes physiques. Ce type de modèle exige des informations complètes sur la configuration et les dimensions des composantes ; tels que le type des échangeurs de chaleur (tubes et calendre, à plaques, condenseur à air ou à eau ... etc.), le nombre de tubes dans la calendre, les diamètres des tubes, le nombre de passes, le nombre de pistons dans le compresseur s'il s'agit d'un compresseur à pistons, le type de réfrigérant, le nombre de ventilateurs dans le condenseur si refroidi à l'air ...etc.

Cependant, une des principales difficultés dans la modélisation des systèmes de réfrigération est le fait qu'un modèle exact de chaque composante peut s'avérer extrêmement complexe ou même impossible à obtenir. Par exemple, dans le cas du compresseur, où le débit du réfrigérant à travers les soupapes, le processus de transfert de chaleur, la présence d'un lubrifiant à l'intérieur de la coque du compresseur...etc., sont presque analytiquement indescriptibles. Aussi, quelques limitations et hypothèses simplificatrices sont la plupart du temps nécessaires et requises pour alléger la simulation.

Pour cette raison, plusieurs auteurs ont adopté une méthode alternative qui en fait se situe entre les deux types de modèles décrits précédemment. Certains articles illustrant ces approches sont brièvement passés en revue dans les paragraphes suivants.

Le modèle de la pompe à chaleur eau-à-eau à surchauffe-commandée développé par **Stefanuk** et coll. (1992), est l'un des modèles les plus détaillés présent dans la littérature. Les auteurs stipulent que leur modèle est dérivé entièrement des lois fondamentales de conservation de la masse, de l'énergie, de la quantité de mouvement et des équations d'état ainsi que les corrélations fondamentales du transfert de chaleur. Les valeurs des paramètres qui décrivent le comportement des différents composants (évaporateur, condenseur, compresseur ....) sont supposées disponibles. Par exemple, les paramètres du compresseur sont choisis en adaptant le modèle aux courbes de performance fournies par le fabricant et qui relient le débit massique et la puissance du courant électrique d'entrée à la température d'évaporation et à la pression de décharge du compresseur. Cependant, elles ne sont presque jamais disponibles dans les catalogues des pompes à chaleur des fabricants. Les comparaisons entre les mesures expérimentales et les prédictions numériques du modèle pour les pressions d'évaporation et de condensation, les taux de transfert thermique dans l'évaporateur et dans le condenseur, ainsi que le COP de la pompe à chaleur sont données. Excepté quelques points avec des erreurs au delà de ±10%, la plupart des résultats sont généralement acceptables. Les prévisions des taux de transfert thermique dans les deux échangeurs de chaleur sont uniformément trop élevées, les auteurs expliquent que la cause de ce phénomène est la prévision surestimée des coefficients de transfert thermique, puisque les coefficients de transfert thermique utilisés dans le modèle sont seulement connus à l'intérieur de ±20%.

Le modèle quasi-statique du système de réfrigération réciproque développé par **Bourdouxhe** et coll. (1994, 1997) fait partie d'une trousse à outils de simulation (Toolkit) pour l'ASHRAE qui se veut d'être à la fois orienté vers des solutions simples avec un minimum de paramètres et d'être quelque part entre les modèles à «curve fitting» et «équations fondamentales». Leur approche consiste à l'utilisation d'un schéma conceptuel comme technique de modélisation afin de représenter l'unité comme un ensemble de composants élémentaires et classiques. Le comportement de chaque composant est alors modélisé par une approche déterminante. Cette approche exige peu de paramètres et de données expérimentales comparée aux modèles développés précédemment. Dans la procédure

d'identification des paramètres, les données expérimentales disponibles, telles que les températures de condensation et d'évaporation, ainsi que les possibles sous-refroidissements et sur-chauffages, sont exigées. Basés sur ces derniers résultats expérimentaux, les paramètres du compresseur sont identifiés. Alors le système de réfrigération en entier est considéré afin d'identifier les coefficients de transfert de chaleur de l'évaporateur et du condenseur. Cependant, ces données expérimentales ne sont pas toujours disponibles dans les catalogues des manufacturiers.

Willatzen et coll. (1998) ont établi un modèle mathématique décrivant les phénomènes transitoires de flux diphasiques pour les évaporateurs et les condenseurs dans un cycle de réfrigération à l'application d'un réfrigérateur domestique. Il est basé sur des équations aux dérivés partielles unidimensionnelles qui représentent la conservation de masse et de l'énergie de la paroi du tube (avec omission des équations de mouvement et en partant du principe que les pertes de charge sont négligeables). Ils ont formulé un jeu d'équations différentielles plus simples en intégrant séparément sur les trois phases (liquide, liquide/vapeur et vapeur) habituellement présentes dans un échangeur de chaleur tout en examinant de près les phases transitoires importantes induites par la régulation On/Off des systèmes de refroidissement à compression de vapeur. Ces équations ont été restructurées par la suite, puis reliées à une base de données sur les principaux frigorigènes purs et en mélanges. De cette manière, ils ont obtenu un modèle d'échangeur de chaleur d'application général et souple. Ce modèle a été testé dans des conditions de fonctionnement très variées et a été aussi employé dans un système de régulation simple pour montrer l'efficacité du modèle pour la conception et la régulation des systèmes.

Svensson (1999) s'est inspiré d'un système à compression de vapeur avec plusieurs hypothèses simplificatrices pour le compresseur. Le condenseur a été séparé en deux zones (condensation et sous-refroidissement), tandis que l'évaporateur a été traité comme une seule zone. Le processus d'expansion au niveau de la vanne de détente a été modélisé comme étant une expansion parfaitement isenthalpique qui maintient une surchauffe constante.

Ge et **Tassou** (2000) ont développé un modèle mathématique pour simuler le fonctionnement du système de réfrigération d'un supermarché. Un tel modèle peut être employé pour la comparaison de différents systèmes et les stratégies de commande en termes de consommation d'énergie et impact du réchauffement global. Le modèle est basé sur

plusieurs sous modèles de composants qui ont été liés ensemble dans l'environnement de TRNSYS. Les sous modèles des composants principaux incluent le compresseur réciproque, le condenseur refroidi à l'air, la valve thermostatique d'expansion, l'étalage froid et la commande. Le modèle du système général a été validé avec les résultats expérimentaux obtenus à partir d'un système en laboratoire et d'un système complet réel dans un supermarché en Écosse. La valeur du modèle est illustrée en déterminant et en comparant l'efficacité du contrôle de la pression de condensation et de la vitesse variable des compresseurs contre une pression de condensation et une vitesse constantes. Les auteurs concluent que même dans les conditions ambiantes de l'été, le système peut être actionné sans problèmes à des pressions de condensation très inférieures à ce qui est fait dans la pratique sous des stratégies de commande à pression fixe. L'utilisation de la commande de vitesse variable sur un des compresseurs peut également fournir un meilleur contrôle de la pression d'aspiration et une économie d'énergie substantielle (jusqu'à 23%) comparée à la commande On/Off.

Browne et **Bansal** (2002) présentent un modèle permettant de prévoir la performance des refroidisseurs d'eau à compression de vapeur en régime transitoire dans un large éventail de conditions de fonctionnement. Le modèle surmonte les hypothèses idéales utilisées pour les modèles antérieurs employés pour la modélisation des échangeurs de chaleur. En particulier, le modèle actuel emploie une méthodologie NTU- ϵ pour le condenseur et l'évaporateur multitubulaire. Cette approche permet de varier les coefficients de transfert de chaleur dans toutes les parties des échangeurs de chaleur, améliorant ainsi l'analogie physique et la précision de la simulation. On peut utiliser ce modèle en disposant simplement de données faciles à obtenir (par exemple, la température de l'eau entrant dans le condenseur et la température de l'eau sortant de l'évaporateur). Par ailleurs un modèle de compresseur simple se basant sur une régression empirique a été employé pour la simulation. Les données obtenues comprennent les variables de performance telles que la puissance électrique requise, le coefficient de performance (COP) ainsi que les états du frigorigène pendant l'intégralité du cycle frigorifique. La méthodologie employée pour ce modèle permet la modélisation de la performance des refroidisseurs utilisant les mélanges de frigorigènes. Ils ont validé le modèle à l'aide des données obtenues pour les refroidisseurs à mono vis et à double vis respectivement. Les données montrent une concordance de ± 10 %.

Swider et coll. (2001) et **Bechtler** et coll. (2001) ont adopté avec succès une nouvelle approche dans le but de modéliser un refroidisseur à compression de vapeur; cette approche utilise une méthode à réseau de neurones artificiels, dite GRBF (Generalised Radial Basis Function) afin de prévoir la performance générale du refroidisseur. Le modèle est développé avec l'objectif de recourir seulement aux paramètres d'entrée qui sont aisément connus de l'ingénieur opérateur, c.-à-d. la température de sortie de l'eau de l'évaporateur, la température d'admission de l'eau de refroidissement au condenseur, et la capacité de l'évaporateur. Le modèle GRBF du refroidisseur prédit le travail du compresseur ainsi que le COP de tout le système avec une précision de ± 5%.

Solati et coll. (2003) ont présenté plusieurs corrélations pour des modèles de base de systèmes de réfrigération à compression de vapeur (compresseurs à vis), dans le but d'évaluer la performance énergétique de ces systèmes. Ils ont été développés en utilisant un modèle thermodynamique détaillé, contenu dans la trousse à outils de l'ASHRAE (Toolkit 1), pour :

1. L'identification des paramètres du système de réfrigération avec des données du catalogue du fabricant.
2. La simulation de la performance énergétique des systèmes de réfrigérations à vis.

Les nouveaux modèles ont été comparés à ceux actuellement utilisés pour les systèmes de réfrigération centrifuges. La performance énergétique des systèmes de réfrigération à vis de deux fabricants différents a été également comparée.

Jin et **Spitler** (2002) ont présenté un modèle d'une pompe à chaleur eau-à-eau, approprié pour être utilisé dans l'analyse énergétique des bâtiments ainsi que la simulation des systèmes CVC-R. Le modèle a été développé afin d'exiger seulement des données généralement disponibles dans les catalogues des manufacturiers dans le but d'estimer les coefficients du modèle. Contrairement à d'autres modèles déterminants plus détaillés, il ne requiert pas les données des mesures internes du système, habituellement indisponibles pour les concepteurs de systèmes du bâtiment et les simulationnistes. Cela fonctionne également aussi bien avec seulement 16 points de repères pour chaque mode, le faisant raisonnablement commode quand les données doivent être manuellement transcrites à partir d'un catalogue. En outre, la performance du modèle se compare favorablement avec le modèle déterminant le plus détaillé précédemment édité, ayant la même erreur RMS que le modèle décrit par **Stefanuk** et coll. (1992). En le comparant aux modèles à équation adaptée, ce modèle

maintient la représentation physiquement basée de la pompe à chaleur, ce qui permet une certaine extrapolation au delà des données du catalogue. Sa performance est sensiblement meilleure quand un nombre limité de points de fonctionnement est utilisé pour l'évaluation des paramètres ou des coefficients.

Fu et coll. (2002) ont développé un modèle de simulation en régime permanent, afin de prévoir la performance des refroidisseurs à vis dans un large champ de paramètres de configuration et de conditions de fonctionnement. Le modèle inclut des sous-modèles pour les composantes clés, telles que le compresseur sans économiseur, compresseur avec économiseur, condenseur à tubes, valve d'expansion, et évaporateur noyé. La méthode modulaire séquentielle et les méthodes successives de substitution ont été combinées ensemble pour effectuer la simulation des refroidisseurs. Les propriétés de convergence de cette technique de simulation ont été également analysées.

Ce modèle peut prévoir la performance du système avec une erreur de ±10% pour une capacité de refroidissement à grande échelle. Une fois leur modèle validé, une analyse de sensibilité sur le système d'économiseur à été réalisée; ils ont constaté que la capacité de refroidissement du compresseur à vis peut être augmentée en ajoutant l'économiseur, mais seulement quand le rapport volumétrique de la compression est plus grand qu'une certaine valeur critique. En même temps le compresseur à vis avec économiseur peut avoir un plus haut COP que celui sans économiseur.

Durant la même année, il y a lieu de signaler l'important travail de **Bendapudi** et **Braun** (2002) qui ont réalisé une revue de la littérature comprenant plus de 40 articles de différents modèles de systèmes de réfrigération à compression de vapeur s'étalant sur une période de 23 ans provenant de différents périodiques et conférences. Ils présentent un résumé de chacun de ces documents en utilisant le même modèle qui comporte huit rubriques: description de l'équipement, le but, les hypothèses, la description mathématique, la solution technique, l'applicabilité, une discussion et des références. Leur rapport fournit donc une mine d'informations dans un format simple qui donne un aperçu utile de l'évolution des approches appliquées à la modélisation de tels systèmes.

Le et coll. (2004) ont développé un modèle de simulation pour un compresseur à vis à huile-injecté pour des applications en processus industriel. Toutes les composantes principales du système sont modélisées dans un format modulaire, telles que le compresseur à vis à huile-

injecté, condenseur à tubes, évaporateur noyé, valve de détente...etc. Il prévoit les paramètres de performance avec une erreur qui ne dépasse pas les 10%. Les résultats simulés se comparent bien avec les températures mesurées de l'eau de refroidissement (à la sortie du condenseur) et de l'eau glycolé (à la sortie de l'évaporateur) à ±2% et ±5%, respectivement. Ils constatent que le COP du système augmente d'environ 25% en réduisant la température de l'eau de refroidissement entrant dans le condenseur de 5°.

Un autre modèle numérique du comportement thermique et dynamique du fluide dans des évaporateurs et condenseurs à double tubes à été développé par **Garçia-Valladares** et coll. (2004). Pour le cas unidimensionnel en régime permanent et transitoire, les équations gouvernantes discrétisées (continuité, quantité de mouvement et énergie) ont été efficacement couplées en utilisant une méthode pas-à-pas implicite. Cette formulation a exigé l'utilisation de corrélations empiriques pour l'évaluation du transfert de chaleur en convection et en effort de cisaillement. Une attention particulière a été portée aux différentes phases du fluide à l'intérieur des échangeurs de chaleur (liquide, vapeur/liquide, vapeur). Toutes les variables de l'écoulement (enthalpies, températures, pressions, vitesses, flux de chaleur,...) en même temps que les propriétés thermo-physiques sont évaluées à chaque point du maillage où le domaine est discrétisé. Les différents aspects et comparaisons numériques avec des résultats analytiques et expérimentaux ont été présentés afin de vérifier et valider le modèle. Les résultats obtenus présentent une bonne concordance avec les travaux antérieurs.

Chan et **Yu** (2006) ont présenté un modèle thermodynamique dans le but d'évaluer la possibilité d'améliorer le coefficient de performance (COP) sous diverses conditions de fonctionnement. Il tient compte des vrais phénomènes physiques du processus, y compris le contrôle de la capacité des compresseurs à vis et la variation des coefficients de transfert thermique dans l'évaporateur et dans le condenseur. Il contient aussi un algorithme pour déterminer comment les ventilateurs du condenseur sont mis en marche en réponse à une température de condensation différente du point de consigne. Les paramètres du modèle ont été identifiés sur la base des données de performance des caractéristiques du refroidisseur et le modèle de ce dernier a été validé en utilisant un large champ de données de fonctionnement d'un refroidisseur à vis refroidi à l'air. Ils trouvent que la différence entre les COPs mesurés et modelés est à moins de ±10% pour 86% des cas. Aussi, le COP du refroidisseur peut augmenter jusqu'à 115% quand la température de condensation du point de consigne est

ajustée, et cela pour n'importe quelle température extérieure donnée. Ils ont aussi proposé une stratégie pour faire fonctionner à un maximum d'efficacité un refroidisseur à vis refroidis à l'air pour satisfaire le plus possible les besoins de réfrigération d'un bâtiment.

Arias et **Lundqvist** (2006), ont proposé une solution à deux options qui peuvent être combinées afin de diminuer la demande énergétique des supermarchés où la consommation d'énergie est très élevée. La première s'applique mieux pour les pays relativement froids tels que l'Europe du nord et le Canada. Elle consiste en la récupération de la chaleur rejetée par les condenseurs pour l'utiliser par la suite pour les besoins de chauffage du bâtiment. L'autre option consiste à faire varier la pression de condensation, afin d'améliorer le coefficient de performance et diminuer la consommation d'énergie du système de réfrigération pour les températures extérieures plus basses. Les auteurs ont employé le logiciel CyberMart pour mettre au point leur modèle numérique du système de réfrigération qui calcule la consommation d'énergie d'un supermarché en Suède. Ils ont validé leurs calculs théoriques par des mesures de différents paramètres tels que les températures, taux d'humidité relative et puissance du compresseur, effectués dans différents supermarchés. Les auteurs affirment que tous les besoins de chauffage d'un supermarché peuvent être comblés en exploitant soigneusement les deux options précitées dans le cadre d'une stratégie de commande adéquate.

1.4 Objectifs du projet :

Le présent projet s'inscrit dans le cadre d'un projet stratégique sur les arénas financé par le CRSNG (Conseil de Recherche en Sciences Naturelles et en Génie du Canada) qui a pour but principal le développement d'un outil numérique capable d'estimer et d'optimiser la consommation d'énergie dans les arénas et curlings. Plusieurs travaux de recherche ont déjà été réalisé dans le cadre de ce projet notamment ceux de **Bellache** et coll. (2005) qui ont développé un modèle numérique 2D en régime permanent utilisant un code CFD capable de prévoir la vitesse de l'air et sa température ainsi que l'humidité absolue dans un aréna à Montréal (Québec) avec ventilation et chauffage. Le code développé calcule le flux thermique vers la glace dû aux phénomènes de convection de l'air, de la condensation de la vapeur et de la radiation à partir des murs et du plafond de l'aréna étudié. Cependant, les calculs ne

tiennent pas compte du resurfaçage, du travail de la pompe et du gain de chaleur à partir du sol.

Ce modèle à été ensuite amélioré par **Bellache** et coll. (2006) pour inclure le phénomène transitoire, les gains de chaleur du sol, les charges dues aux luminaires, le resurfaçage et la dissipation de travail de la pompe dans les tuyaux de saumure. La température du sol à une profondeur de 2m à été considérée comme étant constante et les tuyaux de saumure ont été assimilés à une surface horizontale à température constante égale à la moyenne des températures d'entrée et de sortie de la saumure. Les résultats ont été comparés avec succès avec les mesures expérimentales effectuées sur l'aréna en question par **Ouzzane** et Coll. (2006)

Bien que l'approche de CFD soit très précise et fourni beaucoup de détails dans les résultats, elle requiert cependant une mémoire très importante et un temps de calcul considérable. Par exemple pour une simulation de 24h avec le modèle de **Bellache** et coll. (2006) le temps de calcul sur un ordinateur personnel performant prend un jour complet.

Dés lors, une autre méthode alternative au CFD qui requiert moins de temps de calcul et moins de mémoire à été développée par **Daoud** et coll. (2006, 2007) qui combine plusieurs modèles; zonal, radiation, humidité et condensation et tient en compte le resurfaçage et l'occupation. Ce modèle appelé «Above Ice Model » ou AIM, calcule les flux de chaleur à travers l'enveloppe du bâtiment ainsi que les distributions de températures et d'humidité pour un régime transitoire en 3D durant une année météorologique typique. En particulier, il calcule les flux de chaleur vers la couche de glace dus à la convection, la radiation et la condensation. La température sous la glace est considérée constante et les résultats montrent une bonne concordance avec les données expérimentales et les résultats obtenus par CFD.

C'est à la suite de cette dernière étude que s'inscrit notre travail qui consiste à développer dans un premier temps un modèle général de la structure sous la glace, qui tient compte de sa géométrie 3D, des différentes couches, de l'effet transitoire, des gains de chaleur du sol en dessous et autour de l'aréna ainsi que de la température d'entrée de la saumure. Ce modèle nommé *Below Ice Model* ou BIM vient se coupler à l'*Above Ice model* (ou AIM) développé par **DAOUD** et coll. (2006, 2007) comme le montre la figure1.4. Il suppose une température constante d'entrée de saumure de -9°C dans la dalle de béton et simule une année

entière. Les détails de la modélisation et résultats ont été publié par **Seghouani** et coll. (2009) et constituent le chapitre 2 de la présente thèse.

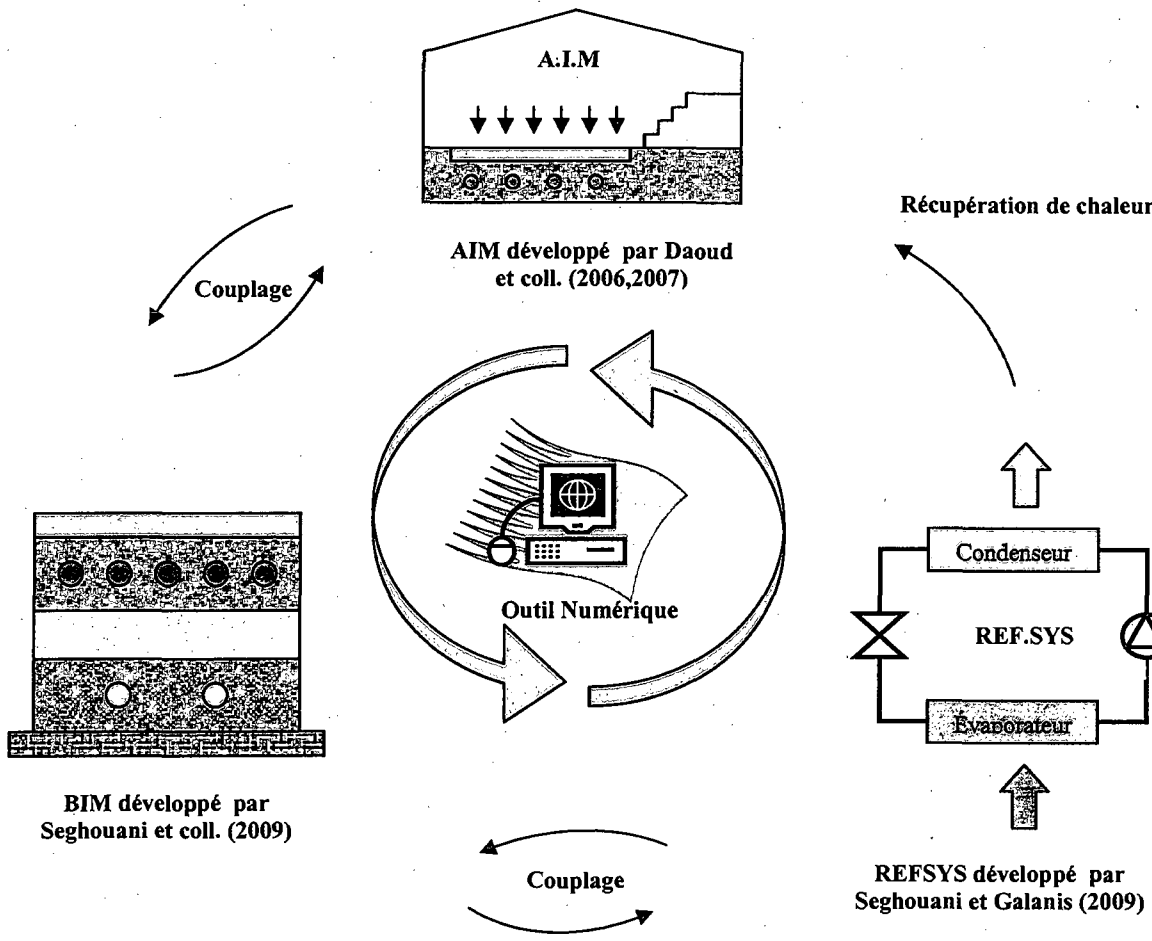

Figure 1.4 Objectif général du projet

La deuxième étape consiste à modéliser numériquement le système de réfrigération de l'aréna à l'étude (C. Houde), qui est constitué de 5 compresseurs, de 2 évaporateurs, ainsi que de 5 condenseurs à air et autant de vannes de détente. La modélisation d'un tel système doit tenir compte de la température de l'air extérieur, de la température de retour de la saumure de la dalle de béton ainsi que de la charge thermique calculée par l'ensemble couplé de l'AIM + BIM. Le système de réfrigération doit alors évacuer cette charge et délivrer la température de saumure de consigne désirée soit -9°C. Les détails de la modélisation et les résultats obtenus ont été publié par **Seghouani** et **Galanis**. (2009) et constituent le chapitre 3 de la présente thèse. Le même système à déjà été modélisé par **Madani** (2008) utilisant une approche

relativement similaire afin d'étudier les effets de la variation de la pression de condensation sur les paramètres thermodynamiques du circuit de réfrigération. Cet auteur a évalué les gains énergétiques découlant du fonctionnant à pression de condensation variable qui permet de profiter du climat canadien spécialement en hiver.

Enfin, la troisième et dernière étape de ce projet (chapitre 4) consiste à coupler le modèle développé du système de réfrigération et l'ensemble AIM + BIM (voir figure1.4). Ainsi, le modèle numérique de l'aréna est complet et l'interaction entre le bâtiment et son système de réfrigération au niveau des évaporateurs (fluide secondaire et primaire) peut être analysée. Ceci permet d'étudier différentes stratégies de contrôle en mode quasi permanent. Aussi, une estimation du potentiel de récupération de chaleur au niveau des condenseurs est effectuée et comparée aux besoins énergétiques du bâtiment.

CHAPITRE 2

PREDICTION OF YEARLY ENERGY REQUIREMENTS OF INDOOR ICE RINKS

Auteurs et affiliation:

L. SEGHOUANI: étudiant au doctorat, Université de Sherbrooke, Faculté de génie, Département de génie mécanique.

A. DAOUD: Chercheur Scientifique, Institut de Recherche d'Hydro-Québec Laboratoire des Technologies de l'Énergie (LTE), Shawinigan, (Québec).

N. GALANIS: professeur, Université de Sherbrooke, Faculté de génie, Département de génie mécanique.

Date d'acceptation: 22 Novembre 2008

État de l'acceptation: version finale publiée

Revue: Energy and Building

Référence: (Seghouani et coll. 2009)

Titre français: Prédictions annuelles des besoins énergétiques des arénas internes.

Résumé :

Dans ce chapitre, un modèle de transfert de chaleur transitoire, entre le sol sous l'aréna et autour de ses fondations avec la saumure circulant dans les tuyaux de la dalle de béton sous la glace fut développé. Par la suite, ce modèle a été couplé avec succès au modèle aéraulique et thermique du bâtiment développé par Daoud et al. (2006) ; celui-ci calcule les différents flux de chaleur qui opèrent au dessus de la glace par convection, radiation et changement de phase. Aussi, plusieurs sous-routines ont été élaborées dans le but d'estimer la consommation d'énergie pour le chauffage et l'humidification (ou pour la climatisation et le réchauffement) de l'air de ventilation.

L'outil de simulation développé a été utilisé pour calculer les charges mensuelles de réfrigération, la consommation d'énergie par le système de ventilation, l'éclairage, la pompe à saumure, le système de chauffage radiant des gradins et le chauffage électrique souterrain utilisé pour prévenir le gel dans le sol.

L'effet du climat de quatre villes d'Amérique du Nord (climats très différents) est analysé ainsi que les effets de la température d'entrée de saumure dans la dalle de béton, de l'épaisseur de la glace, de l'hystérésis du thermostat qui contrôle la température de l'air au dessus des estrades et de l'effet du *set back* nocturne du thermostat. Enfin, quatre corrélations exprimant la consommation d'énergie du système de ventilation en fonction de la température sol-air sont formulées.

Mots clés: Méthode zonale, Conduction au sol, Échanges radiatifs, Convection, Condensation, Charge de réfrigération.

Abstract

A model of the transient heat transfer between the ground under and around the foundations of an indoor ice rink and the brine circulating in pipes embedded in the concrete slab under the ice has been coupled with a previously developed model calculating heat fluxes towards the ice by convection, radiation and phase changes. Subroutines calculating the energy consumption for heating and humidifying (or cooling and reheating) the ventilation air have also been added to the model. The resulting simulation tool has been used to calculate monthly refrigeration loads and energy consumption by the ventilation system, the lights, the brine pump, the radiant heating system of the stands and the underground electric heating used to prevent freezing and heaving for four North American cities with very different climates. Correlations expressing the energy consumption of the ventilation air stream in terms of the sol-air temperature are formulated.

Keywords: zonal method, ground conduction, radiation exchanges, convection, condensation, refrigeration load

Nomenclature

A	area, m^2
C_p	Specific heat, *J/kg K*
C_d	Discharge coefficient
g	Acceleration of gravity, m/s^2
h	height, *m*
k	Thermal conductivity, *W/(m.K)*
$\dot{m}_{i,j}$	Airflow between zones i and j, *kg/s*
$\dot{m}_B$	Brine flow rate, *kg/s*
M	Mass, *kg*
P	Static pressure, *Pa*
q_{cd}	Conductive flux, W/m^2
q_{cv}	Convective flux, W/m^2
q_{rd}	Radiative flux, W/m^2
q_{cond}	Condensation flux, W/m^2
q_{rs}	Heat flux due to resurfacing, W/m^2
Q_{Cool}	Cooling rate, *W*
Q_{Heat}	Heating rate, *W*
Q_{Humid}	Energy rate due to humidification, *W*
Q_{Reheat}	Energy rate due to reheating, *W*
Q_H	Electrical power in sand layer, *W*
Q_{Ice}	Heat rate into node 1 calculated by AIM, *W*
Q_{node}	Lateral heat transfer to node n, *W*
R	Thermal resistance, $m^2 \cdot K/W$
S_{node}	Surface for lateral heat transfer at node n, m^2
t	Time, hour
T	Temperature, *K*
T_b	Brine temperature, *K*

T_{gr} Temperature of ground surface, *K*

T_{node} Temperature at node n, *K*

$T_{sol\text{-}air}$ Sol-air temperature, *°C*

U_{node} Average conductance for lateral heat transfer at node n, $W/m^2 K$

$\dot{W}_g$ Moisture source term, *kg/s*

z_1, z_2 Top and bottom depths of ground segment, *m*

Abreviations

AIM Above Ice Model

BIM Below Ice Model

IST Ice Surface Temperature

Subscripts and Superscripts

i Cell i or surface i

i,j Between surface or cell i and j

p present time step

p+1 next time step

Greek symbols

Δt Time step, *hour*

ε_{ij} Constant depending on flow direction (±1)

ρ Air density, kg/m^3

ω Absolute humidity, $kg_{moisture}/kg_{dry\ air}$

2.1 Introduction

Indoor ice rinks are large buildings without internal partitions and with high energy consumption. They have a complex energy system in which a large ice sheet is cooled and maintained at a low temperature by a refrigeration system, while the stands are heated (or cooled) to ensure comfortable conditions for the spectators. Also, the building is ventilated to ensure good air quality. The movement of the ventilation air through these wide open areas and the simultaneous operation of heating and cooling equipments increase energy consumption and greenhouse gas (GHG) emissions.

A study by Lavoie et al. (2000) shows that the potential for energy savings in a typical ice rink in Quebec is roughly 620 MWh/year and the potential GHG emission reduction is 146 tons-equivalent CO_2/year. Since there are 435 indoor ice rinks in Quebec and several thousand in North America, it would be interesting to improve their energy efficiency while preserving good ice quality and comfort for the spectators. To achieve this objective precise methods for the calculation of the corresponding loads are necessary.

Three different methods are commonly used for the thermal modeling of buildings: the Nodal method, Computational Fluid Dynamics (CFD) and the Zonal method. The first one is the simplest and is implemented by representing the inside volume of the entire building, or of large parts thereof, by a single node. Therefore the Nodal method does not necessitate an important computing capacity but, on the other hand, it does not provide a detailed description of the indoor conditions. The application of such a model to ice rinks (or other large buildings without internal partitions such as supermarkets or gymnasia) can lead to very imprecise results because the mass fluxes between different parts of the inside volume are extremely difficult to estimate.

On the other hand, the modeling of an ice rink for CFD calculations is very complex due firstly to their size and geometry, and secondly to the variety of the heat and mass transfer mechanisms which take place therein. Thus, the model must take into account heat transfer through the envelope and heat gains from the ground, air motion within the building due to forced and natural convection, vapour diffusion and condensation on the ice sheet, heat transfer by radiation between all internal surfaces, conduction in the ice and floor as well as heat generation by the lights, the resurfacing operations, the refrigeration system, etc. Hence, the literature review revealed few CFD studies for large buildings such as ice rinks. Jones and

Whittle (1992) described the status and capabilities of CFD for building air flow prediction while Jian and Chen (1995) as well as Yang et al. (2000) used a CFD code to evaluate air quality in large ventilated enclosures. However, these studies did not calculate heating and refrigeration loads and ignored the interaction between the indoor and outdoor environments.

More recently Bellache et al. (2005a, 2005b) have carried out numerical simulations in 2D and steady state conditions using a CFD code which predicts velocity, temperature and absolute humidity distributions in an indoor ice rink with ventilation and heating. The CFD code also calculates the heat fluxes toward the ice due to convection from the air, to condensation of vapour and to radiation from the walls and ceiling. However, these calculations did not take into account the contributions of ice resurfacing, system pump work and ground heat to the refrigeration load.

This 2D CFD model was later improved by Bellache et al (2006) by including transient phenomena, heat transfer through the ground and energy gains from lights as well as the effects of resurfacing and dissipation of pump work in the coolant pipes. The ground at a depth of 2 m was assumed to have a constant temperature while the horizontal plane through the centers of the brine pipes was assumed to be an isothermal surface with temperature equal to the average of the supply and return brine temperatures.

Ouzzane et al. (2006) contributed preliminary experimental measurements for a Canadian indoor ice rink which provide a better understanding of its thermal and energy behaviour. These measured values were also used for the verification and calibration of the numerical model developed by Bellache et al. (2006). The main drawback of the CFD approach is that it requires considerable computer memory and CPU time for the simulations. Thus, the transient 2D model by Bellache et al (2006) requires approximately 24 hours of calculations on a modern desktop computer to simulate the response of an ice rink over a period of one day.

An alternative method to CFD, which requires less calculation time and computer memory, was developed by Daoud et al. (2006, 2007, 2008). It combines a zonal airflow model, a radiation model, a humidity transport and condensation model and takes into account resurfacing and occupation. This above ice model (AIM) predicts the heat fluxes through the envelope as well as the temperature and absolute humidity distributions for a 3D transient regime during an entire typical meteorological year. In particular it calculates the heat fluxes

into the ice sheet by convection, radiation and condensation. The temperature below the ice sheet was assumed uniform and constant. The results show a satisfactory agreement with corresponding measurements and CFD calculations.

The present article describes a second part in the development of a global 3D transient model of an ice rink. The Below Ice Model (BIM) was developed using an implicit unidirectional electrical analogy, taking into account the secondary loop and brine movement and the heat gain from the ground (with changing meteorological conditions). The BIM was coupled successfully with the previously mentioned Above Ice Model (AIM). The combined model eliminates the assumption of constant temperature below the ice sheet used in AIM. Instead the temperature of the brine entering the pipes below the ice sheet must be specified. The combined model evaluates the return brine temperature, the total refrigeration load, the ice surface temperature, the heat gain from ground, as well as the energy consumption of the ventilation system and of the radiant heaters. Parametric studies were undertaken in order to evaluate the impact of the climate, brine inlet temperature, ice thickness and other parameters on the calculated results and their results are presented in the last part of the present paper.

2.2 Description and Modeling

2.2.1 Ice rink description

Figures 2.1 and 2.2 show a schematic representation of the studied ice rink «Camilien Houde» located in Montreal (Canada). The building is 64.2 m long, 41.5 m wide and its height is 9.2 m. The ice surface is 61 m long, 25.9 m wide and is surrounded by a narrow corridor. The space above the stands is heated by 8 radiant heaters (22 kW x 8) which are controlled by a thermostat. Seven inlets supply a stream of ventilation air. Its flow rate is 4270 L/s except during resurfacing of the ice when it is increased to 10384 L/s to evacuate the combustion gases of the resurfacing vehicle. The air exits through 4 outlets on the walls. Heat gains from lighting are 10 W/m^2 above the ice and 5 W/ m^2 above the stands; those due to the presence of the audience are also taken into account while the number of spectators is specified according to a weekly schedule (Bellache et al. (2006), Daoud (2007)). The ice resurfacing takes place several times per day, lasts 12 minutes and is modeled as a 1mm film of hot water at 60 °C. Its

frequency, specified in the schedule mentioned above, is higher in the evenings and weekends. The stands, corridors and boards are also modeled in the AIM.

The ground structure beneath the ice rink is represented in Figure 2.1 and comprises horizontal layers of ice (50 mm), concrete (150 mm), thermal insulation (100 mm), sand (200mm) and, finally, soil. The total depth of this structure included in the calculation domain is 4 m.

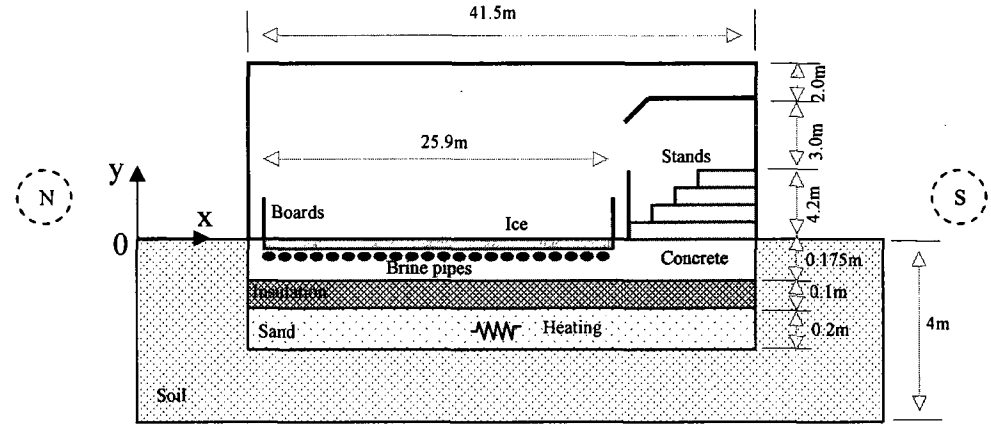

Figure 2.1 Schematic section of the ice rink and the different layers under the ice (not to scale)

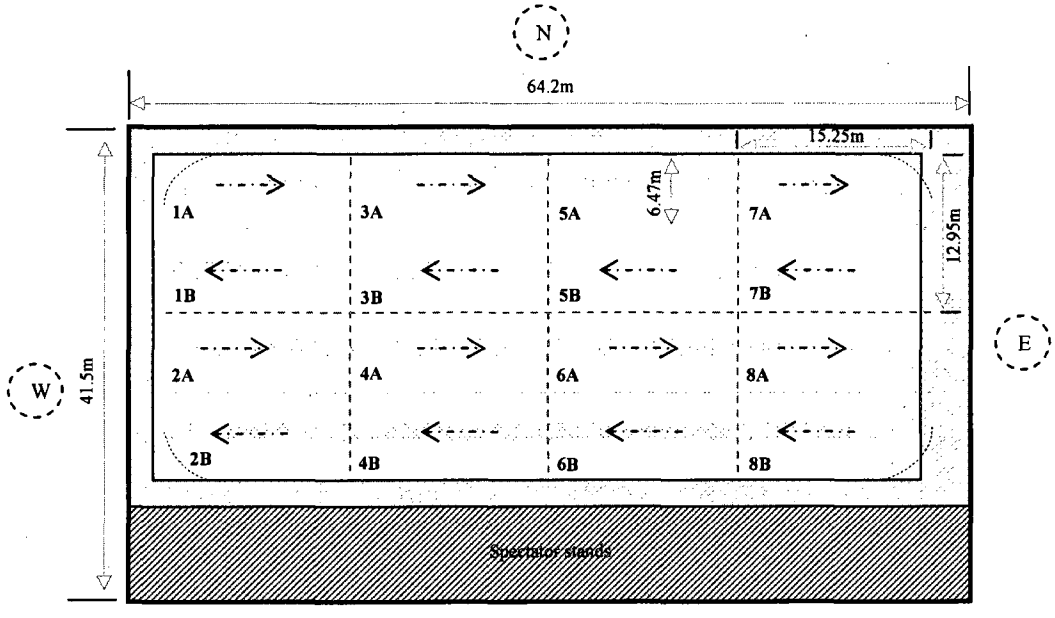

Figure 2.2 Top view of the ice showing the different zones and the flow of the brine

The secondary coolant used to maintain the ice at the desired temperature is calcium chloride brine. It is supplied from a header located at the west end of the ice sheet and circulates in the concrete slab at a depth 57.5 mm below the ice surface within 74 uniformly distributed, four-pass polyethylene tubes (25 mm ID). The spacing between tubes is 87.5 mm. The main collector has an internal diameter of 150 mm. The flow rate of the pump is 28.5 L/s.

An electrical heater of 8 kW is activated in the sand layer when the ground temperature at a depth of 4 m is below 4 °C to prevent freezing under the concrete slab which can cause damage to the underground structure and ice.

2.2.2 Model of air movement and heat exchanges above the ice (AIM)

The air movement and heat exchanges occurring in the rink above the ice surface are simulated using a 3D transient model with 64 zones (Daoud et al. (2006, 2007, 2008)). It consists of six coupled submodels solved with the "onion" method. The first submodel is the energy model which uses the Multizone Building Model (type 56) of TRNSYS (2000). It is based on two relations. The first one expresses energy conservation inside each thermal zone i:

$$\left(Mc_p\right)_i \frac{dT_i}{dt} = (q_{cv}A)_i + \sum_j \dot{m}_{j\to i} c_p T_j \qquad (2.1)$$

while the second expresses energy conservation for each internal surface in contact with the air in the building:

$$q_{cd} = q_{cv} + q_{rd} + q_{cond} + q_{rs} \qquad (2.2)$$

The conductive flux through the wall is evaluated using the transfer functions method while the convection flux between the wall surface and the air inside the building is calculated using a constant heat transfer coefficient (3 W/m^2K). The radiation flux between internal surfaces of the building is provided by a submodel (radiative transfer submodel) based on the Gebhart method (Gebhart (1971)). The condensation flux is attributed to the ice surface when its temperature is below the dew point of the air above it. It is provided by a submodel (humidity transport submodel) which calculates the absolute humidity of the air in every thermal zone inside the building using the following conservation equation:

$$M_{air,i}\frac{d\omega_i}{dt} = \Sigma_{i,j}\dot{m}_{i,j}(\omega_j - \omega_i) + \dot{W}_{g,i} \quad (2.3)$$

Finally, q_{rs} corresponds to the heat flux occurring when the resurfacing operation deposits approximately 0.5 m^3 of water at 60 °C on the ice surface. It is calculated using the equation recommended by ASHRAE (2002).

The airflow $m_{i,j}$ between thermal zones used in equation 2.1 is provided by the zonal airflow submodel. The formulation used expresses the mass flow crossing the common surface between two zones i and j in terms of their pressure difference. Thus, in the case of a vertical interface

$$\dot{m}_{i,j} = \varepsilon_{i,j} \cdot Cd \cdot \sqrt{2\rho_i} \cdot A_{i,j}\left|P_j - P_i\right|^{\frac{1}{2}} \quad (2.4)$$

While in the case of a horizontal interface

$$\dot{m}_{i,j} = \varepsilon_{i,j} \cdot Cd \cdot \sqrt{2\rho_i} \cdot A_{i,j}\left|P_j - P_i - \frac{1}{2}(\rho_i g h_i + \rho_j g h_j)\right|^{\frac{1}{2}} \quad (2.5)$$

The coefficient ε_{ij} is equal to +1 when flow is from zone i to zone j and equal to -1 for flow from zone j to zone i.

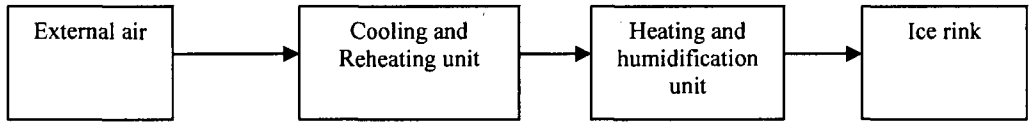

Figure 2.3 Schematic representation of the ventilation system

A new submodel not described in our previous publications Daoud et al. (2006, 2008). is used to simulate the behaviour of the ventilation system. It consists of two units (see figure 2.3). The first one is used for cooling, dehumidifying and reheating the external air when its temperature is above 23 °C while the second unit is for heating and humidifying it when its temperature is below 15 °C. When the temperature of the entering air is between 23 and 15 °C none of the units is in operation unless the humidity level is too high or too low. The humidity controls are such that the relative humidity of the air entering the ice rink is maintained between 20% and 33%. The equations modeling the operation of these two units are the mass and energy conservation equations for a gas-vapour mixture in a steady state, steady flow

process. It should be noted that the results presented here assume that only outdoor air is handled by the ventilation system (no recirculation).

The final submodel evaluates the ventilation effectiveness by calculating the age of the air in every zone of the ice rink.

The data exchange between these six submodels is represented in figure 2.4. It takes place several times at every timestep until the outputs of each submodel vary by less than 10^{-3}.

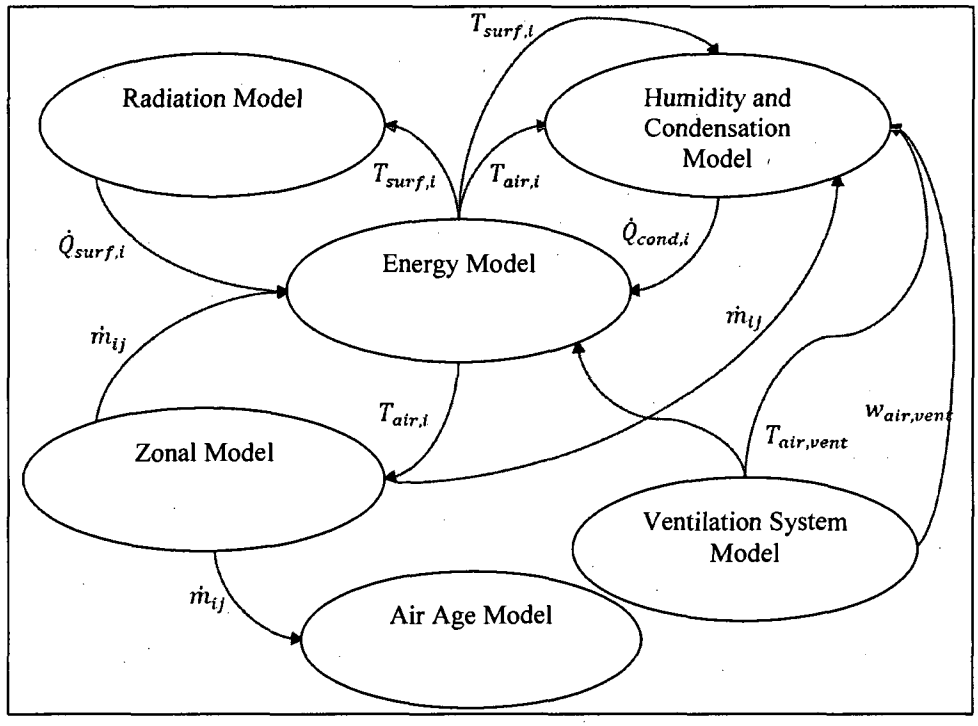

Figure 2.4 Information flow in the Above-Ice Model (AIM)

2.2.3 Below ice modeling (BIM)

The modeling of the ice rink ground structure shown in figures 2.1 and 2.2 is of a substantial nature. Indeed, the concrete slab is one of the most important parts of an ice rink. It forms and maintains the ice by removing heat from it, using a secondary coolant (brine) circulating in the embedded network of pipes.

The BIM is based on the transient one-dimensional conduction equation and the electrical circuit analogy. For that, the ice surface is divided in 8 equal square surfaces (1 to 8) shown in figure 2.2, which correspond to those used by the zonal submodel of the AIM. Each of these surfaces is subdivided into two parts (A and B). The brine flows from west to

east under part A of the eight surfaces and in the opposite direction under part B (see figure 2.2). Thus, the brine enters at 1A or 2A with a constant temperature $T_{b,in}$ and exits at 1B or 2B with a temperature $T_{b,out}$ which is not the same for the North and South brine loops.

Heat transfer between the tubes is neglected since the brine temperature increases by less than 2 °C between inlet and outlet. This justifies the hypothesis of one-dimensional vertical heat transfer between the different layers of the ground structure. However, the BIM takes into consideration heat exchanges between the horizontal layers and the outdoor or the indoor appropriate ground surface as explained below. Therefore, it takes into account three-dimensional phenomena.

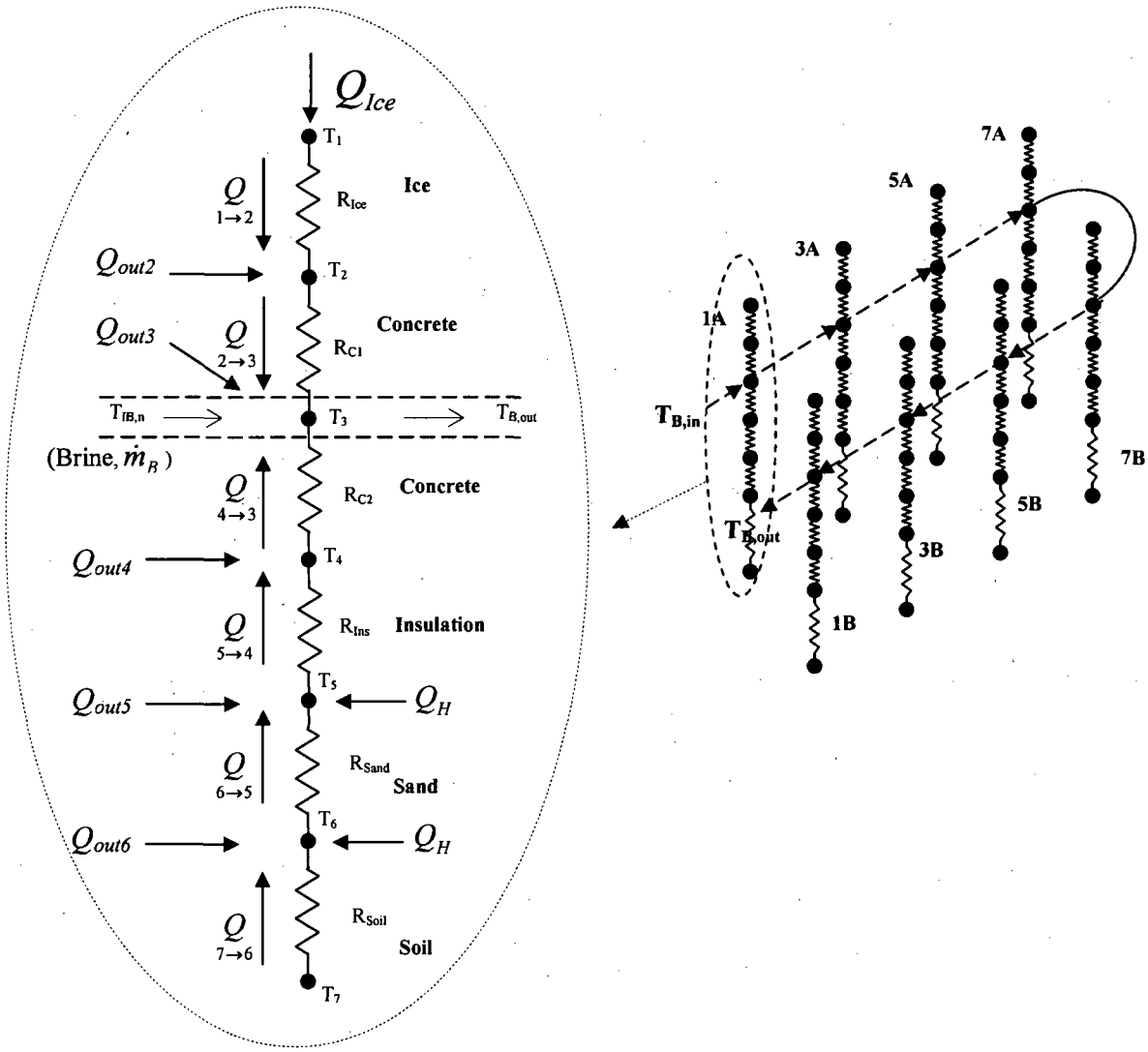

Figure 2.5 Thermal circuit model for below ice structure (1A, 1B ...etc identify zones in figure 2.2)

Figure 2.5 shows the equivalent electrical circuit under one half of the ice. At each of the 16 subdivisions of the ice surface shown in figure 2.2 the heat flux calculated by AIM enters the ice at node 1. The electrical heating in the sand layer is added to nodes 5 and 6. The temperature of node 7 is considered as given by the following correlation based on the deep soil (4 m) temperature data for Montreal (EnergyPlus).

$$T_7 = 3.34 - 4.78\cdot10^{-3}t - 1.97\cdot10^{-7}t^2 + 1.15\cdot10^{-9}t^3 - 2.66\cdot10^{-13}t^4 + 2.15\cdot10^{-17}t^5 - 5.91\cdot10^{-22}t^6 \quad (2.6)$$

Where t is in hours.

The heat exchanges between the horizontal layers and the outdoor or indoor ground surface are added at nodes 2 to 6. They are evaluated using the ASHRAE method (ASHRAE 2005) and are divided in two halves attributed to the circuits under parts A and B. This method uses the formula:

$$Q_{node} = U_{node}\cdot S_{node}\cdot(T_o - T_{node}) \quad (2.7)$$

Where the below-grade average U-factor is given by:

$$U_{node} = \frac{2\cdot k_{soil}}{\pi(z_2 - z_1)} \times \left[\ln\left(z_2 + \frac{2\cdot k_{soil}\cdot R}{\pi}\right) - \ln\left(z_1 + \frac{2\cdot k_{soil}\cdot R}{\pi}\right)\right] \quad (2.8)$$

For nodes 4, 5 and 6 on the north, east and west sides of the ice rink T_o is the temperature of the ground surface outside the ice rink. It is calculated at each time step by the following correlation based on the surface soil temperature data for Montreal (EnergyPlus):

$$T_{gr} = -2.56 - 1.31\cdot10^{-2}t - 6.88\cdot10^{-6}t^2 - 1.79\cdot10^{-10}t^3 - 2.02\cdot10^{-13}t^4 + 2.42\cdot10^{-17}t^5 - 7.93\cdot10^{-22}t^6 \quad (2.9)$$

where t is in hours.

On the south side T_o is taken as constant (equal to the temperature in the changing rooms). On the three other sides, for nodes 2, 3 and 4, T_o is taken as the temperature of the concrete surface in the corridors surrounding the ice surface which is calculated by the AIM.

The brine enters each subdivision and absorbs the heat coming from nodes 2 and 4. Its temperature therefore increases and it enters the next subdivision where the process is repeated. Each of the 16 subdivisions (parts A and B of surfaces 1 to 8 in figure 2.2) is modeled in the same manner and only the entering brine temperature and the lateral heat exchanges calculated by Eq. 2.7 vary from one to another. Thus there are 7 unknown temperatures under each of the 16 subdivisions (at nodes 1 to 6 and at the brine outlet) or 118 unknown temperatures altogether.

The implicit discretisation of the transient energy balance for each node under each subdivision leads to a system of linear equations which can be represented by the matrix equation

$$A \cdot T = B \tag{2.10}$$

where T is the vector of the seven unknown temperatures. The expressions of the 7x7 matrix A and of the vector B are given in the appendix.

This system of linear equations is solved by inversing matrix A since this direct method is suitable for small-size systems. The solution starts under surface 1A and then continues to 3A, 5A etc. following the direction of flow. The temperature of all the nodes is thus obtained for each of the 16 subdivisions. Then, the temperature of each level below the ice is obtained by averaging the 16 corresponding node temperatures. The final outlet temperature of the brine is calculated by assuming that the two streams from 1B and 2B are mixed adiabatically. The heat rates from the ice to the brine and from the soil to the brine are also evaluated and therefore the total refrigeration load is calculated. A FORTRAN subroutine of this model was incorporated as a new type in TRNSYS (2000).

2.2.4 Coupling of the AIM and BIM

The coupling of the BIM with the AIM was realised using the «Onion» method. Figure 6 shows a schematic representation of the coupling method. During one time step, the BIM calculates the temperature T_2 between the ice and the concrete for each of the 8 zones. It provides them as inputs to the AIM in which they are used as boundary conditions. This

model calculates the 8 total heat fluxes towards the ice and returns them as inputs to the BIM. Several such data exchanges take place until outputs of each model vary by less than 10^{-3}. Then time is incremented and this procedure is repeated.

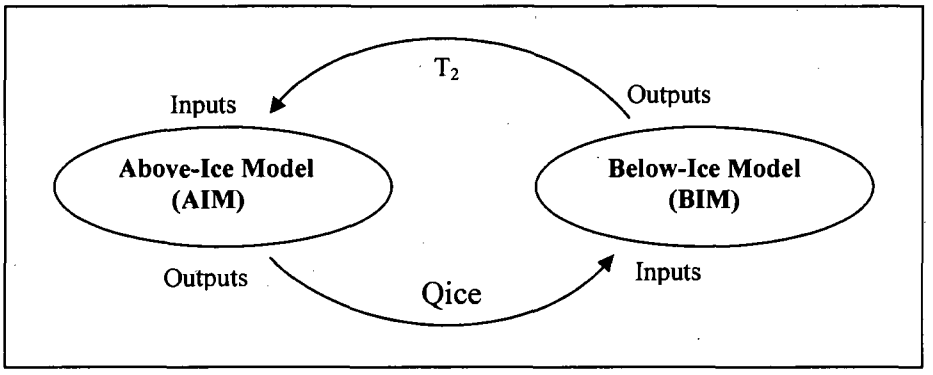

Figure 2.6 Schematic representation of the Onion coupling between AIM and BIM

For the simulations performed in the present project hourly average weather data for a typical meteorological year (temperatures of the air and the ground at 0 m and 4 m depth as well as solar radiation (EnergyPlus)) is used. In order to ensure the periodicity of the results (values at the end of the 365th day must be identical to those at the beginning of the first one) we carried out simulations over 17 months by repeating the meteorological data for January to May and did not consider the results of the initial five months to be sure that the effects of the arbitrary initial values are eliminated.

The choice of time step is based on four considerations. The first is that TRNSYS accepts only time steps of the form 1/N where N is an integer. The second is the duration of resurfacing (12 minutes) which means that the time step should not exceed 0.2 hours. The third is the need to minimize the time required for the calculation of the results over the 17 month period which implies that the time step must be large. Finally, a small time step is necessary to capture more transient details. As a compromise between these considerations we have opted for a time step equal to 0.1 hours. With this choice the entire yearly simulation requires about 80 hours on a personal computer (with an Intel Core 2 Duo 6400 2.13 GHz processor and 2 Go of RAM). This is a considerable improvement over an equivalent CFD two-dimensional simulation which requires 24 hours to calculate the results for a single day (Bellache et al. 2006)

2.3 Model validation

The AIM was successfully validated in previous studies (Daoud et al. (2006, 2007, 2008)) The predictions of the more complete numerical model presented here are validated by comparison with measurements recorded in the Camilien Houde ice rink over relatively short periods in 2005 and 2006 (Ouzzane et al. (2006)). Table 2.1 presents such a comparison of the measured and calculated brine outlet temperature and ice surface temperature. Measured values are the averages of recorded temperatures while calculated values are monthly averages for the typical meteorological year. Although these conditions are not identical, the small seasonal variation of these results makes this comparison acceptable. The agreement between measured and calculated values of these temperatures shows that the proposed model predicts satisfactorily these values. The maximum relative difference is less than 10%, which is acceptable since the simulations did not take into account the refrigeration system which regulates the inlet brine temperature. This difference is principally due to the boundary condition used for the simulation (constant brine inlet temperature $T_{b,in}$= -9°C) and to imprecision of the measurements.

Table 2.1 Comparison between measured and calculated temperatures

	Measured	**Calculated**
Return brine temperature (°C)	-7.3	From -7.8 to -8.0
Ice surface temperature (°C)	From -5.5 to -6.3	From -5.2 to -6.0

Similar agreement has also been established between the measured and calculated values of the heat flux into the ice. The former was obtained by integrating the readings of four heat flux sensors installed under the ice sheet. The corresponding daily mean values for October 1, 2005 are: 94.9 W/m^2, 56.6 W/m^2, 90.6 W/m^2 and 113.0 W/m^2 (Ouzzane et al. (2006)). Disregarding the second sensor which gives significantly lower values than the other three, the mean value of the experimentally measured heat flux is 99.5 W/m^2. On the other hand, the model predicts an average total heat flux of 108 W/m^2 for October which is about 8 % higher than the measurements. In view of the fact that these values do not correspond to identical climate conditions, their agreement is judged to be acceptable.

In view of these results we consider that the proposed model can be used with confidence for the calculation of typical yearly refrigeration loads and for parametric studies which aim to establish the effect of design and operation conditions on these loads.

2.4 Parametric analysis

The analysis in this section starts from a "base case scenario" which corresponds to meteorological conditions for a typical year in Montreal (lat. N 45°47', long. W 73°75'), a constant brine inlet temperature to the slab equal to -9 °C, an ice thickness of 5.08 cm, an under slab insulation thickness equal to 10 cm, a setpoint of 15 °C with a nocturnal set back of 7 °C and an hysteresis of ±0.2 °C for the electronic thermostat, while the underground heating (8 kW) is in operation when the ground temperature at a depth of a 4 m is below 4 °C. The results of this transient simulation are compared with corresponding results obtained by varying the parameters defining the base case scenario one at a time.

2.4.1 Effects of the climate

Results have been calculated for typical meteorological years for the cities of Edmonton (lat. N 53°31', long. W 114°5'), Houston (lat. N 29°58', long. W 95°22') and Pittsburgh (lat. N 40°30', long. W 80°13'). They are compared with those for the base case at Montreal. As indicated by the values in Table 2.2 these climatic conditions vary from very warm and humid during the summer in Houston to very cold and dry in winter in Edmonton.

Table 2.2 Comparison of climatic conditions in the cities under consideration

	Heating Dry Bulb (99 %)	**Cooling Dry Bulb (2%)**	**Mean Coincident Wet Bulb**
Edmonton	-30.5°C	24.0°C	15.7°C
Houston	-0.4°C	33.5°C	24.9°C
Montreal	-21.8°C	25.8°C	19.5°C
Pittsburgh	-14.1°C	28.7°C	20.6°C

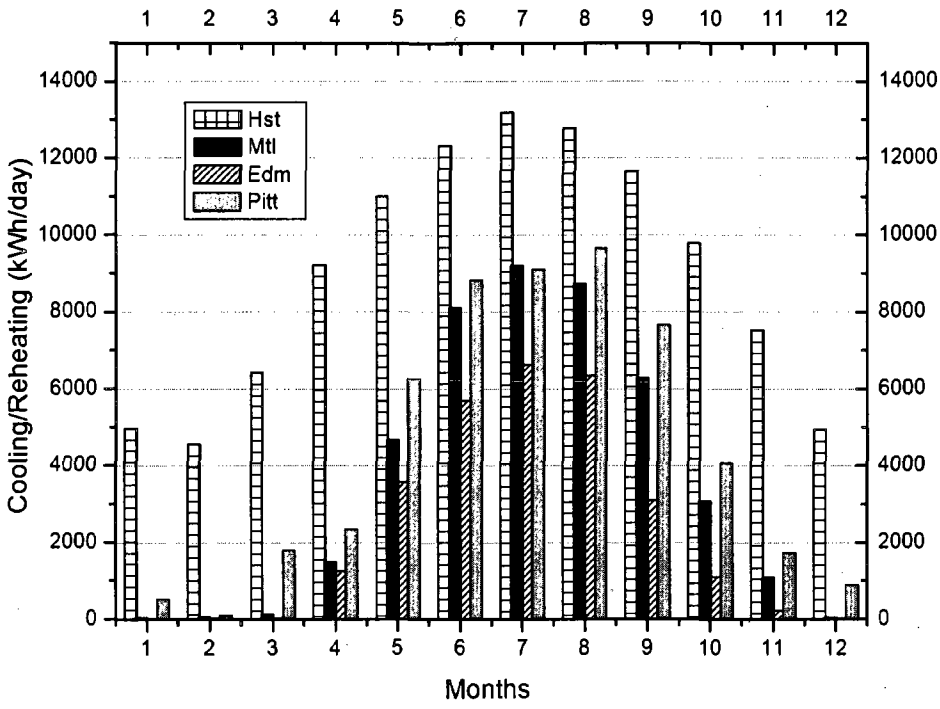

Figure 2.7 Effect of the climate on the cooling and reheating energy consumption of the ventilation system

Figures 2.7 and 2.8 illustrate the effects of the climate on the average daily energy consumption of the ventilation system which, as mentioned before, is constituted of two units (cf. figure 2.3). In particular, figure 2.7 shows that the energy consumption of the first unit, which dehumidifies the ventilation air by cooling and reheating it, is greatest for Houston where it is significant throughout the year. On the other hand, for the other three cities this quantity is essentially zero during the winter months but becomes important during the summer. The seasonal variation of this quantity as well as its relative magnitude between the four cities under consideration is consistent with the meteorological data of table 2.2.

The same is true for the results in figure 2.8 which shows the energy consumption of the second unit of the ventilation system. This one heats and humidifies the incoming ventilation air and is therefore high in winter and essentially zero in summer, largest for Edmonton and lowest for Houston. It is interesting to note that the peak energy consumption for cooling-reheating is for every city higher than the one for heating-humidification.

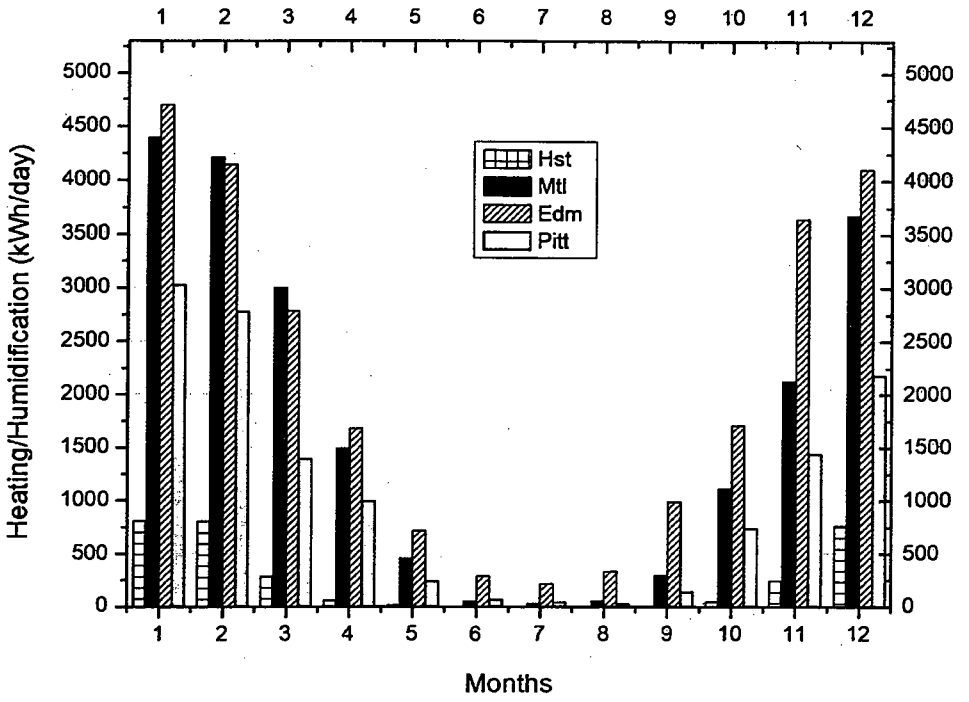

Figure 2.8 Effect of the climate on the heating and humidification energy consumption of the ventilation system

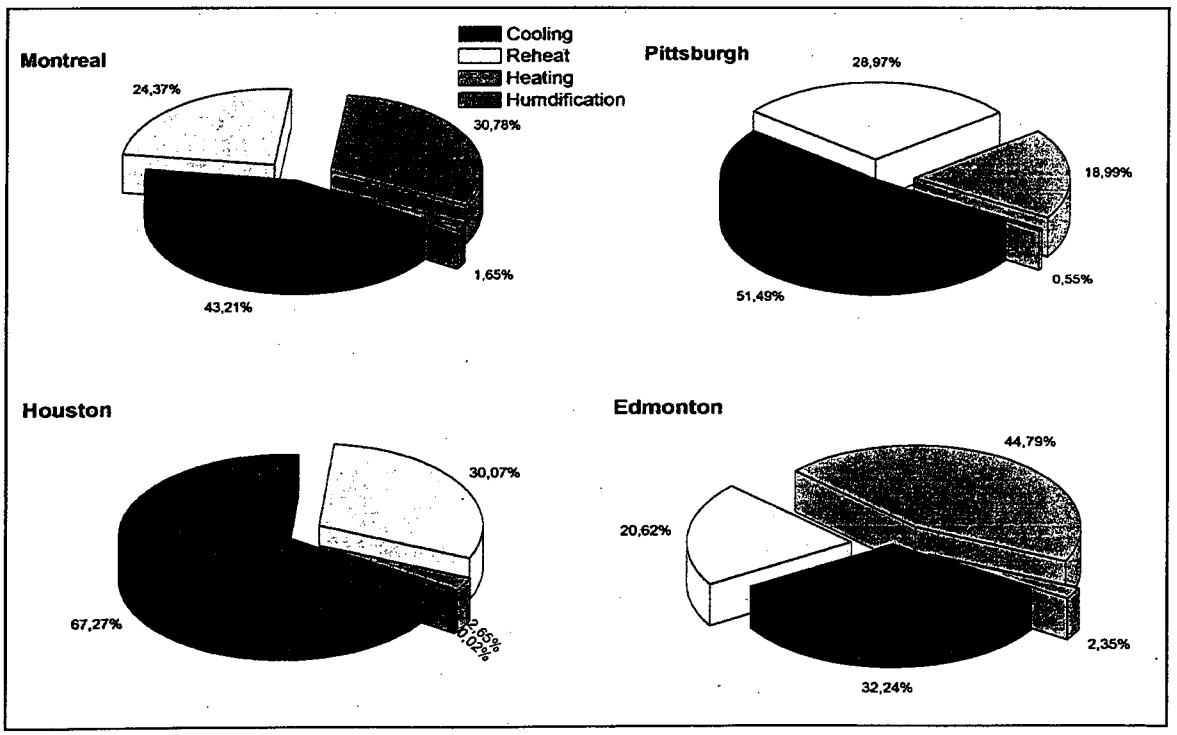

Figure 2.9 Effect of the climate on the annual energy consumption of the ventilation system

The predicted total annual energy consumption of the ventilation system for Edmonton, Houston, Montreal and Pittsburgh is 1278 MWh, 4033 MWh, 1435 MWh and 2228 MWh respectively. The distribution of this total among the four processes is shown in figure 2.9. Cooling uses the largest part in Houston, Pittsburgh and, surprisingly, Montreal while in Edmonton the largest part is used for heating. Humidification requires a very small part of the total energy consumption in all cases.

The impact of the climate on the temperature of the ice surface (IST) is quite small ($\approx$ 1 °C) since this variable is essentially determined by the temperature of the brine which for these simulations is the same throughout the year for all four cities. Therefore the values of IST are not presented here. However, it should be noted that these values are somewhat influenced by the temperature of the air above the ice which depends on whether the radiant heating is on and whether the ventilation air is heated or cooled. Thus the IST for all cities is slightly higher in winter, when heating is required, than in summer, when the ventilation air requires cooling. Similarly, the IST during the summer is a little bit higher in Edmonton than in Houston since the former city requires much less cooling of the ventilation air and necessitates heating of the stands as shown in figure 2.10. This last Figure also shows that the radiant heating of the stands exhibits the expected seasonal behaviour, that it is significantly smaller in Houston and quite important in Edmonton even during the summer. It should be noted that the daily energy consumption of the radiant heaters is for all cities significantly lower than the corresponding values of the ventilation system (sum of consumption shown in figures 2.7 and 2.8).

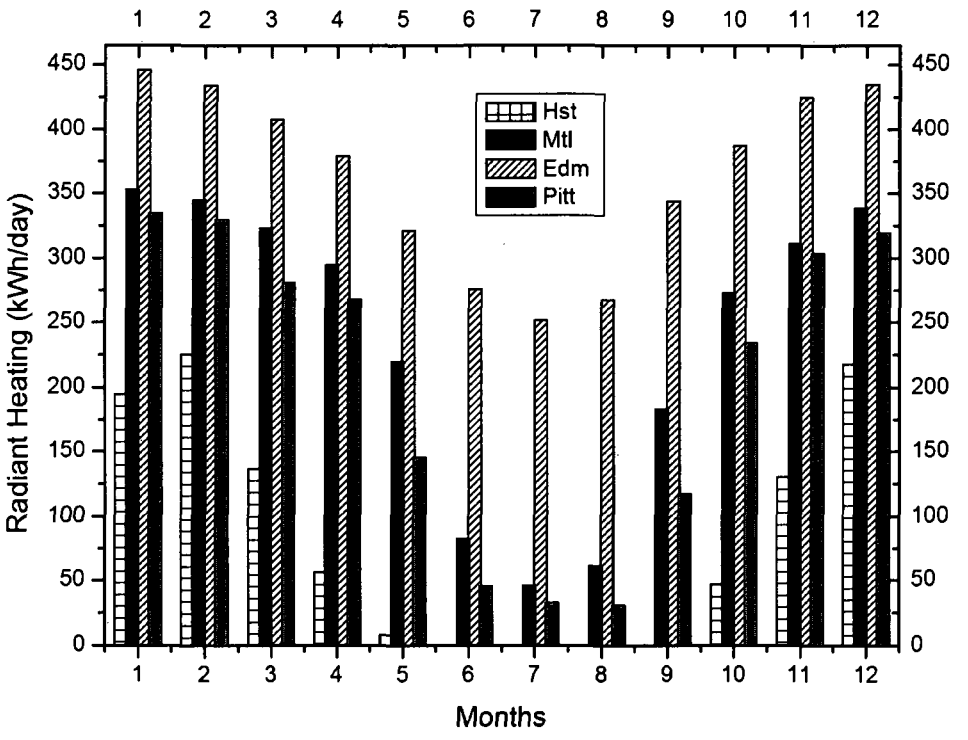

Figure 2.10 Effect of the climate on the energy consumption of the radiant heating

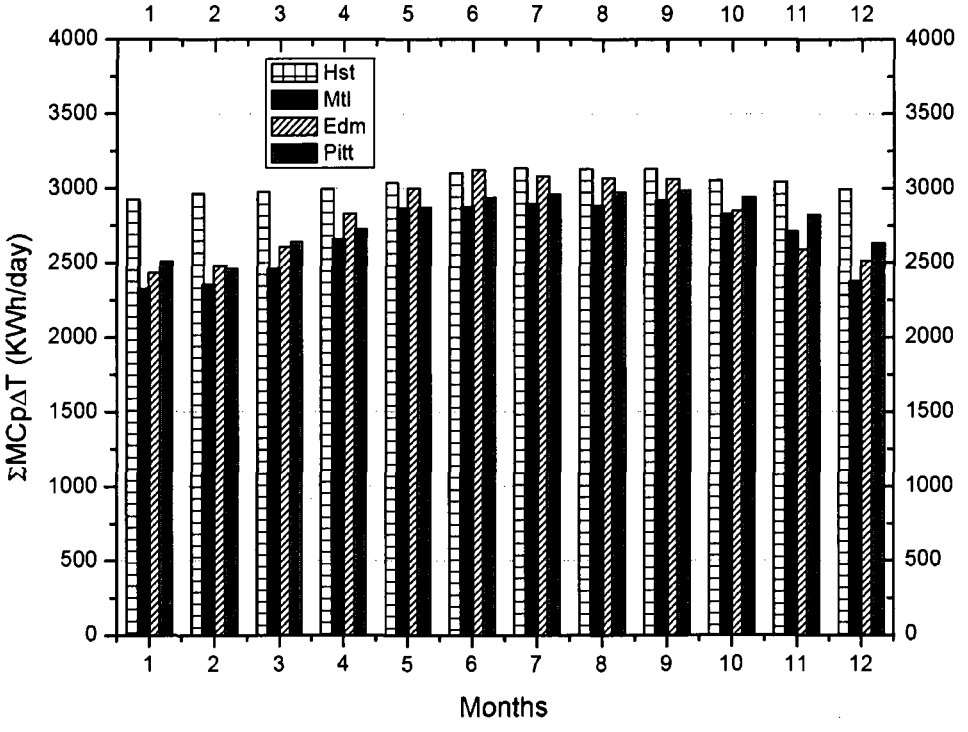

Figure 2.11 Effect of the climate on the refrigeration load

Figure 2.11 shows the influence of the climate on the refrigeration load, i.e. on the sum of the heat reaching the brine from the ice and from the ground. This quantity is greatest for Houston where the seasonal variation is also the least pronounced. This result is consistent with the climatic conditions which signify that the envelope and indoor air are warmer in Houston and that, therefore, heat fluxes towards the ice by both radiation and convection are also higher in this city. Furthermore, because the humidity is higher in Houston the corresponding heat flux due to condensation of water vapour on the ice is also higher in this city. The combination of all these effects explains the results shown in this figure.

Table 2.3 Annual energy consumption of different systems and annual refrigeration load for each city (MWh)

	Annual refrigeration load	Annual energy consumption of different systems					
		Ventilation system	Radiant heating	Underground heating	Lighting	Brine pump	Total
Edmonton	1023	1278	133	40.4	148.7	98.1	1698.2
Houston	1110	4033	30	0	148.7	98.1	4309.8
Montreal	979	1435	86	30.1	148.7	98.1	1797.9
Pittsburgh	1018	2228	74	0	148.7	98.1	2548.8

Table 2.3 compares the annual refrigeration load and the corresponding energy consumption of the different systems for each city. It confirms the fact that the refrigeration load is greatest for Houston and shows that this quantity is always smaller than the energy consumption by the ventilation system. It is important to note that the refrigeration load does not vary significantly (less than 7.5% of the average value) between these four locations despite their very different climates. This is attributed to the fact that the indoor conditions are quite similar due to the controls on the ventilation system and the radiant heaters. However, it is expected that the energy consumption of the refrigeration system will be higher in locations with warm climates since the condensation temperature and pressure will be higher than in locations with cold climates.

Table 2.3 also shows that the energy consumed by the lights and the brine pump does not depend on the climate in accordance with the modeling assumptions. Lighting consumes more energy than the radiant heaters for each of the four locations under consideration while

the same is true for the energy used by the brine pump in three of the four cities. The greatest and smallest contributors to the total energy consumption are the ventilation system and the underground heater respectively for each of the four cities under consideration. Finally, the total annual energy consumption is highest, by a considerable margin, in Houston (where summer operation requires considerable quantities of energy for cooling and dehumidification) and lowest in Edmonton.

Table 2.4 Monthly underground electrical heating for each city (MWh)

	Jan	Feb	Mar	Apr	May	Jun	Jul	Aug	Sep	Oct	Nov	Dec
Edmonton	5.8	5.8	5.8	5.8	5.8	3.9	Off	Off	Off	Off	1.7	5.8
Montreal	5.8	5.8	5.8	5.8	4.8	Off	Off	Off	Off	Off	Off	2.1
Pittsburgh	Off	Off	Off	Off	Off	Off	Off	Off	Off	Off	Off	Off
Houston	Off	Off	Off	Off	Off	Off	Off	Off	Off	Off	Off	Off

Table 2.4 shows the energy consumption by the underground heater which is activated to avoid freezing and heaving of the ground under the concrete slab. Its operation is not at all necessary in the case of the warmer climates (Houston and Pittsburgh) while in Edmonton and Montreal it is in operation for approximately 7 and 5 months respectively.

2.4.2 Effects of the hysteresis of the thermostat

The influence of this parameter is established by comparing the results for an electronic thermostat with a hysteresis of ±0.2 °C with those for a conventional bimetallic thermostat with a hysteresis of ±1.5 °C. The set point is 15 °C in both cases.

Figure 2.12 shows that the refrigeration load is always higher in the case of the electronic thermostat. The difference varies from approximately 125 kWh/day in summer to 200 kWh/day in winter. This result can be explained by the fact that the radiant heating is turned on more frequently with an electronic thermostat in order to maintain the temperature in the zone occupied by the spectators at (15 ± 0.2) °C; therefore the corresponding average air and envelope temperatures are slightly higher and result in increased convective and radiative fluxes towards the ice. However, the energy savings associated with the conventional thermostat are achieved at the expense of the spectators comfort since in that case the air temperature above the stands oscillates between 13.5 °C and 16.5 °C. The smaller difference

in summer energy consumption between the two cases under consideration is due to the fact that the radiant heating load is greatly reduced during these warm months.

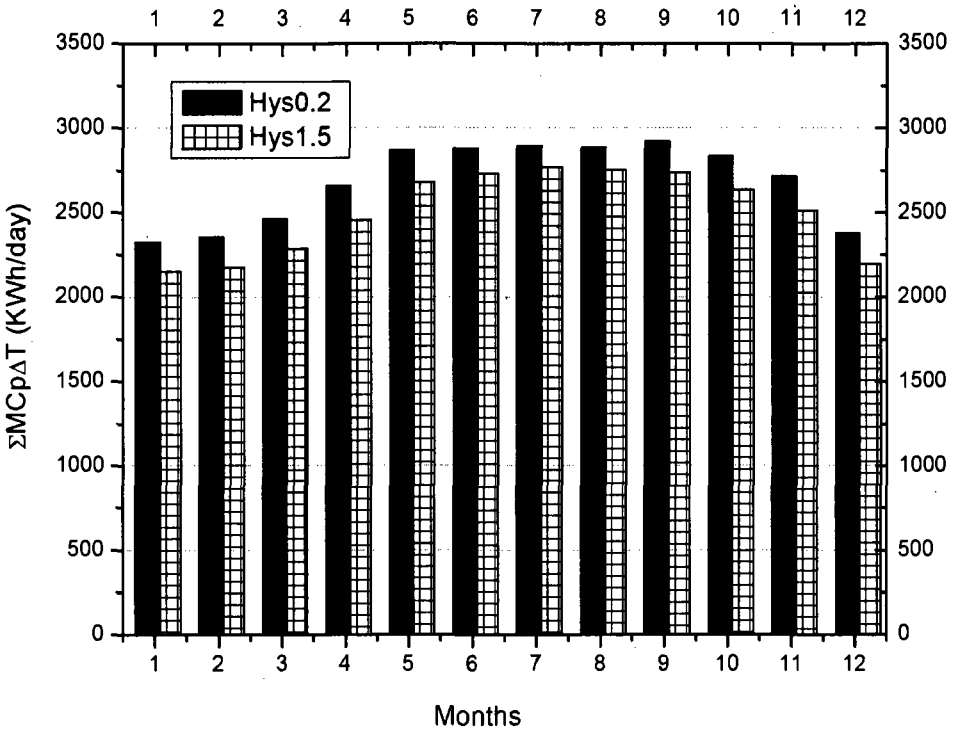

Figure 2.12 Effect of the thermostat hysteresis on the refrigeration load

It should also be noted that the type of thermostat influences the ice temperature, i.e. its quality. Thus the temperature of the ice surface is higher for the base case (electronic thermostat) by approximately 0.25 °C in winter and 0.15 °C in summer.

2.4.3 Effect of the nocturnal set back

Two cases are compared in this section. The first one is the base case in which the thermostat controlling the radiant heating elements is set to 15 °C during the day and 7 °C during the unoccupied night hours, while in second case the thermostat is set to 15 °C throughout the day.

Figure 2.13 shows that the use of a thermostat with nocturnal set back (base case) reduces the refrigeration load. However, this reduction is very small (it varies from 25

kWh/day during the winter to 50kWh/day during the summer). It is due to the decrease of the operation time of the radiant heating elements and the corresponding reduction of the air and envelope temperatures which in turn lower the convective and radiative fluxes towards the ice. The corresponding effect on the IST is insignificant (reduction of 0.1 °C when nocturnal set back is used) since these flux reductions are small compared to their respective values. Finally, it is important to note that the heat flux from the ground to the brine is totally unaffected by the use, or not, of the nocturnal set back since the conditions below the concrete slab are independent of those prevailing within the ice rink.

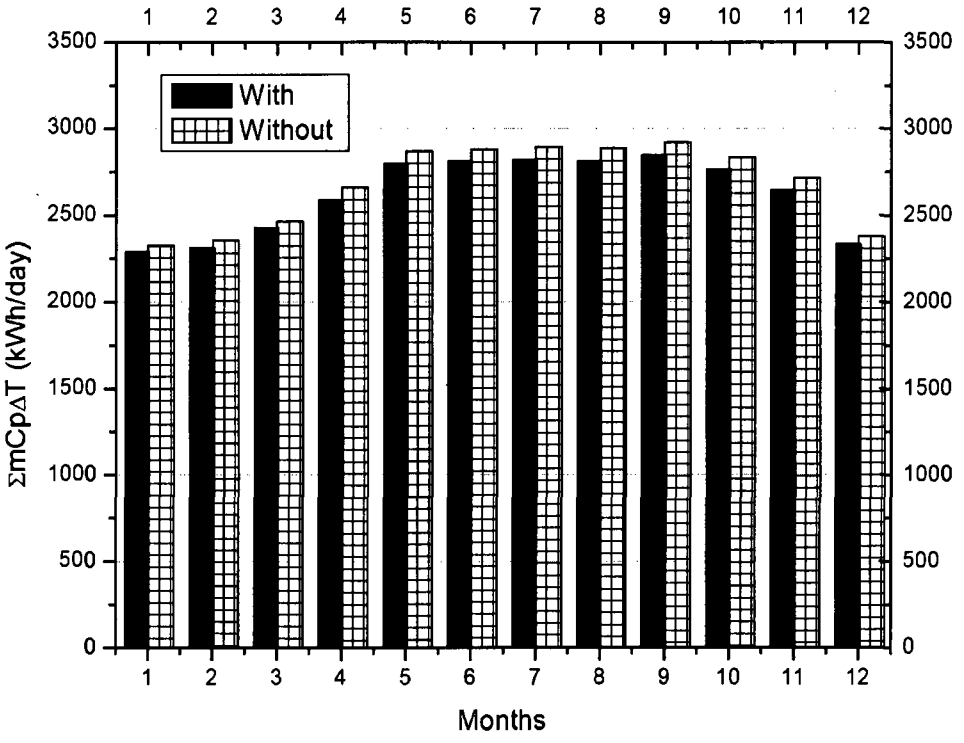

Figure 2.13 Effect of the nocturnal set back on the refrigeration load

2.3.4 Effect of the brine inlet temperature

Three different constant brine inlet temperature were used for this study ($T_{b,in}$ = -8, -9 and -10 °C). Figure 2.14 shows that the refrigeration load increases when the inlet brine temperature decreases. The increase is about 100 kWh/day for each decrease of $T_{b,in}$ by 1 °C. This behaviour is qualitatively logical since the brine acts as a heat sink while the conditions

of the heat sources above and below the concrete slab remain the same for these three simulations.

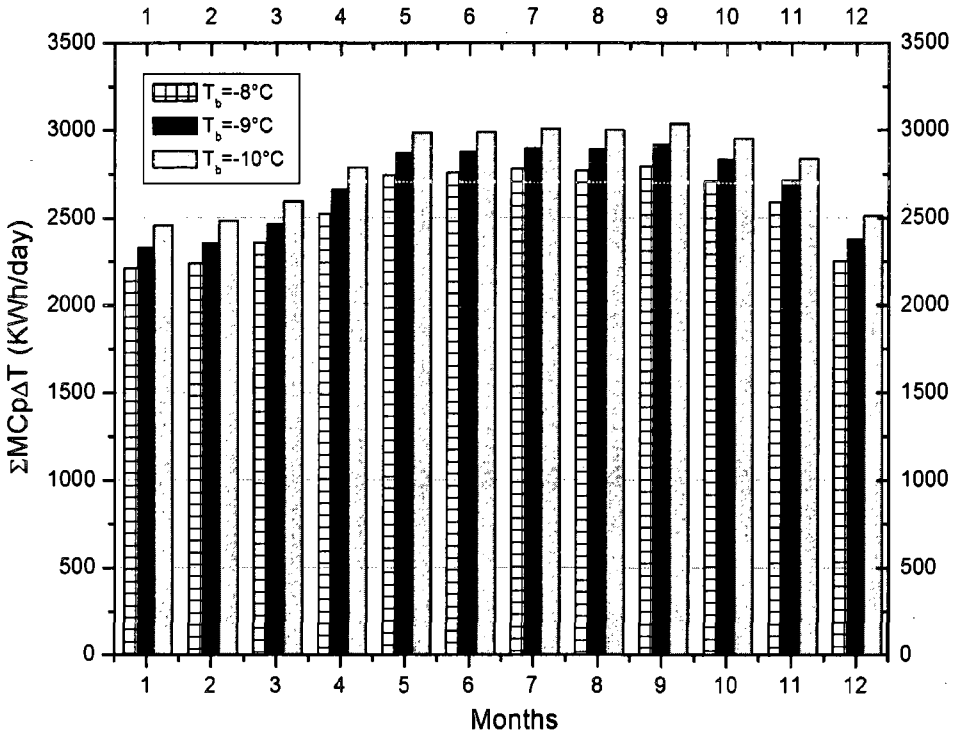

Figure 2.14 Effect of the brine inlet temperature on the refrigeration load

A ±1 °C increase or decrease of the inlet brine temperature causes respectively an augmentation or diminution of ±0.8 °C of the ice surface temperature, for all months of the year. An analogous observation can be made for the outlet brine temperature which increases or decreases by the same amount as the inlet brine temperature.

2.4.5 Effect of the ice thickness

Figure 2.15 shows that the refrigeration load decreases slightly with the increase of the ice thickness. It is reduced by 8 to 10 % when the ice thickness triples (from 2.54 to 7.62cm). This is due to the corresponding increase of the thermal resistance of the ice sheet which also causes a small increase of the IST (ice surface temperature). The increase of the latter is greater in summer due to the augmentation of the convection and radiation fluxes during this warm season.

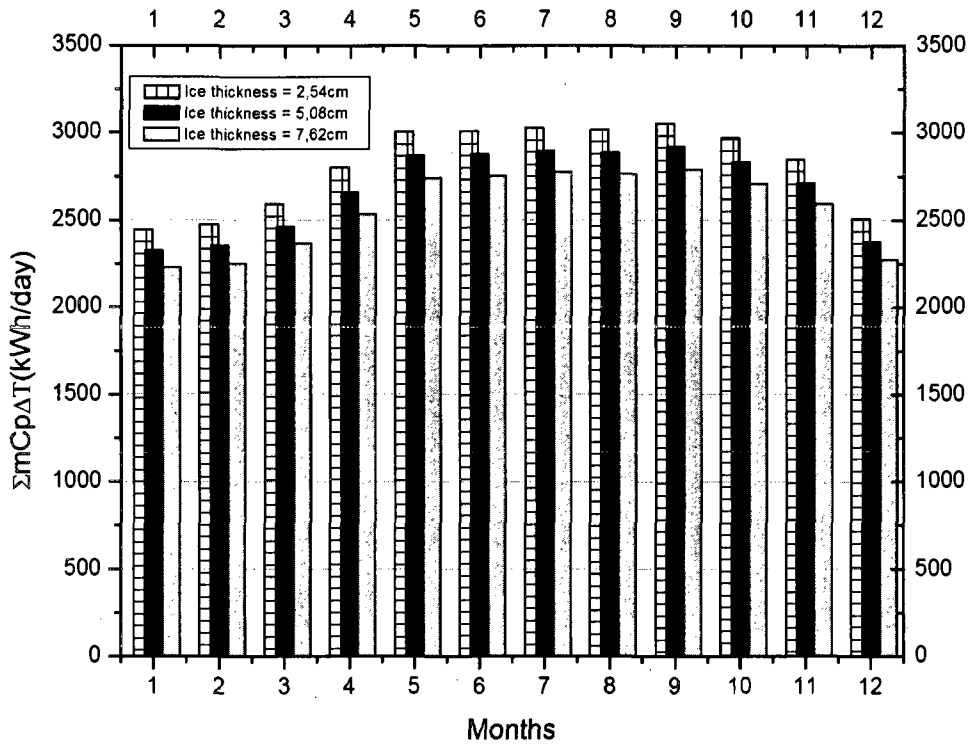

Figure 2.15 Effect of the ice thickness on the refrigeration load

Furthermore, tables 2.5 and 2.6 show that, when the ice thickness is increased by 5 cm, the temperature difference between the ice surface and the brine increases by 14% (from 2.8 °C to 3.26 °C) for the month of January and by 18% (from 3.54 °C to 4.17 °C) for the month of July. These results should not be generalised. They have been calculated by fixing the brine inlet temperature and do not necessarily apply to other control strategies (such as, for example, cases where the ice surface temperature is kept constant).

Table 2.5 Effect of the ice thickness on the temperatures of the ice and the brine (Jan)

Ice thickness (cm)	Temperatures (°C) (January)		
	Ice surface	Brine (inlet)	Difference
2.54	-6.20	-9.0	2.8
5.08	-5.97	-9.0	3.03
7.62	-5.74	-9.0	3.26

Table 2.6 Effect of the ice thickness on the temperatures of the ice and the brine (Jul)

Ice thickness (cm)	Temperatures (°C) (July)		
	Ice surface	Brine (inlet)	Difference
2.54	-5.46	-9.0	3.54
5.08	-5.13	-9.0	3.87
7.62	-4.83	-9.0	4.17

2.4.6 Effect of the insulation thickness

Figure 2.16 shows that an increase of the underground insulation thickness from 10 cm to 30 cm reduces the heat rate transferred to the brine pipes from the soil by approximately 25% for all months of the year. It should also be noted that the change of insulation thickness has an insgnificant effect on the heat rate from the ice to the brine pipes. However, the effect of this reduction of the heat rate from the soil on the total refrigeration load is not significant since the former is less than 10% of the latter (cf. figure 2.15). The most important impact of added underground insulation is to reduce the risk of freezing under the concrete slab which can cause heaving and damage to the ice. Figure 2.17 which shows the average temperature of node 5 situated at the sand-insulation interface clearly illustrates this effect. Furthermore, as this insulation thickness is increased the energy consumption of the electrical element in the sand can be reduced without increasing the danger of freezing.

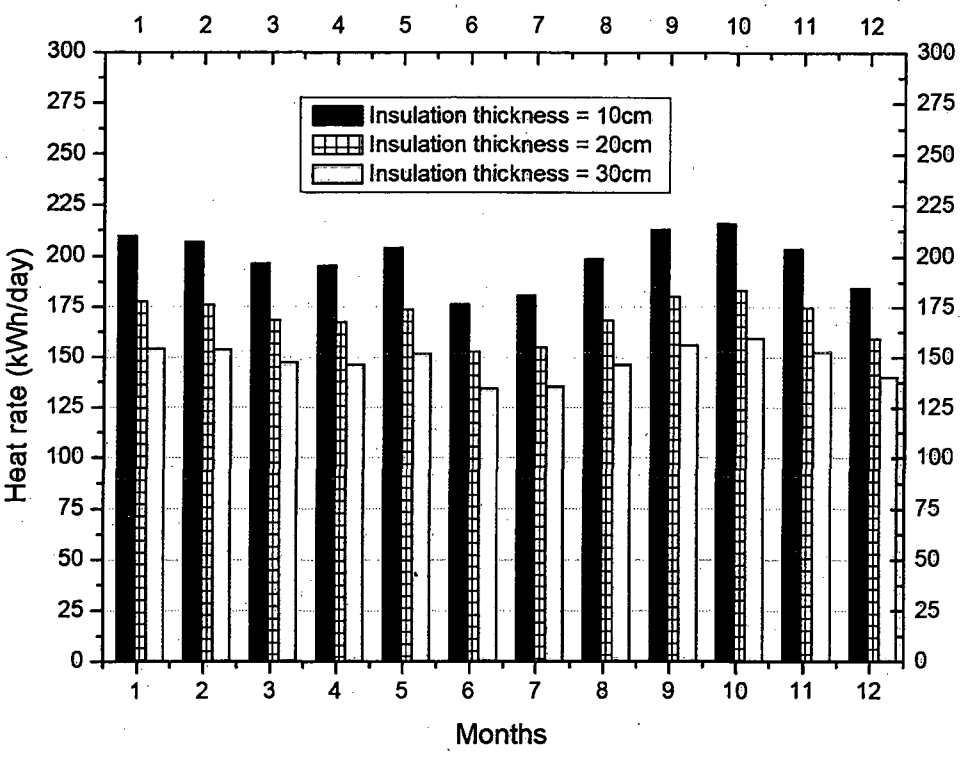

Figure 2.16 Effect of the insulation thickness on the heating rate from the soil

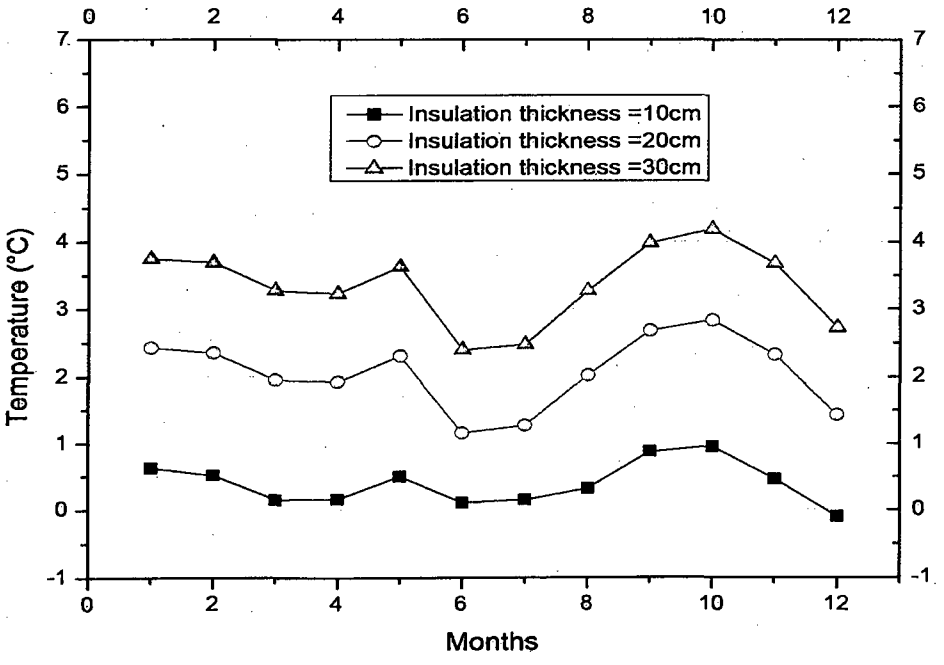

Figure 2.17 Effect of the insulation thickness on the temperature of the insulation-sand interface

2.5 Non-linear correlations of energy loads

This section presents four correlations between the monthly mean value of the energy consumption (in kWh/day) of the different processes taking place in the ventilation system and the corresponding sol-air temperature (in °C) calculated with the expression and parameters proposed by ASHRAE (2001). They are based on numerous simulations carried out at the four selected cities (Montreal, Edmonton, Houston and Pittsburgh).

Cooling load correlation:

$$Q_{Cool} = 283.96 + 189.1 \cdot T_{Sol-Air} + 4.85 \cdot T_{Sol-Air}^2 \quad (2.14a)$$

Reheating load correlation:

$$Q_{Reheat} = 8.63 + 192.58 \cdot T_{Sol-Air} - 2.217 \cdot T_{Sol-Air}^2 \quad (2.14b)$$

Heating load correlation:

$$Q_{Heat} = 1943.1 - 140.23 \cdot T_{Sol-Air} + 1.89 \cdot T_{Sol-Air}^2 \quad (2.14c)$$

Humidification load correlation :

$$Q_{Humid} = 44.9 - 10.95 \cdot T_{Sol-Air} + 0.79 \cdot T_{Sol-Air}^2 \quad (2.14d)$$

Figures 2.18 and 2.19 show that these fairly simple correlations agree quite well with the calculated values. These results also show that the energy consumption by the heating and cooling processes depend heavily on $T_{Sol-Air}$ while those by the reheat and, in particular, humidification processes are less dependent on this parameter.

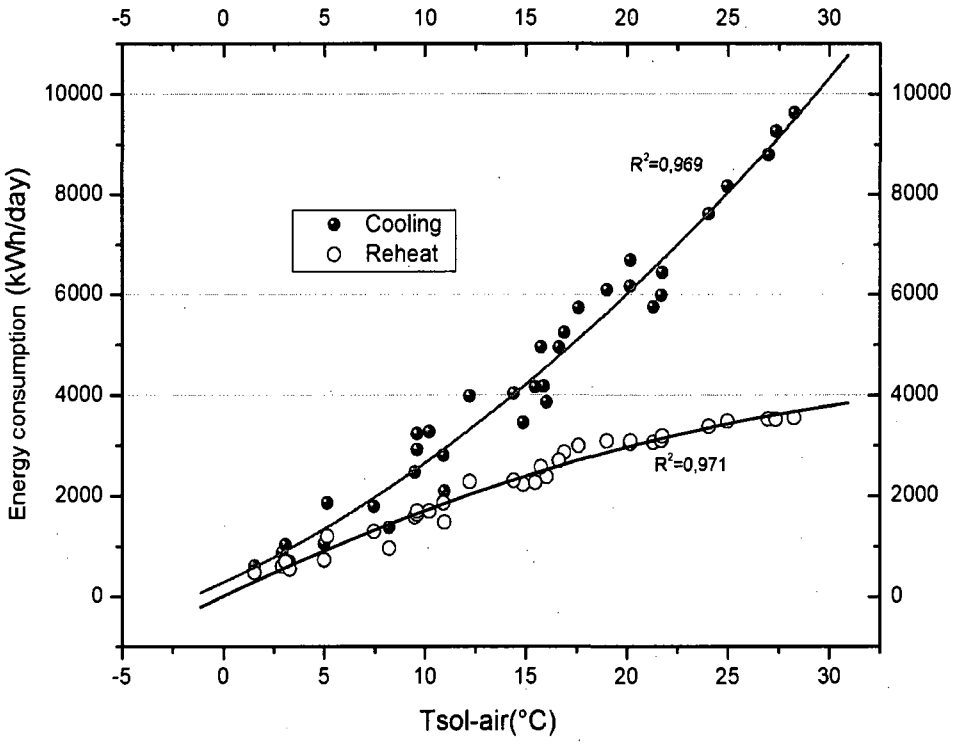

Figure 2.18 Energy consumption of ventilation system (cooling/reheat) vs Sol-Air Temperature

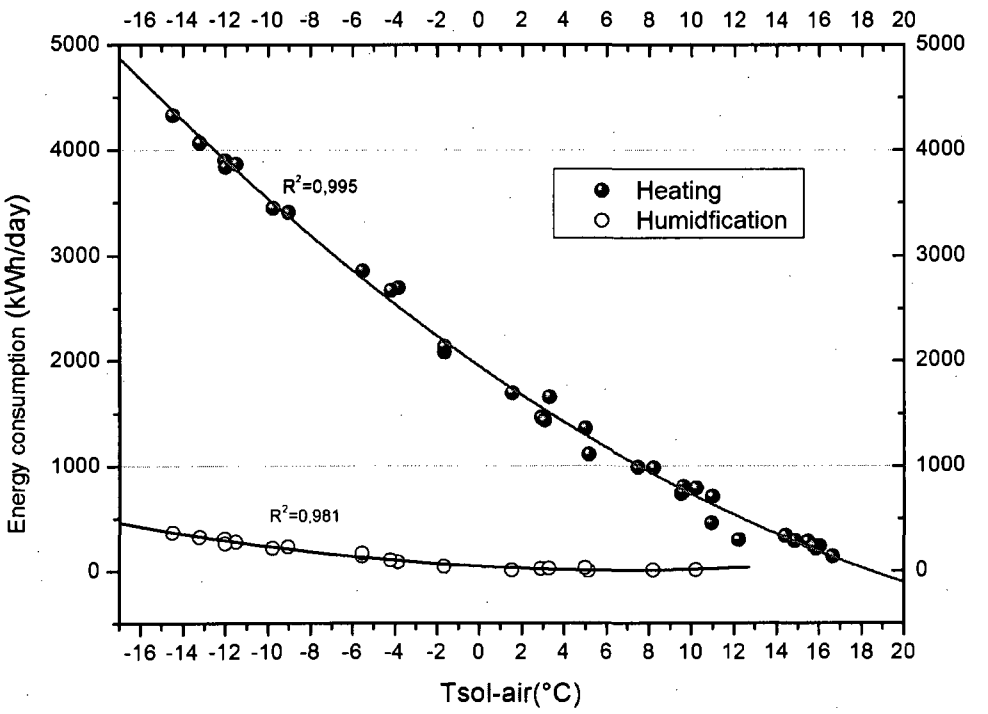

Figure 2.19 Energy consumption of the ventilation system (heating/humidification) vs sol-air temperature

2.6 Conclusion

A transient model which calculates heat transfer through the ground towards the brine pipes imbedded in the concrete slab under the ice of an indoor ice rink has been formulated and coupled with a previously developed one which calculates heat fluxes in the building by convection, radiation and phase changes. The resulting simulation tool has been enriched with subroutines which calculate the energy consumption for heating and humidifying, or cooling and reheating, the ventilation air. After validation with experimental results, this tool was used to evaluate the refrigeration load as well as the energy consumed by the radiant heaters of the stands, each process of the ventilation system,, the lights, the brine pump and the underground electric heater over a typical year at four North American locations (Edmonton, Houston, Montreal, Pittsburgh) with very different meteorological conditions. The results of this analysis show that:

- The annual refrigeration load does not vary significantly (less than ± 7.5 % from the mean value) between these four locations despite their very different climates.
- The annual energy consumption by the ventilation system is significantly influenced by the meteorological conditions; it is highest in hot and humid locations and is always greater than the corresponding refrigeration load.
- The annual energy consumptions by the radiant heaters and by the underground electric heater are very small compared to the refrigeration load even in the coldest of the four cities under consideration.

The main results of the other parametric studies are the following:

- The use of an electronic thermostat with a low hysterisis (± 0.2 °C) rather than a bimetallic one with a high hysteresis (± 1.5 °C) increases the refrigeration load by more than 10 % if the same set point is used in both cases; however the energy savings associated with the bimetallic thermostat are achieved at the expense of the spectator's comfort.
- The use of a thermostat with nocturnal set back results in a small reduction of the refrigeration load.
- A reduction of the brine temperature causes an increase of the refrigeration load and an almost equal reduction of the ice surface temperature.
- An increase of the ice thickness causes a decrease of both the refrigeration load and the ice surface temperature.

- An increase of the underground insulation thickness causes a slight decrease of the refrigeration load and reduces significantly the danger of ground freezing and heaving.

Finally, four correlations expressing the energy consumptions for heating and humidifying, or cooling and reheating, the ventilation air in terms of the sol-air temperature have been proposed.

Appendix

The expressions of the 7x7 matrix A and of the vectors B and T in Eq. 2.10 are:

$$A=\begin{pmatrix} A(1,1) & -1/R_{Ice} & 0 & 0 & 0 & 0 & 0 \\ 1/R_{Ice} & A(2,2) & 1/R_{c1} & 0 & 0 & 0 & 0 \\ 0 & 1/R_{c1} & A(3,3) & 1/R_{c2} & 0 & 0 & -\dot{m}_B \cdot C_{PB} \\ 0 & 0 & 1/R_{c2} & A(4,4) & 1/R_{Ins} & 0 & 0 \\ 0 & 0 & 0 & 1/R_{Ins} & A(5,5) & 1/R_{Sand} & 0 \\ 0 & 0 & 0 & 0 & 1/R_{Sand} & A(6,6) & 0 \\ 0 & 0 & 2 & 0 & 0 & 0 & -1 \end{pmatrix} \quad \text{(A.1)}$$

$$B=\begin{pmatrix} Q_{Ice}+\left((M\cdot Cp)_{eq1}/\Delta t\right)\cdot T_1^p \\ -\frac{1}{2}\cdot U_2\cdot S_2\cdot T_{gr}-\left((M\cdot Cp)_{eq2}/\Delta t\right)\cdot T_2^p \\ -\dot{m}_B\cdot Cp_B\cdot T_{In}-\frac{1}{2}\cdot U_3\cdot S_3\cdot T_{gr}-\left((M\cdot Cp)_{eq3}/\Delta t\right)\cdot T_3^p \\ -\frac{1}{2}\cdot U_4\cdot S_4\cdot T_{gr}-\left((M\cdot Cp)_{eq4}/\Delta t\right)\cdot T_4^p \\ -Q_H-\frac{1}{2}\cdot U_5\cdot S_5\cdot T_{gr}-\left((M\cdot Cp)_{eq5}/\Delta t\right)\cdot T_5^p \\ -Q_H-\frac{1}{2}\cdot U_6\cdot S_6\cdot T_{gr}-\left((M\cdot Cp)_{eq6}/\Delta t\right)\cdot T_6^p-\left(1/R_{Soil}\right)\cdot T_7 \\ T_{in} \end{pmatrix} \quad \text{(A.2)}$$

And $$T=\left(T_1^{p+1}\ T_2^{p+1}\ T_3^{p+1}\ T_4^{p+1}\ T_5^{p+1}\ T_6^{p+1}\ T_{Out}^{P+1}\right) \quad \text{(A.3)}$$

Here the coefficients in Eq. A1 are

$$
\begin{aligned}
A(1,1) &= \left((M \cdot Cp)_{eq1}/\Delta t\right) + 1/R_{Ice} \\
A(2,2) &= -\left(1/R_{Ice} + 1/R_{C1} + \tfrac{1}{2}\cdot U_2 \cdot S_2 + \left((M \cdot Cp)_{eq2}/\Delta t\right)\right) \\
A(3,3) &= -\left(1/R_{C1} + 1/R_{C2} + \tfrac{1}{2}\cdot U_3 \cdot S_3 + \left((M \cdot Cp)_{eq3}/\Delta t\right)\right) \\
A(4,4) &= -\left(1/R_{Ins} + 1/R_{C2} + \tfrac{1}{2}\cdot U_4 \cdot S_4 + \left((M \cdot Cp)_{eq4}/\Delta t\right)\right) \\
A(5,5) &= -\left(1/R_{Sand} + 1/R_{Ins} + \tfrac{1}{2}\cdot U_5 \cdot S_5 + \left((M \cdot Cp)_{eq5}/\Delta t\right)\right) \\
A(6,6) &= -\left(1/R_{Soil} + 1/R_{Sand} + \tfrac{1}{2}\cdot U_6 \cdot S_6 + \left((M \cdot Cp)_{eq6}/\Delta t\right)\right)
\end{aligned}
\qquad \text{(A.4)}
$$

And the equivalent thermal capacity in Eqs. A2 and A4 is calculated as follows:

$$\left(M \cdot C_p\right)_{eq1} = \frac{1}{2}\cdot M_{Ice} \cdot C_{P_{Ice}} \qquad \text{(A.5a)}$$

$$\left(M \cdot C_p\right)_{eq2} = \frac{1}{2}\cdot M_{Ice} \cdot C_{P_{Ice}} + \frac{1}{2}\cdot M_{C1} \cdot C_{P_C} \qquad \text{(A.5b)}$$

$$\left(M \cdot C_p\right)_{eq3} = \frac{1}{2}\cdot M_B \cdot C_{PB} \qquad \text{(A.5c)}$$

$$\left(M \cdot C_p\right)_{eq4} = \frac{1}{2}\cdot M_{C2} \cdot C_{P_C} + \frac{1}{2}\cdot M_{Ins} \cdot C_{P_{Ins}} \qquad \text{(A.5d)}$$

$$\left(M \cdot C_p\right)_{eq5} = \frac{1}{2}\cdot M_{Ins} \cdot C_{P_{Ins}} + \frac{1}{2}\cdot M_{Sand} \cdot C_{P_{Sand}} \qquad \text{(A.5e)}$$

$$\left(M \cdot C_p\right)_{eq6} = \frac{1}{2}\cdot M_{Sand} \cdot C_{P_{Sand}} + \frac{1}{2}\cdot M_{Soil} \cdot C_{P_{Soil}} \qquad \text{(A.5f)}$$

CHAPITRE 3

QUASI-STEADY STATE MODEL OF AN ICE RINK REFRIGERATION SYSTEM

Auteurs et affiliation:

L. SEGHOUANI: étudiant au doctorat, Université de Sherbrooke, Faculté de génie, Département de génie mécanique.

N. GALANIS: professeur, Université de Sherbrooke, Faculté de génie, Département de génie mécanique.

Date d'acceptation: 05 mai 2008

État de l'acceptation: version finale publiée

Revue: Building Simulation: An International Journal

Référence: (Seghouani et Galanis. 2009)

Titre français: Modèle d'un système de réfrigération d'un aréna en régime quasi-permanent.

Résumé :

Dans ce chapitre, un modèle en régime quasi-permanent pour un système de réfrigération s'inspirant de celui de l'aréna Camilien Houde de Montréal a été développé sur la base d'une combinaison de relations thermodynamiques, de corrélations de transfert de chaleur et de relations élaborées à partir de données disponibles dans le catalogue du manufacturier.

Le système étudié comprend cinq compresseurs, cinq condenseurs à air, cinq vannes de détente et 2 évaporateurs de type « tubes et calendre ». Le réfrigérant principal est le R-22 et le fluide secondaire est la saumure qui sort du système à une température de consigne d'environ -9 ° C. Le modèle a été validé par comparaison avec des valeurs mesurées et des données du catalogue du manufacturier.

Il a ensuite été utilisé pour simuler la performance du système de réfrigération sur une année météorologique typique. Les résultats pour une journée représentative incluent notamment, le nombre de compresseurs en fonctionnement à tout moment, leur consommation d'énergie, le COP du cycle et du système, ainsi que la chaleur rejetée par les condenseurs et les débits massique de l'air de refroidissement. Ils montrent que la pression d'évaporation est essentiellement constante tandis que la pression de condensation varie d'environ 1600 à 2000 kPa. Le COP du système quant à lui varie entre 1,9 et 2,5. Les résultats sur une année montrent que la chaleur rejetée lors du changement de phase dans les condenseurs est environ quatre fois plus grande que celle rejetée lors de la désurchauffe et aussi mettent en évidence l'intérêt de la récupération de la chaleur de ces deux processus.

Enfin, le modèle est utilisé pour illustrer les avantages d'une stratégie de contrôle qui limite le nombre maximum de compresseurs fonctionnant simultanément à quatre, au lieu de cinq, lors des fréquentes opérations de resurfaçage de la glace. Cette stratégie se traduit par une diminution de 10% de l'énergie utilisée par les moteurs de compresseurs et de 20% de diminution de la demande de la puissance de pointe. Mais en contre partie durant ces courtes périodes, la température de la saumure augmente à la sortie des évaporateurs d'environ 0,5° C.

Mots clés : Système de réfrigération; échangeurs de chaleurs, Aréna; Charges thermiques; Efficacité énergétique.

Abstract

A quasi-steady model for the refrigeration system of an indoor ice rink was developed based on a combination of thermodynamic relations, heat transfer correlations and data available in the manufacturer's catalogue. The system includes five compressors, rejects heat to the ambient air and uses R-22 to keep a stream of brine at a temperature of approximately -9°C. The model has been validated by comparison with measured values and with data from the manufacturer's catalogue. It was then used to simulate its performance over a typical meteorological year. Results for a representative day include the number of compressors in operation at any given moment, their power consumption, the COP of the cycle and of the system, as well as the heat rejected by the condensers and the corresponding mass flow rate of the cooling air. They show that the evaporation pressure is essentially constant while the condensation pressure varies from about 1600 to 2000 kPa. The COP of the system varies between 1.9 and 2.5. Results for the entire year show that the heat rejected during phase change is approximately four times that due to desuperheating and demonstrates the interest of recovering heat from both processes. Finally, the model is used to illustrate the advantages of a control strategy which limits the maximum number of simultaneously operating compressors to four. This strategy results in a 10% decrease of the energy used by the compressor motors and a 20% decrease of the peak power demand but increases the temperature of the brine at the exit from the chillers by approximately 0.5°C during short periods following the ice resurfacing operations.

Keywords: Refrigeration system; Heat exchangers; Ice rink; Thermal load; Energy efficiency.

Nomenclature

A	Surface (m^2)
A_c	Net cross sectional free-flow area (m^2)
C	Clearance
CF	Correction factor
Cp	Specific heat (kJ/kg.K)
D	Tube diameter (m)
D_h	Hydraulic diameter $(D_h = 4 \cdot A_c / P_W)$ (m)
D_c	Fin collar outside diameter (m)
f	Friction factor
G	Mass velocity $(N_{fan} \cdot \dot{m}_{air} / A_c)$ ($kg/m^2.s$)
Gz	Graetz number $(\mathrm{Re}\,\mathrm{Pr}\,Dh/L)$
h	Heat transfer coefficient ($W/m^2.K$)
i	Specific enthalpy (kJ/kg)
k	Thermal conductivity (W/m.K)
L	Length of condenser tubes (m)
$\dot{m}$	Mass flowrate (kg/s)
n	Polytropic exponent
N_C	Number of compressors in operation
N_{fan}	Number of fans in operation
N_R	Number of tube rows in condenser
Nu	Nusselt number
P	Pressure (Pa)
PD	Piston displacement (m^3/s)
Pr	Prandtl number
P_w	Total wetted perimeter (m)
Q_R	Refrigeration load (kW)
Q_R^*	Refrigeration load per compressor (kW)
Re	Reynolds number
R_f	fouling resistance ($m^2.K/W$)

s	Space between fins (m)
T	Temperature (°C, K)
t	Time (s or hrs)
U	Overall heat transfer coefficient ($W/m^2.K$)
v	Specific volume (m^3/kg)
$\dot{W}$	Power (kW)
x	Quality

Subscript and Abbreviations

1, 1′, 2, 2′, 3′, 3, 4	see figure 2
2p	Two phase region
b	Brine (side of evaporator)
c	Compressor
cd	Condenser
des	Desuperheating
ev	Evaporator
i	Inside
in	Inlet
liq	Liquid
LMTD	Logarithmic mean temperature difference
m	compressor motor
o	Outside
out	Outlet
p	Polytropic
R	Refrigerant
sat	Saturation
sub	Subcooling
sup	Superheating
t	Tube
v	volumetric

Greek letters

Δ	Difference
η_o	Overall surface fins efficiency
η_{vol}	Volumetric efficiency
μ	Dynamic viscosity (Pa.s)
ρ	Density (kg/m^3)
ψ	Dimensionless number

3.1 Introduction

Indoor ice rinks use large quantities of energy and contribute significantly to the increase of greenhouse gases in the atmosphere. A study by Lavoie et al. (2000) estimated that the potential for the reduction of energy consumption and GHG emission for a typical ice rink in Quebec, Canada are 620 MWh/year and 146 tonnes/year (in CO_2 equivalent) respectively. There are several thousand such ice rinks in North America and an important fraction of these potential reductions can be obtained by improving their refrigeration system and its integration with the HVAC system of the building. Therefore the present study was undertaken in order to develop a reliable model for such systems which will then be used to evaluate different strategies for the reduction of energy consumption and GHG emissions.

Two main types of models for refrigeration systems can be found in the literature: the Curve Fitting Model and the Fundamental Model. In the first case the model uses data for each component of the refrigeration system provided in the manufacturer catalogue to generate a mathematical fit between the relevant parameters without any physics contained in the equations. The second type of model, the Fundamental Model, relies on detailed equations for the heat transfer processes and on thermodynamic laws and requires complete information on the configuration and dimensions of the components. One of the main difficulties in the modeling of refrigeration systems is the fact that an exact model for the reciprocating compressor is extremely complex. Complicated flow through valves and heat transfer processes, the presence of a lubricant within the compressor shell, the refrigerant oil mixture concentration and the corresponding thermophysical properties are almost analytically indescribable. For this reason, some authors used and alternative method which falls between the two types of models previously described. Some articles illustrating these approaches are briefly reviewed in the following paragraphs. Most describe steady, or quasi-steady, models that are more appropriate for annual energy calculations.

Fisher & Rice (1983) presented a steady-state model for an air-to-air reciprocating vapour compression heat pump based on thermodynamics principles and heat transfer relations. They used manufacturer maps and curve fitting for the compressor model and developed their model with the objective of only requiring input data that is readily available in manufacturer's catalogues.

Cecchini & Marchal (1991) proposed a simplified numerical code for simulating refrigerating and air-conditioning equipment. This model did not describe in detail the operation of the system's components but characterizes it with a few parameters deduced from experimental data. The simulation calculates heating and cooling capacities and electrical power input for any operating condition.

Stefanuk et al. (1992) developed and used a model to simulate a steady-state water-to-water vapour compression heat pump with superheat control. It was derived entirely from the basic conservation laws of mass, energy, momentum and the equation of state as well as fundamental correlations of heat and mass transfer. It predicts system performance over the full operating range of a heat pump. Good agreement with experimental results was found for the cases studied.

Nyers & Stoyan (1994) modeled the evaporator of a refrigeration system with detailed heat transfer equations. The focus was on the response of the evaporator to system controls. The expansion valve and compressor were modeled using algebraic equations with lumped parameters. Other interesting works using first principles to model the complete refrigeration system have been published by Sami & Dahmani (1996), Xiandong et al. (1997) and Xuejun et al. (1999).

Popovic & Shapiro (1995) described a compressor model which requires eight input quantities and determines mass flow rate, refrigerant outlet state and compressor power with a 10% relative error.

Bourdouxhe et al. (1997, 1994) produced a simulation toolkit for ASHRAE which uses a small number of parameters that are accurate enough for annual energy calculations of building systems. They used a quasi-static approach and assumed an ideal thermodynamic cycle with isothermal refrigerant in the condenser and evaporator.

Williatzen et al. (1998) presented a mathematical model describing the transient phenomena of two-phase flow for evaporators and condensers in a refrigeration cycle with application to a domestic refrigerator. The heat exchanger was separated in three zones (liquid, two-phase and vapour regions).

Svensson (1999) modeled a basic vapour compression system with several simplifying assumptions for the compressor. The condenser was separated in two zones (condensing and

subcooling) while the evaporator was treated as a single zone. The expansion device was modeled as a perfect isenthalpic process maintaining constant superheat.

Sreedharan & Haves (2001) compared three chiller models (including the ASHRAE toolkit model and the DOE-2 chiller model) with experimental data and concluded that all three displayed similar levels of accuracy.

Jin & Spitler (2002) presented a steady-state simulation model for a water-to-water reciprocating vapour compression heat pump, based on thermodynamics principles and heat transfer relations. It includes several parameters that are estimated from catalogue data using a multi-variable optimization and was developed with the objective of only requiring input data that is readily available in manufacturer's catalogues.

The literature review of models of vapour compression equipment by Bendapudi & Braun (2002) includes 40 papers spanning a period of 23 years from different journals and conference proceedings. They present a summary of each of these papers using the same general template which includes eight headings: equipment description, purpose, assumptions, mathematical description, solution technique, applicability, discussion and references. It therefore provides a wealth of information in a simple format which gives a useful overview of the evolution of the modeling approaches applied to such systems.

The principal goal of the present paper is to describe and validate a numerical model of an indoor ice rink refrigeration system, which can be used to simulate its operation, to estimate its annual energy consumption and to analyse different energy saving strategies. The system under consideration includes several compressors, evaporators and condensers while previous publications treated simple systems with only one component of each type. The modeling approach uses a combination of the Fundamental method -especially for heat exchangers where well established correlations for phase changes were used- and the Curve Fitting method coupled with thermodynamics laws for the compressor. The expansion valve is modeled as a perfect isenthalpic device maintaining constant superheat. In future work this model of the refrigeration system will be coupled to the models of the building and the concrete slab with brine pipes described in our previous articles (Daoud & Galanis, 2006; Daoud et al., 2008; Seghouani et al., 2009).

3.2 Refrigeration system description and basic assumptions

The refrigeration system under study is that of the Camilien Houde ice rink situated in Montreal, Canada. The thermal behaviour and refrigeration loads of this building have been analysed previously (Daoud and Galanis, 2006; Daoud et al., 2008; Seghouani et al., 2009).

Figure 3.1 shows a schematic representation of this system which is essentially constituted of:

- Two parallel shell and tubes evaporators with three compartments each, shell diameter 0.5m, evaporator length 1.778m, baffle spacing 0.393m, 342 tubes in two passes, total surface of tubes 49.1m^2, internal and external tube diameters respectively 15.75mm and 19.05mm, tube length 2.4m, pitch 23.812mm, triangular configuration of tubes.
- Five open-drive four-cylinder compressors (Carrier 5H40 model) with maximum speed 1750 rpm, piston displacement 0.04359m^3/s, clearance 0.08.
- Five air-cooled condensers (Larkin RC8, 0768 model) with 2.743m length, 2.038m width, 168 copper tubes in six passes and three rows, internal and external tube diameters respectively 9.525mm and 11.525mm, tube length 2.667m, total surface (tubes + fins) 91.338m^2, number of aluminum fins 390 per meter, fin pitch 2.56mm, fin thickness 0.25mm, height and width of fins 25mm. There are four fans per condenser with a flow rate of 5.89 kg/s per fan.
- Five thermostatic expansion valves (Parker)
- One split-case brine pump: 1200 rpm, 56.7 L/s, 18.7 kW
- Primary refrigerant: R-22
- Secondary refrigerant: calcium chloride brine solution (concentration 20% by mass)

The refrigeration system was initially constituted of six compressors (three per evaporator). However, in February 2005 a compressor was removed from the second chiller. Thus, as shown in figure 3.1, the first chiller is connected to three compressors and the second chiller is connected to two compressors while the brine flow rate is shared between these two chillers.

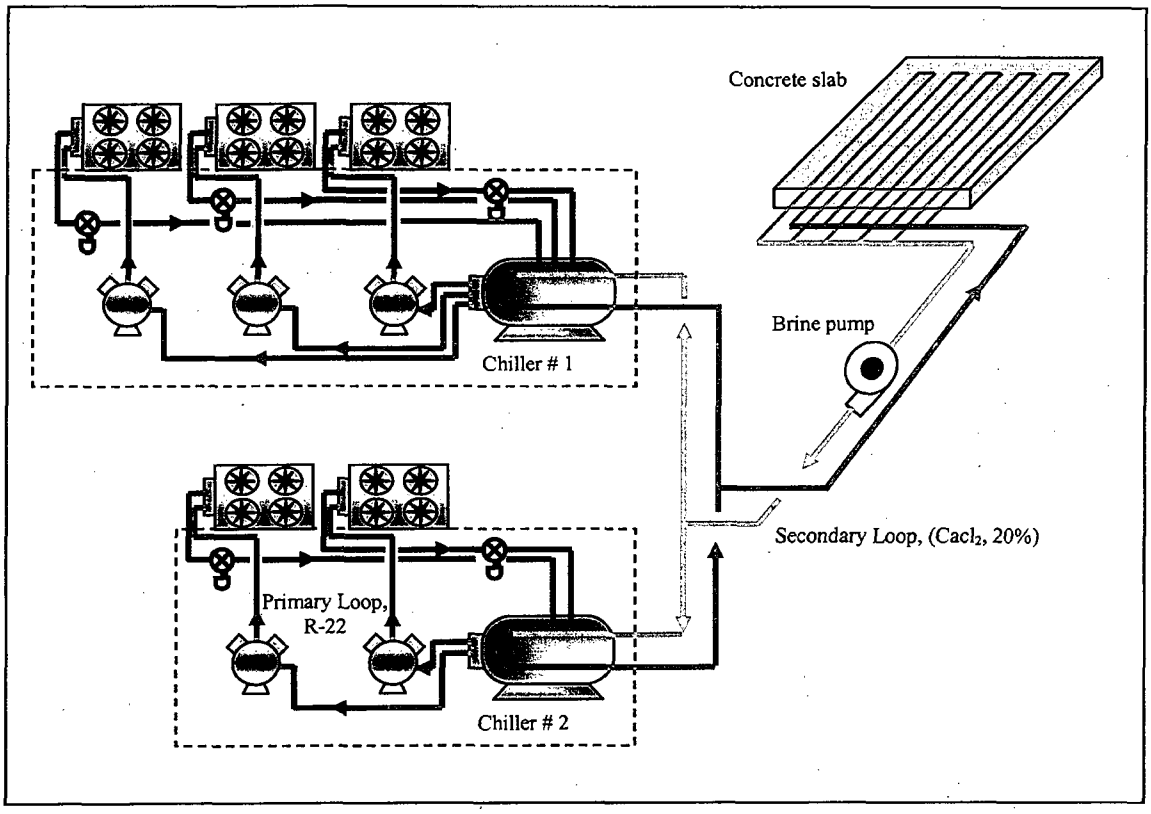

Figure 3.1 Schematic representation of the refrigeration system and the secondary loop (Camilien Houde Ice Rink)

For the simulation it was assumed that the refrigeration system is constituted of five identical units represented schematically in figure 3.2. The characteristics of the compressor and condenser of each of these units are those specified above while the corresponding evaporator surface is equal to that of one of the three compartments in the tube and shell evaporator of figure 3.1. The brine flow rate is always the same (56.7 L/s) and is divided equally between the units in operation at any given instant. The other modeling assumptions are:

- Steady state conditions
- Negligible pressure drop in all the pipes and heat exchangers
- Negligible heat losses to the environment
- Polytropic compression
- Isenthalpic expansion

These assumptions were also used in most of the articles mentioned in the introduction.

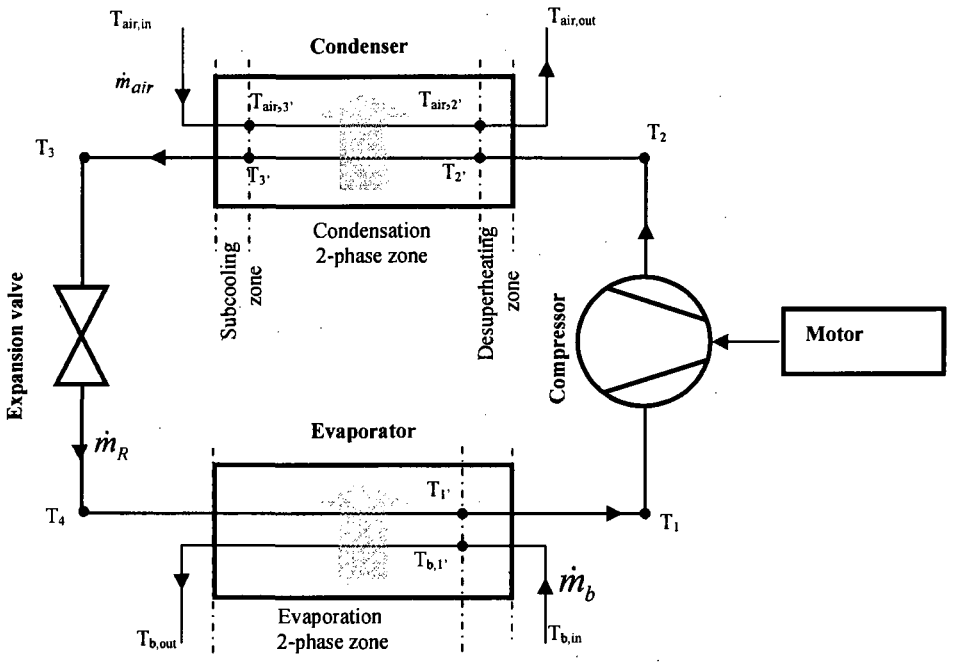

Figure 3.2 Schematic representation of the basic refrigeration unit

Finally, the thermodynamics properties of the brine are taken constant at -8 °C since measurements show that its temperature changes by approximately 1 °C between the inlet and outlet of the evaporator and that it varies by approximately ±1 °C over a period of several months.

Figure 3.3 shows the thermodynamic states of the refrigerant on a temperature-enthalpy diagram as well as the corresponding temperatures of the brine in the evaporator and those of the air in the condenser. The procedure described in the next section is used to calculate the pressure and temperature of the refrigerant at each of the states identified in figure 3.3 as well as the corresponding outlet temperatures of the air and brine every 360 seconds (Δt = 0.1 hr) over an entire year. The relations used to calculate these quantities include the conservation equations for mass and energy, certain correlations derived from the data in the manufacturer's catalogue as well as the time dependent ambient air temperature ($T_{air,in}$), the refrigeration load (Q_R) and the inlet brine temperature ($T_{b,in}$) calculated according to our earlier work (Daoud and Galanis, 2006; Daoud et al., 2008; Seghouani et al., 2009).

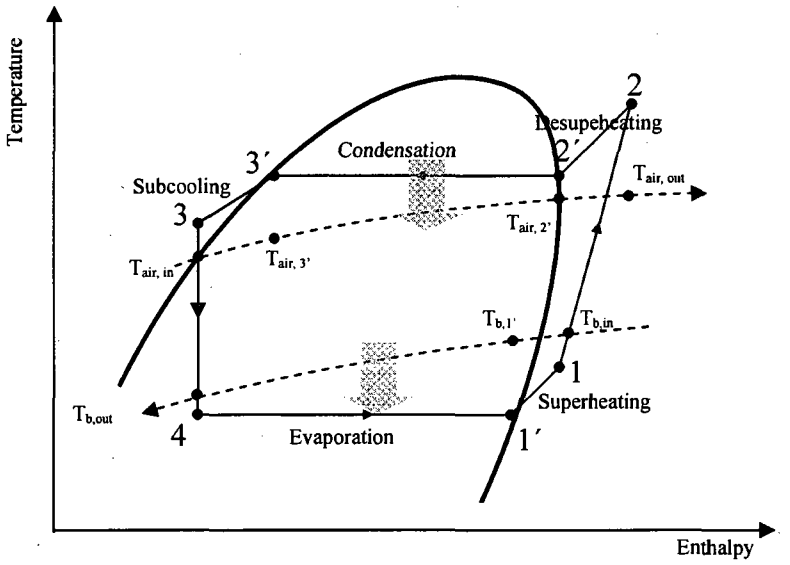

Figure 3.3 Temperature-enthalpy diagram for the basic refrigeration unit

3.3 Modeling procedure

Figure 3.4 shows the adopted procedure for the calculation of the operating conditions of the refrigeration system under study. The refrigerant and physical characteristics defined earlier, the values of subcooling ($T_{3'}$-T_3) and superheating (T_1-$T_{1'}$) as well as the thermophysical properties of the air and the brine (including the desired brine outlet temperature $T_{b,out}$) are specified. Then the code reads from an appropriate file the refrigeration load (Q_R), the brine inlet temperature ($T_{b,in}$) and the outside air temperature ($T_{air,in}$). These last three values are time dependent. The calculation for a given instant t proceeds according to the following steps:

1.a The determination of the number of refrigeration units (cf. figure 3.2) in operation is based on the analysis of measured values which show that the refrigeration load per compressor never exceeds 65kW. Therefore

$$N_C = 1 \quad \text{if} \quad Q_R \leq 65 \text{ kW} \tag{3.1a}$$

$$N_C = 2 \quad \text{if} \quad 65 < Q_R \leq 130 \text{ kW} \tag{3.1b}$$

$$N_C = 3 \quad \text{if} \quad 130 < Q_R \leq 195 \text{ kW} \tag{3.1c}$$

$$N_C = 4 \quad \text{if} \quad 195 < Q_R \leq 260 \text{ kW} \tag{3.1d}$$

$$N_C = 5 \quad \text{if} \quad Q_R > 260 \tag{3.1e}$$

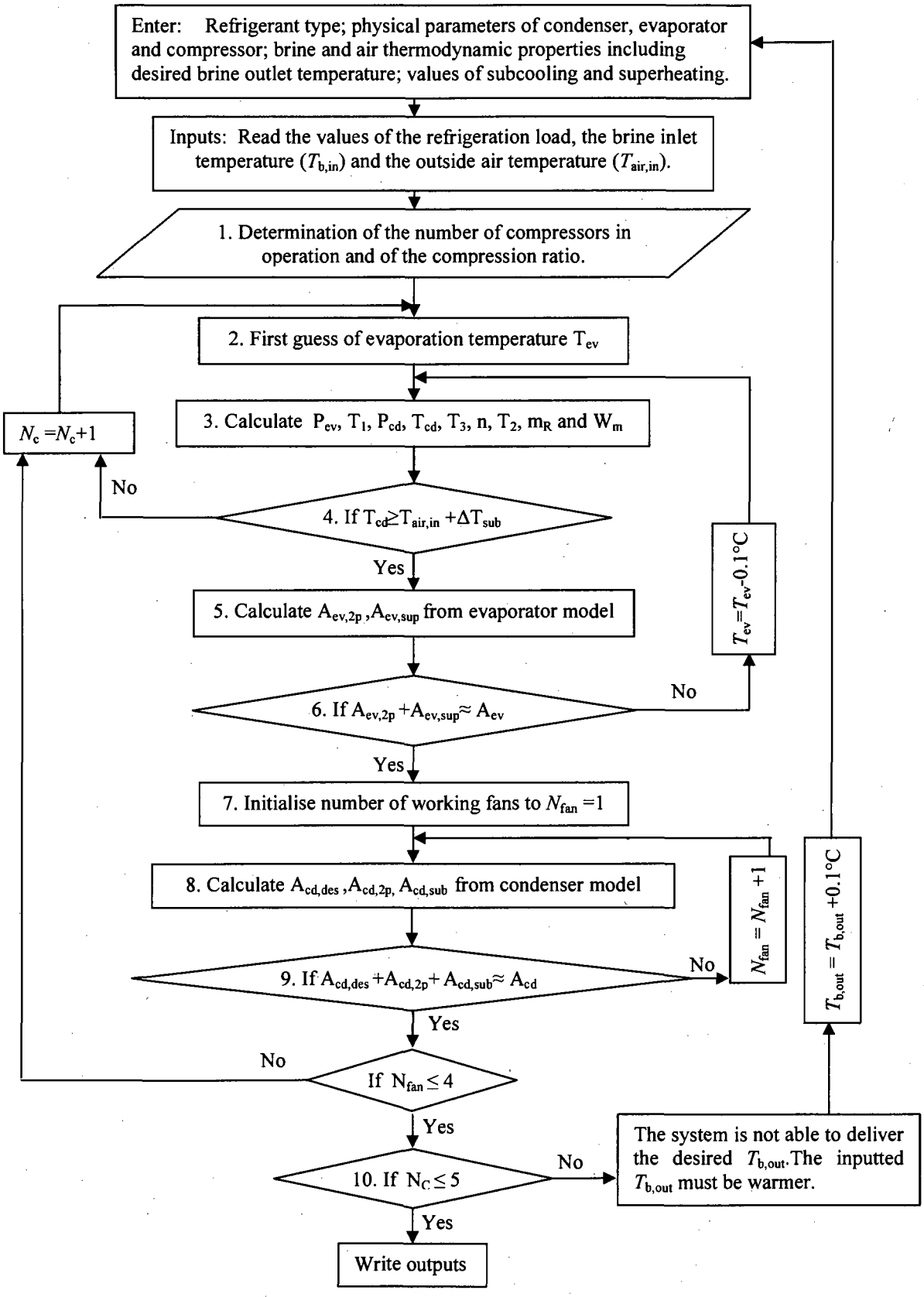

Figure 3.4 Procedure for the calculation of the system's performance

As is the case in all quasi-steady simulations, such an approach can be interpreted in two different ways. The first focuses on a particular instant of the simulation and considers that a compressor which is in operation produces a constant fraction X of its nominal capacity during the entire following timestep. The second focuses on the interval $\Delta t = 0.1$ hr between two consecutive instants of the simulation and considers that the compressor operates during a fraction X of the timestep at its nominal capacity. With both interpretations the quantity of energy transferred during the interval is the same.

1.b The refrigeration load for each unit in operation is therefore

$$Q_R^* = Q_R / N_C \tag{3.2}$$

The value of Q_R^* is then used to determine the compression ratio P_{cd}/P_{ev} from a correlation based on the values in the manufacturer's catalogue (see figure 3.5). The evaporation temperatures for the 18 points included in the figure are between -34 and -18 °C while the condensation temperatures are between 27 and 54 °C. As shown in this figure the correlation returns values of the compression ratio which are within ±12% of the manufacturer's data in 17 out of 18 cases. The mean of the absolute values of the percentage difference between corresponding values of the predicted and catalogue values of P_{cd}/P_{ev} is 6.3% for the 18 cases in figure 3.5. It should be noted that operation of the compressor at the conditions shown in figure 3.5 requires an oil cooler and water-cooled heads.

2. A first value for the evaporation temperature is assumed :

$$T_{ev} = T_{b,in} - \Delta T_{sup} = T_4 = T_{1'} \tag{3.3}$$

where $\Delta T_{sup} = 8°c$

3. The corresponding pressure P_{ev} is then obtained from the refrigerant data using the REFPROP software

$$P_{ev} = f(T_{ev})_{sat} \tag{3.4}$$

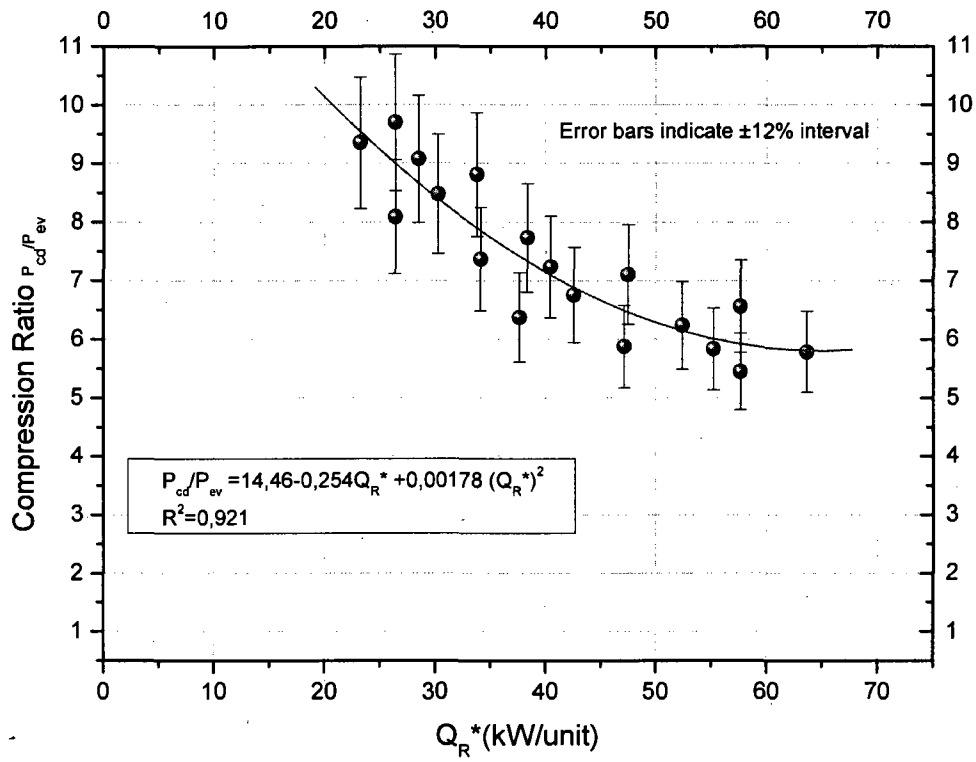

Figure 3.5: Compression ratio versus Load (manufacturer's data and correlation)

The refrigerant temperature at the compressor inlet is

$$T_1 = T_{ev} + \Delta T_{sup} \tag{3.5}$$

The other thermodynamic properties of the refrigerant (enthalpy, entropy, density ...) at states 1 and 1′ are also evaluated using REFPROP.

Furthermore, the corresponding condensation pressure can be evaluated using the known compression ratio (figure 3.5)

$$P_{cd} = \left(14.46 - 0.254 \cdot Q_R^* + 0.00178 \cdot \left(Q_R^*\right)^2\right) \cdot P_{ev} \tag{3.6}$$

While the condensation temperature T_{cd} and the thermodynamic properties of the refrigerant at states 2′ and 3′ are evaluated using REFPROP.

$$T_{cd} = T_{sat}\left(P_{cd}\right) = T_{3'} = T_{2'} \tag{3.7}$$

The temperature at the exit of the condenser is

$$T_3 = T_{cd} - \Delta T_{sub} \tag{3.8}$$

The polytropic exponent n is evaluated from a correlation based on data in the manufacturer's catalogue (see figure 3.6)

$$n = 0.842 \cdot \exp\left(-\left(P_{cd}/P_{ev}\right)/0.925\right) + 1.227 \tag{3.9}$$

Therefore the temperature at the compressor exit, its volumetric efficiency, the refrigerant mass flow rate and the polytropic compressor power are:

$$T_2 = T_1 \cdot \left(\frac{P_{cd}}{P_{ev}}\right)^{\frac{n-1}{n}} \tag{3.10}$$

$$\eta_{vol} = \left[1 + C - C \cdot \left(\frac{P_{cd}}{P_{ev}}\right)^{1/n}\right] \tag{3.11}$$

$$\dot{m}_R = \eta_{vol} \cdot \frac{PD}{v_1} \tag{3.12}$$

$$\dot{W}_{pol} = \dot{m}_R \left[\frac{n}{n-1} P_{ev} v_1 \left(\left(\frac{P_{cd}}{P_{ev}}\right)^{\frac{n-1}{n}} - 1\right)\right] \tag{3.13}$$

The other thermodynamic properties of the refrigerant (enthalpy, density ...) at states 2, 2′, 3′ and 3 are also evaluated using REFPROP. It should also be noted that the expansion of the thermostatic valve is assumed to be isenthalpic. Therefore the quality and density at state 4 can also be evaluated since its pressure and enthalpy are known.

The power input to the motor driving the compressor can be evaluated by the following correlation obtained from the manufacturer's data

$$\dot{W}_m = \dot{W}_{pol} \Bigg/ \left(0.77423 + 0.03969 \cdot \left(\frac{P_{cd}}{P_{ev}}\right) - 0.00442 \cdot \left(\frac{P_{cd}}{P_{ev}}\right)^2\right) \tag{3.14}$$

4. A first test is performed at this point by comparing the temperature at the condenser outlet T_3 to that of the outside air $T_{air,in}$. If the former is higher than the latter the calculation proceeds to step 5. Otherwise the number of refrigeration units (or equivalently the number of compressor N_C) is incremented, and the procedure returns to step 1b.

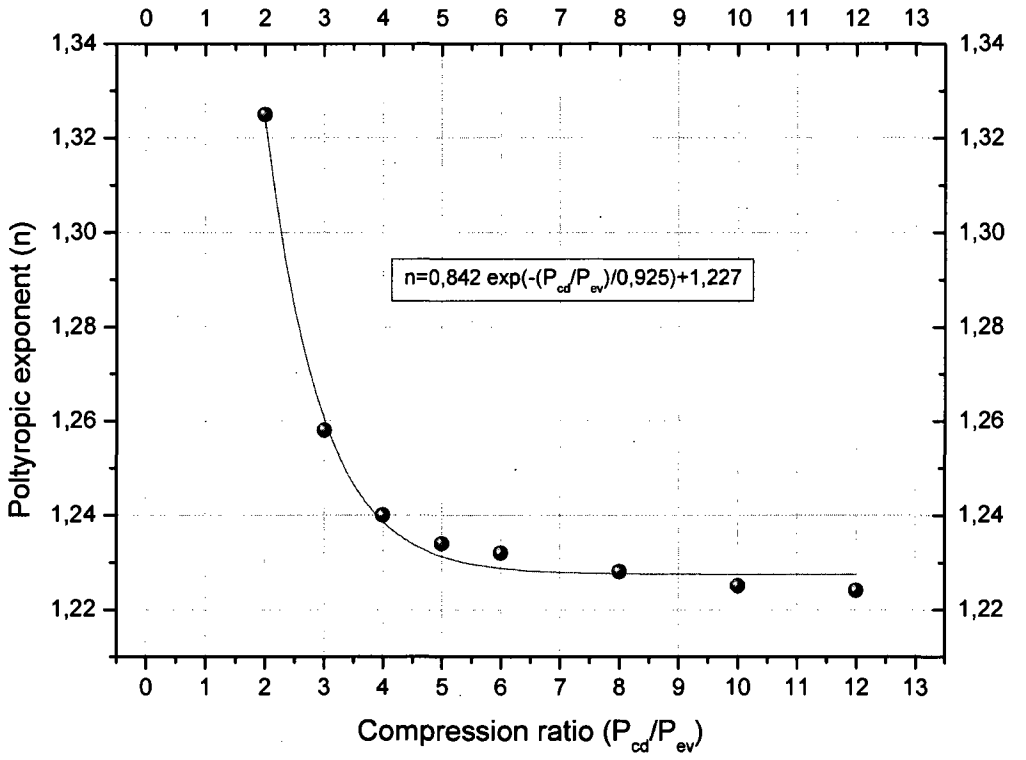

Figure 3.6 Polytropic exponent versus Compression ratio (manufacturer's data and correlation)

5. This step uses the evaporator model to calculate the heat exchange surfaces for the two-phases (2p) and superheated (v) zones. The corresponding equations are :

$$\dot{m}_R \cdot (i_{1'} - i_4) = \frac{\dot{m}_b}{N_C} \cdot Cp_b \cdot (T_{b,out} - T_{b,1'}) = U_{ev,2p} \cdot A_{ev,2p} \cdot CF_{ev} \cdot \text{LMTD}_{ev,2p} \quad (3.15a)$$

$$\dot{m}_R \cdot (i_1 - i_{1'}) = \frac{\dot{m}_b}{N_C} \cdot Cp_b \cdot (T_{b,1'} - T_{b,in}) = U_{ev,sup} \cdot A_{ev,sup} \cdot CF_{ev} \cdot \text{LMTD}_{ev,sup} \quad (3.15b)$$

It should be noted that the mass flow rate of the brine which circulates on the shell side is divided by the number of compressors in operation. The resulting mass flow rate therefore represents the corresponding brine flow rate for each refrigeration unit in operation.

By taking into consideration the resistance of the evaporator tubes and the fouling resistance, the overall heat transfer conductance for each zone (2p and v) can be expressed as follows

$$U_{ev,phase} = \left(\frac{D_{ev,o}}{D_{ev,i} \cdot h_{ev,phase}} + \frac{D_{ev,o} \cdot \ln(D_{ev,o}/D_{ev,i})}{2 \cdot k_{wall}} + R_{f,o} + \frac{1}{h_{ev,b}} \right)^{-1} \quad (3.16)$$

Next, it is necessary to calculate the convection heat transfer coefficients for each refrigerant phase and also for the shell side of the evaporator.

5.a Brine side of the evaporator:

The heat transfer coefficient outside the tube bundles is calculated from the McAdams correlation (Kakaç and Liu 2002) for the baffled shell-side heat transfer coefficient:

$$h_{ev,b} = 0.36 \cdot (k_b/D_{eq}) \cdot \left(\frac{D_{eq} \cdot G}{\mu} \right)_b^{0.55} \cdot \left(\frac{C_p \cdot \mu}{k} \right)_b^{1/3} \cdot \left(\frac{\mu_b}{\mu_{wall}} \right)^{0.14} \quad (3.17)$$

which is valid for $2000 < \left(\frac{D_{eq} \cdot G}{\mu} \right)_b < 1 \times 10^6$

The properties in this relation are evaluated at the average brine temperature in the shell.

5.b Refrigerant side of the evaporator (separated in two zones):

In the superheated zone, the simplified correlation given by Petukhov (1970) is used to obtain the heat transfer coefficient for the single phase refrigerant (vapour). The Nusselt number is given by

$$NU = \frac{(f/2) \cdot \mathrm{Re} \cdot \mathrm{Pr}}{1.07 + 12.7 \cdot (f/2)^{1/2} \left(\mathrm{Pr}^{2/3} - 1 \right)} \quad (3.18)$$

The Fanning friction factor is calculated from the correlation for smooth circular ducts given by

$$f = (1.58 \cdot \ln \mathrm{Re} - 3.28)^{-2} \quad (3.19)$$

Equation (3.19) predicts the results in the range $10^4 < \mathrm{Re} < 5 \cdot 10^6$ and $0.5 < \mathrm{Pr} < 200$ with 5 to 6 % error, and in the range $0.5 < \mathrm{Pr} < 2000$ with 10% error.

For the transition region where the Reynolds numbers are between 2300 and 10^4, the Gnielinski correlation (Gnielinski 1976) is recommended:

$$NU = \frac{(f/2)\cdot(\mathrm{Re}-1000)\cdot \mathrm{Pr}}{1+12.7\cdot(f/2)^{1/2}\left(\mathrm{Pr}^{2/3}-1\right)} \tag{3.20}$$

Therefore, we can calculate the convection heat transfer coefficient for a single phase

$$h = \left(NU \cdot \bar{k}\right)/D_{\mathrm{i}} \tag{3.21}$$

In the two phases zone of the evaporator the heat transfer coefficient is evaluated from the Shah correlation (Shah 1982):

$$h_{\mathrm{ev,2p}} = \psi \cdot h_{\mathrm{liq}} \tag{3.22}$$

Here, h_{liq} is the all-liquid convection heat transfer coefficient for the liquid phase which is calculated from the Dittus-Boelter correlation (Kakaç and Liu 2002).

$$h_{\mathrm{liq}} = 0.023\left[\frac{G_{\mathrm{ev}}(1-x)\cdot D_{\mathrm{i,ev}}}{\mu_{\mathrm{R,liq}}}\right]^{0.8} \mathrm{Pr}^{0.4}\,\frac{k_{\mathrm{liq}}}{D_{\mathrm{i,ev}}} \tag{3.23}$$

The coefficient ψ in eq. 3.22 depends on the convection number, the boiling number and the Froude number (Shah 1982)

After the three convection heat transfer coefficients have been calculated the values of $U_{\mathrm{ev,sup}}$ and $U_{\mathrm{ev,2p}}$ are obtained from eq. 3.17 and those of the surfaces $A_{\mathrm{ev,sup}}$ and $A_{\mathrm{ev,2p}}$ from eq. 3.15a and 3.15b.

6. A second test is now performed by comparing the sum of the two calculated surfaces $A_{\mathrm{ev,sup}}$ and $A_{\mathrm{ev,2p}}$ to the given total surface of the evaporator A_{ev}. If the sum is within ±5% of A_{ev} the calculation continues with step 7a. Otherwise, the evaporation temperature is reduced by 0.1°C and the procedure returns to step 3.

7.a The number of fans is initialised $(N_{\mathrm{fan}} = 1)$

7.b The mass flow rate of air in the condenser is calculated $(\dot{m}_{\mathrm{air}} = 5.89 \cdot N_{\mathrm{fan}}\ \mathrm{kg/s})$

8. The condenser is modeled by expressing energy conservation for each of three zones: desuperheating (2 to 2′), condensing (2′to 3′) and subcooling (3′to 3). The corresponding expression are

$$\dot{m}_R \cdot (i_2 - i_{2'}) = N_{fan} \cdot \dot{m}_{air} \cdot Cp_{air} \cdot (T_{air,out} - T_{air,2'}) = U_{cd,des} \cdot A_{cd,des} \cdot CF_{cd} \cdot \text{LMTD}_{cd,des} \quad (3.24a)$$

$$\dot{m}_R \cdot (i_{2'} - i_{3'}) = N_{fan} \cdot \dot{m}_{air} \cdot Cp_{air} \cdot (T_{air,2'} - T_{air,3'}) = U_{cd,2p} \cdot A_{cd,2p} \cdot CF_{cd} \cdot \text{LMTD}_{cd,2p} \quad (3.24b)$$

$$\dot{m}_R \cdot (i_{3'} - i_3) = N_{fan} \cdot \dot{m}_{air} \cdot Cp_{air} \cdot (T_{air,3'} - T_{air,in}) = U_{cd,sub} \cdot A_{cd,sub} \cdot CF_{cd} \cdot \text{LMTD}_{cd,sub} \quad (3.24c)$$

The overall heat transfer conductance for each zone is

$$U_{cd,phase} = \left(\frac{A_{cd,o}}{A_{cd,i} \cdot h_{cd,phase}} + \frac{A_{cd,o} \cdot \ln(D_{cd,o}/D_{cd,i})}{2\pi \cdot k_{wall} \cdot L} + \frac{R_{f,o}}{\eta_o} + \frac{1}{\eta_o \cdot h_{cd,air}} \right)^{-1} \quad (3.25)$$

Next it is necessary to calculate the convection heat transfer coefficients for the refrigerant in each zone and for the air.

8.a Refrigerant side of the condenser (three zones are considered)

For single phase refrigerant (desuperheating and subcooling zones) the convection heat transfer coefficient was calculated using equation (3.18) or (3.20) depending on the value of the Reynolds number.

For the two phase refrigerant we use the correlation by Cavallini and Zecchin (1974)

$$h_{cd,2p} = 0.05 \cdot \text{Re}_{R,eq}^{0.8} \cdot \text{Pr}_{R,des}^{0.33} \frac{k_{R,des}}{D_{i,cd}} \quad (3.26)$$

Where the equivalent Reynolds number is defined by:

$$\text{Re}_{R,eq} = \text{Re}_{des} \left(\frac{\mu_{R,des}}{\mu_{R,sub}} \right) \left(\frac{\rho_{R,sub}}{\rho_{R,des}} \right)^{0.5} + \text{Re}_{R,sub} \quad (3.27a)$$

$$\text{Re}_{R,sub} = \frac{G_{ev} \cdot (1-x) \cdot D_{i,cd}}{\mu_{R,sub}} \quad (3.27b)$$

$$\text{Re}_{R,des} = \frac{G_{ev} \cdot x \cdot D_{i,cd}}{\mu_{R,des}} \quad (3.27c)$$

8.b Air side of the condenser

The air side convection heat transfer coefficient was estimated using Webb's correlation (Webb, 1990) for heat exchangers with flat plate fins

$$\begin{cases} Nu_{cd,air} = 0.4\, Gz^{0.73} (s/D_c)^{-0.23} N_R^{0.23} & \text{for } Gz \le 25 \\ Nu_{cd,air} = 0.53\, Gz^{0.62} (s/D_c)^{-0.23} N_R^{0.31} & \text{for } Gz > 25 \end{cases} \quad (3.28)$$

The calculation in this step proceeds as follows. First the air temperatures $T_{air,3'}$, $T_{air,2'}$ and $T_{air,out}$ are calculated from equations 24. Then the logarithmic temperature differences $LMTD_{cd,sub}$, $LMTD_{cd,2p}$ and $LMTD_{cd,des}$ are evaluated from their definition. Next equations 3.26, 3.27 and 3.28 are used to calculate the convection heat transfer coefficients and the overall conductance for each zone is calculated from equation 3.25. Finally the heat transfer surface for each zone ($A_{cd,des}$, $A_{cd,2p}$ and $A_{cd,sub}$) is calculated from equations 3.24.

9. The third test is performed by comparing the sum of the three calculated surfaces ($A_{cd,des}$, $A_{cd,2p}$, $A_{cd,sub}$) to the given total surface of the condenser A_{cd}. If the sum is not within ±5% of A_{cd}, the number of fans is increased and the calculation continues with step 7b. If the sum is within ±5% of A_{cd} and $N_{fan} \le 4$ the calculation proceeds to step 10. On the other hand, if $N_{fan} > 4$ the solution is unacceptable since there are only four fans per condenser in the system under study. In such a case, the number of compressors (refrigeration units) is increased and the procedure restarts at step 2.

10. If the above procedure leads to $N_C \le 5$ the model has converged to physically acceptable operating conditions. Time is then incremented and the procedure is repeated for the next timestep. On the other hand if $N_C > 5$ the solution, although mathematically and thermodynamically correct, is not acceptable since there are only five compressors (five refrigeration units) in the system under study. This solution implies that the system can not deliver the desired outlet brine temperature $T_{b,out}$. Therefore its value is increased and the whole procedure is repeated for the same timestep by replacing its previous value by the new one.

Since the calculations are repeated every 6 minutes for an entire year the results are in the form of a set of 87600 vectors (365days x 24 hrs/day x 10 calc/hr) which include the calculated values of all the system's operating variables (evaporation and condensation pressures, compressor polytropic power, power input to the motor, exit brine and air temperatures, etc.) at each instant.

3.4 Model Validation

The developed model for the Camilien Houde ice rink refrigeration system was validated in two steps.

Firstly, the performance of the system was compared to the manufacturer's data. Eight of the 87600 vectors containing the results were chosen at random and the calculated values of the evaporation and condensation temperatures as well as those of W_m, the power input to the motor driving the compressor, and Q_R, the refrigeration capacity, are presented in table 3.1. The corresponding values of W_m and Q_R obtained for the same T_{ev} and T_{cd} by interpolation in the manufacturer's catalogue are also specified in this Table. The agreement is similar to that reported in other studies. Thus, in the case of W_m the difference in 7 of the 8 cases is less than 7% while in the case of Q_R it is less than 5% in 5 out of 8 cases. Overall this is deemed to be acceptable in view of the assumptions incorporated in the model and the uncertainty of the empirical correlations.

Table 3.1 Comparison between manufacturer's values and calculated results

T_{ev}(°C)	T_{cd}(°C)	Power of the compressor motor (kW)			Refrigeration Capacity (kW)		
		Calculated	Measured	Difference	Calculated	Measured	Difference
-20.0	41.37	18.85	19.14	1.5 %	47.71	48.31	1.1 %
-19.5	36.59	19.43	18.97	2.3 %	57.25	54.13	5.4 %
-19.25	35.15	19.5	18.98	2.8 %	59.64	48.86	18,0 %
-19.75	42.16	18.85	16.12	14.5 %	47.71	48.49	1.6 %
-18.7	42.0	19.06	20.42	6.6 %	49.64	51.34	3.3 %
-19.25	42.19	18.67	17.43	6.6 %	47.62	53.76	11,0 %
-18.42	42.22	19.18	20.06	4.3 %	50.05	51.87	3.5 %
-19.36	48.70	17.68	18.83	6.1 %	37.32	41.07	9.1 %

Secondly, calculated values of the evaporation and condensation pressures, refrigerant mass flow rate and number of compressors in operation were validated by comparing them to those obtained experimentally by Ouzzane et al. (2006). The measured outdoor air temperature, inlet and outlet brine temperatures and brine mass flow rate were taken as inputs for the model. Table 3.2 specifies the values of these inputs and compares the calculated and measured values of these four significant outputs. The agreement is considered to be very good. The small differences between calculated and measured evaporation and condensation pressures and mass flow rates are due to the imprecision of the measurements and to the simplifying assumptions of the model.

Table 3.2 Comparison between measured and calculated values

	Inputs				Outputs			
	Brine mass flow rate	Outdoor air temperature	Inlet brine temperature	Outlet brine temperature	Evaporation pressure	Condensation pressure	Refrigerant mass flow rate	Number of compressors in operation
Measured	62.88 kg/s	-13 °C	-5.88 °C	-7.01 °C	263.4 kPa	1549 kPa	0.335 kg/s	4
Calculated					268.5 kPa	1571.8 kPa	0.346 kg/s	4
Difference (%)					1.9	1.5	3.3	0

3.5 Results and discussion

In this section the response of the modeled refrigeration system to the time-dependent input data (Q_R, $T_{B,in}$ and $T_{air,in}$) is analysed and discussed for two time periods. A short period of 240 timesteps corresponding to a typical day (the 1st of March was chosen for this purpose) illustrates the variation of operating conditions (evaporation and condensation pressures, number of compressors in operation, etc.) due to the diurnal variations of the refrigeration load and of the ambient air temperature. A long period of 87600 timesteps corresponding to a typical year is used to compare monthly energy consumption by the compressors, the fans, etc. for two control strategies of the system. The results were calculated using yearly distributions of the ambient temperature and refrigeration load described in an earlier publication (Seghouani et al. 2009). The pumping power was added to this load resulting in Q_R while the corresponding brine temperature at the inlet of the evaporator was obtained from Eq. 3.30.

3.5.1 Transient results for a typical day (March 1st)

The time dependent input data is shown in figure 3.7. The outside air temperature $T_{air,in}$ for the day under consideration (from ENERGYPLUS) decreases from -5.6°C to -11°C during the night, starts rising after sunrise, reaches a maximum of -1°C around 16h and then decreases. The corresponding total refrigeration load Q_R, calculated with the code described in a previous article (Seghouani et al. 2009), is the sum of heat fluxes into the ice (by convection, radiation and phase changes), heat gains from below the concrete slab and the pump power (5kW) which is dissipated by friction. As seen in figure 3.7 this quantity decreases slightly from 0h00 to 8h00 due to the fact that there are no activities in the ice rink during the night (no lights, etc.) and then rises from 8h00 until noon when the first resurfacing operation takes place. During the first half of the day the load is between 100 and 75 kW. The second half of the day is characterised by high peaks which reach more than 300 kW and correspond to the resurfacing of the ice which is achieved by spreading water at 60°C on its surface.

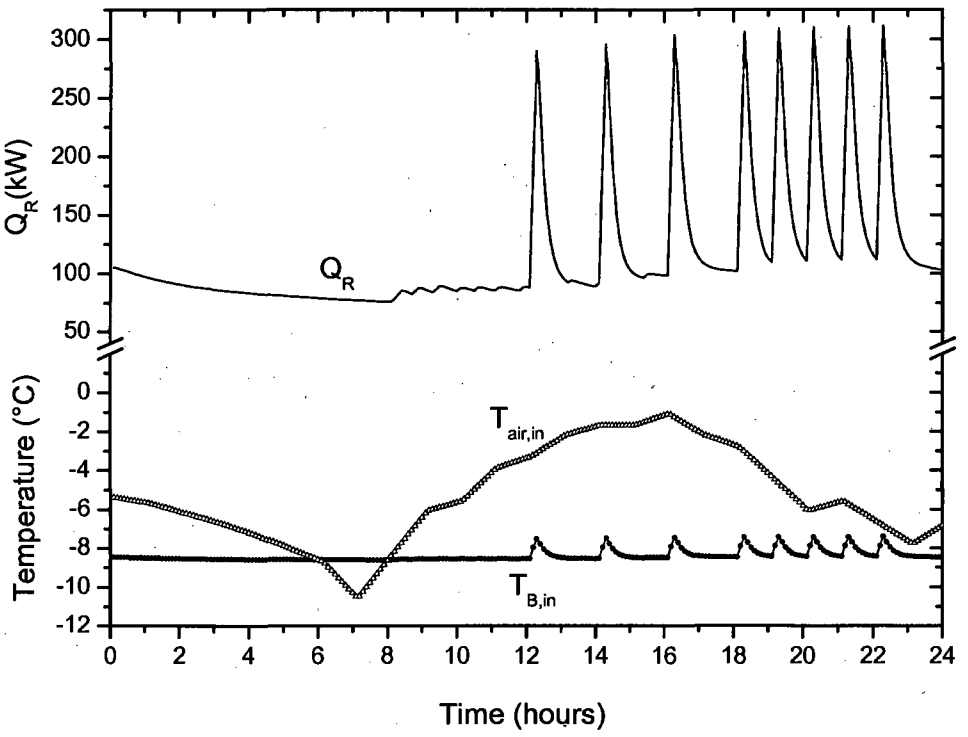

Figure 3.7 Diurnal variations of the inputs for March 1st

The temperature of the brine entering the refrigeration system $T_{b,in}$ is the third input and is calculated from the relation

$$Q_R = \dot{m}_b \cdot Cp_b \cdot (T_{b,in} - T_{b,out}) \tag{3.30}$$

The brine temperature coming out of the refrigeration system and entering the concrete slab (figure 3.1) is considered to be constant at -9°C for the calculation of Q_R (Seghouani et al., 2009).

Figure 3.8 shows the calculated response of the system to the input data for this particular day. The number of compressors, or units, in operation (left axis) is three from 0h00 to 0h30 and then falls to two due to the decrease of the refrigeration load Q_R (see figure 3.7). During this transition the mass flow rate of air per condenser increases since Q_R^* increases. The number of compressors in operation stays at two until noon while the mass flow rate of the cooling air decreases between 0h30 and 8h00 (due to the decrease of the outside air

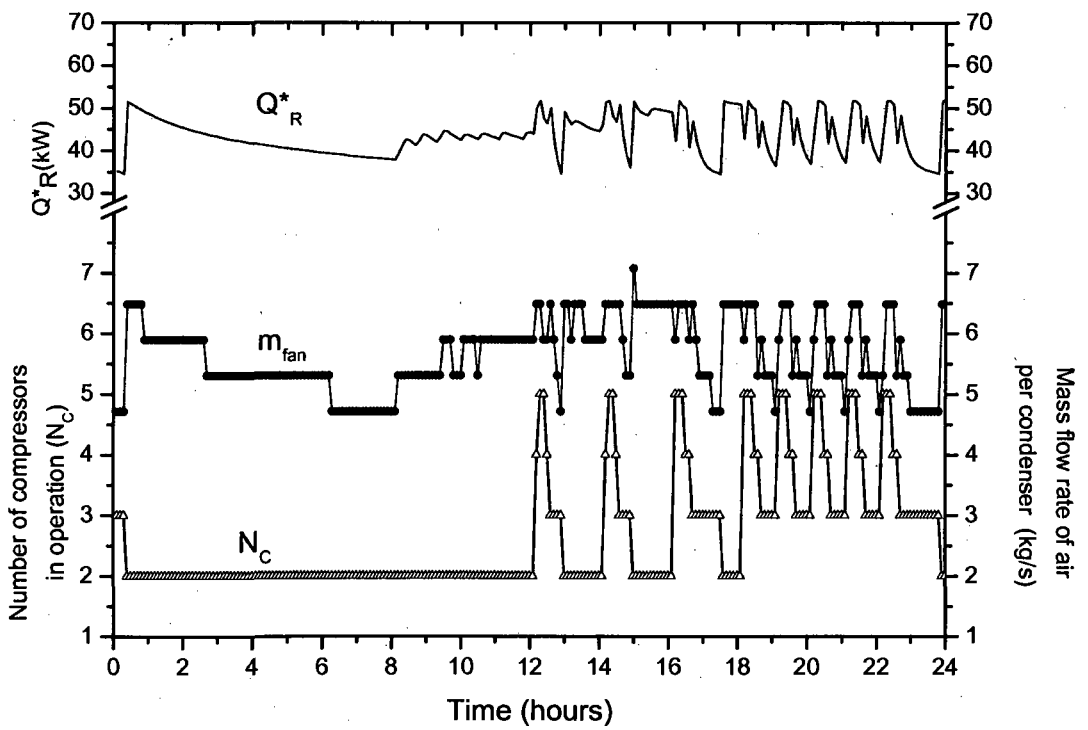

Figure 3.8 Number of compressors in operation, mass flow rate of air per condenser and refrigeration load per unit for March 1st

temperature) and increases after sunrise as the activities in the ice rink intensify. During the resurfacing operations the number of compressors in operation is maximum (five) for two or three timesteps. Between noon and 18h00, when the time interval between successive resurfacing operations is fairly long, the system can recover from the high load corresponding to these operations and can return gradually to a state with only two compressors in operation. On the other hand, from 18h00 to midnight when the frequency of resurfacing operations increases, the minimum number of compressors in operation is three. This is due to the increased activity in the ice rink and the inertia of the system which does not have sufficient time between resurfacing operations to return to a more normal condition. Peak values of the refrigeration load per unit Q_R^* occur more often than those for Q_R but are less pronounced as a result of the variation of the number of compressors in operation. Thus the values for Q_R^* vary between approximately 35 and 52 kW. Therefore the ratio of the maximum to minimum values of Q_R^* is approximately 1.5 while the corresponding ratio for the total load Q_R is approximately 4. On the other hand the mass flow rate of air per condenser increases during resurfacing in order to evacuate the increased heat quantity. Finally, it should be noted that during this particular day the outside temperature is fairly low (figure 3.7) and therefore the maximum number of operating fans per condenser is only two.

Figure 3.9 shows the condensation and evaporation pressures during this day. The evaporation pressure is essentially constant at about 260 kPa since the temperature of the brine remains always constant. On the other hand, the condensation pressure varies between 1600 and 2000 kPa due to the combined effect of the air temperature (figure 3.7) and the refrigeration load per unit (figure 3.8). Between 0h30 and 8h00 this refrigeration load Q_R^* decreases, therefore P_{cd} rises as indicated by the manufacturer's data in figure 3.5 and by equation 6. The peak values of the condensation pressure occur after the start of the resurfacing operations and again shortly afterwards. The latter are due to the rise of Q_R^* as the number of compressors in operation decreases gradually from 5 to 3 (figure 3.8) during these periods.

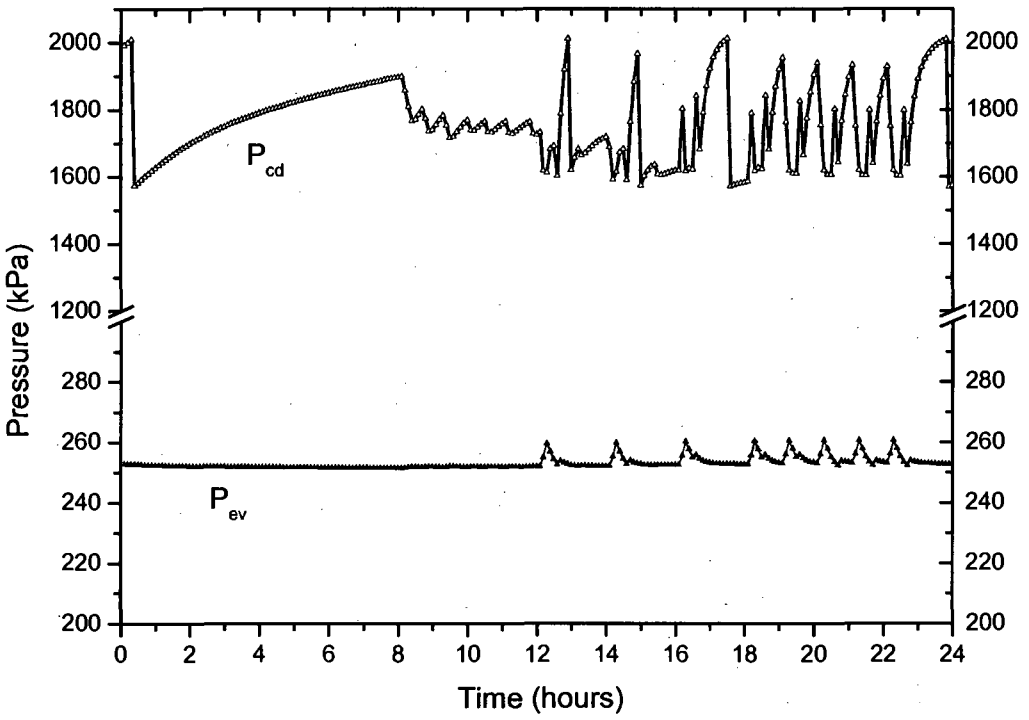

Figure 3.9 Variation of the condensation and evaporation pressures with time on March 1st

Figure 3.10 illustrates the corresponding diurnal variation of the power for all the compressors and fans in operation at any instant. The polytropic power of the compressors (Eq. 3.13) is of course lower than the power input to the motors (Eq. 3.14) due to mechanical losses. During resurfacing operations the number of compressors in operation is maximum and therefore the required power consumption is also highest. The total power for the fans is very small compared to the corresponding value for the compressors. This is partly due to the fact that the day under consideration is relatively cold (figure 3.7) so that only one or two fans per condenser are needed to reject the heat from the refrigerant. However even during hot days, when all four fans per condenser are in operation, their power consumption remains small compared to that of the compressors.

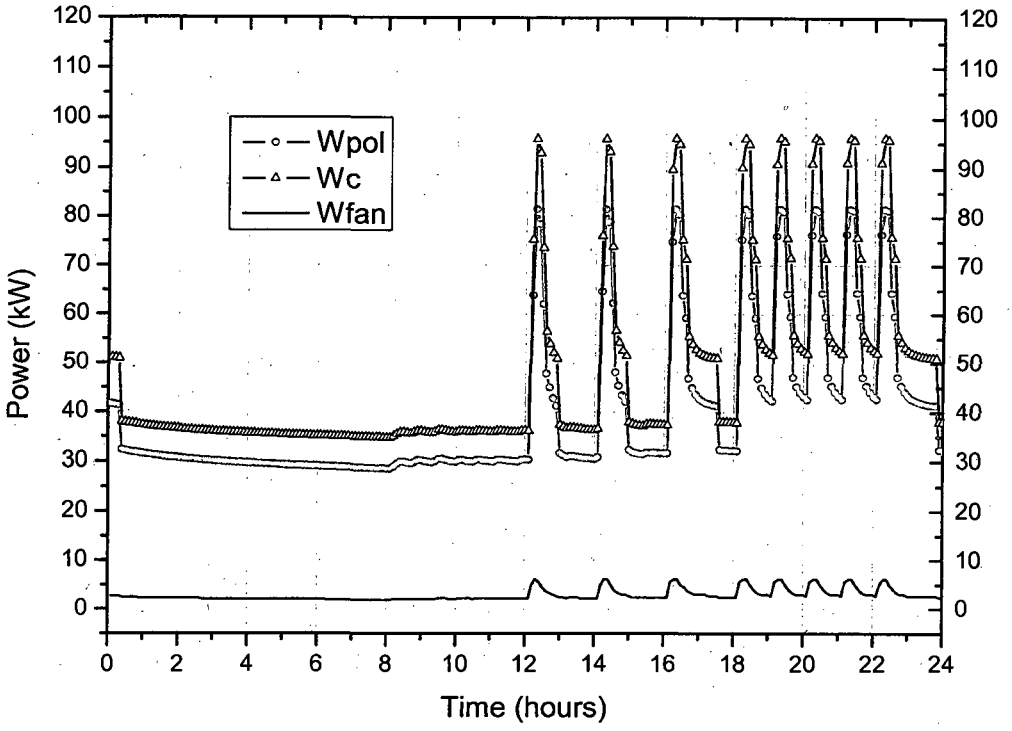

Figure 3.10 Power required by the fans and the compressors on March 1st

Figure 3.11 shows the variation of the COP for the refrigeration cycle and for the system. The former is based on the polytropic compressor power (Eq. 3.13) while the latter is based on the power input to the compressor and fan motors (Eq. 3.14):

$$\mathrm{COP}_{\mathrm{Cyc}} = (i_1 - i_4)/(i_2 - i_1) \tag{3.31}$$

$$\mathrm{COP}_{\mathrm{Sys}} = \dot{m}_{\mathrm{b}} \cdot Cp_{\mathrm{b}} \cdot \left(T_{\mathrm{b,in}} - T_{\mathrm{b,out}}\right) \Big/ \left(N_{\mathrm{C}} \cdot \left(\dot{W}_{\mathrm{m}} + N_{\mathrm{fan}} \cdot \dot{W}_{\mathrm{fan}}\right)\right) \tag{3.32}$$

Therefore the system COP is smaller since $\dot{W}_{\mathrm{m}} > \dot{W}_{\mathrm{pol}}$ (see figure 3.10). From 0h00 to 8h00 they both decrease due to the refrigeration load diminution illustrated in Figures 8 and 9. During the resurfacing operations both COPs increase and just after this short period they fall significantly due to the decline of the refrigeration loads Q_{R} and Q_{R}^{*}.

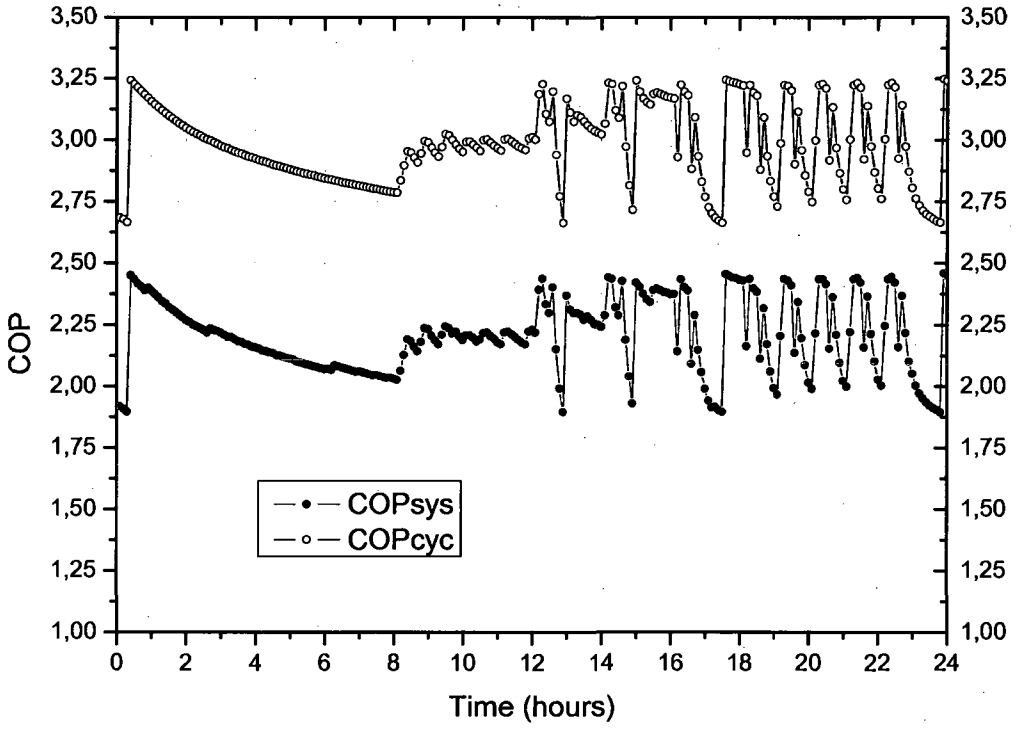

Figure 3.11 Coefficients of performance for the refrigeration system and for the refrigeration cycle for March 1st

Figure 3.12 shows the variation of the brine temperature at the inlet and outlet from the refrigeration system for the day under consideration. The former is represented by the top curve and constitutes an input to the model as stated earlier. It is important to remember that the system is modeled in a way that the outlet brine temperature returning to the concrete slab below the ice sheet (see figure 3.1) will normally be equal to -9°C. However, during resurfacing the refrigeration system is sometimes not able to absorb the corresponding important load Q_R and, therefore, the outlet brine temperature is warmer than -9°C as represented in figure 3.12 by the two lower curves. These two curves represent the outlet brine for two operating strategies: in one case all five units are allowed to operate during periods of high load while in the second case the maximum number of units in operation is limited to

four in order to limit the peak electrical demand of the system. As shown by the results of Figure 3.12 the effect of these two strategies on the returning brine temperature is only visible during the short resurfacing periods and is rather small: when the maximum number of simultaneously operating compressors is limited to four the returning brine temperature during these periods is slightly warmer (-8.35°C) than if all five compressors are allowed to operate simultaneously (-8.77°C). During the rest of the day both operating strategies meet the design requirement of a -9°C returning brine temperature. The effect of each of these operating strategies on the annual energy consumption is analyzed in the next section of the present paper while their influences on the ice sheet temperature will be studied in the future by coupling the present model with the one described by Seghouani et al. (2009).

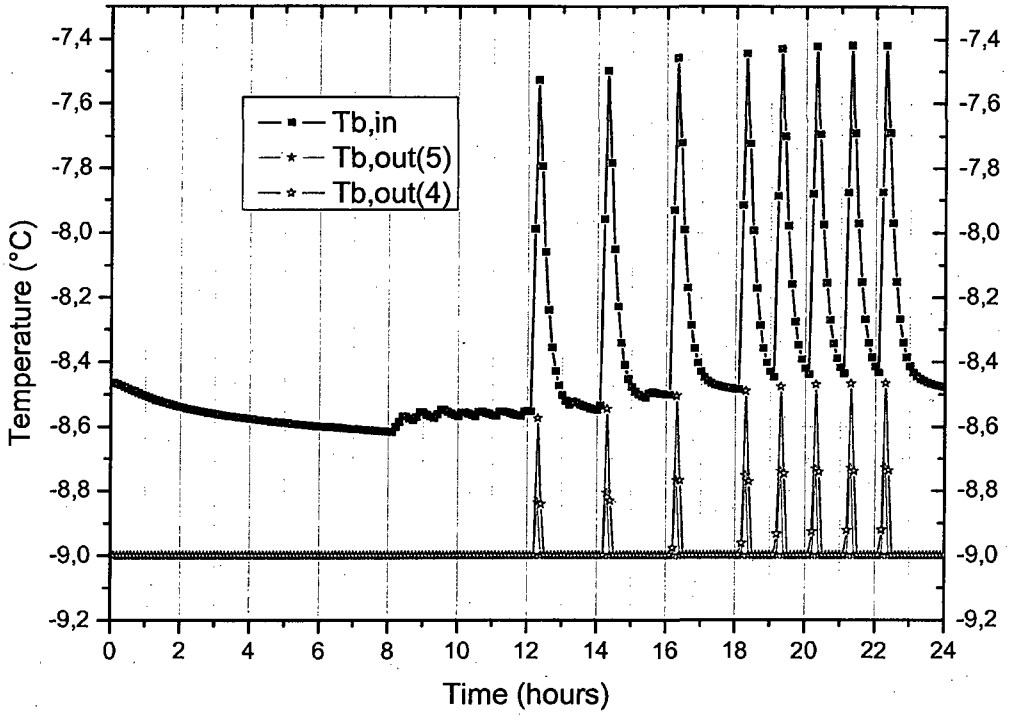

Figure 3.12 Inlet and outlet brine temperatures for two functioning strategies

3.5.2 Monthly energy calculations for a typical year

Figure 3.13 shows a comparison of the average daily energy transferred to the refrigerant in the evaporators for the two operating strategies described earlier (maximum number of units in simultaneous operation equals 4 or 5). It clearly shows that with a maximum of five compressors in operation the refrigeration load treated by the system is higher than with four compressors. The difference can reach almost 150 kWh/day during the summer months while in winter it is slightly smaller than 100 kWh/day. As already mentioned, the peak power demand when the maximum number of compressors in simultaneous operation is lowered from 5 to 4 is reduced by approximately 20% while the maximum temperature of the brine at the outlet of the evaporator increases by approximately 0.5 °C. The seasonal effect on this energy quantity is clear and qualitatively predictable. Its value is lower in winter than in summer due to the colder ambient and soil temperatures which reduce heat fluxes towards the brine in the ice rink.

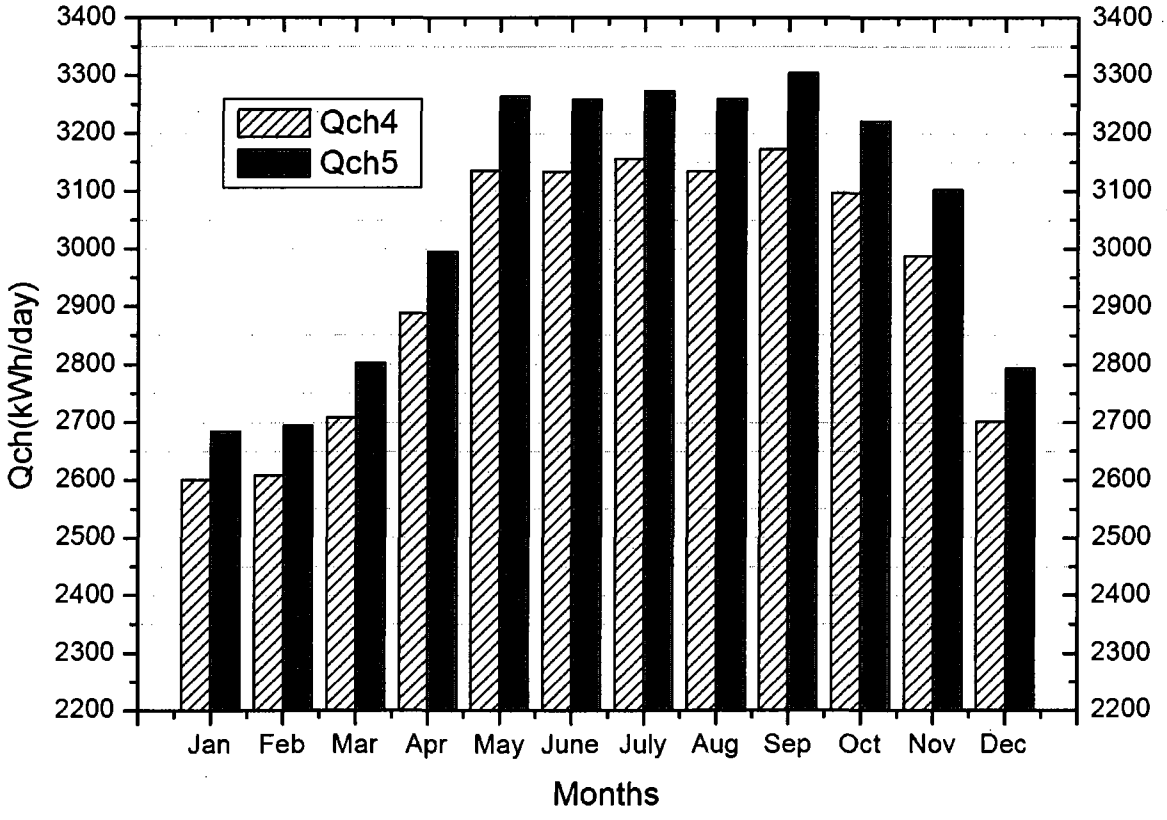

Figure 3.13 Average daily refrigeration loads at the evaporator for two operating strategies

Figure 3.14 compares the average daily energy consumption by the motors driving the compressors for the two operating strategies under consideration. Logically, this quantity is lower when the maximum number of units in simultaneous operation is 4. Thus the annual energy consumption of the motors driving the compressors can be reduced by almost 10% by this simple control strategy with a small increase in the temperature of the ice. The values in figure 3.14 rise progressively from January to May and can exceed 1400 kWh/day during the summer months. After September they decrease significantly due to the decrease of the refrigeration load (figure 3.13).

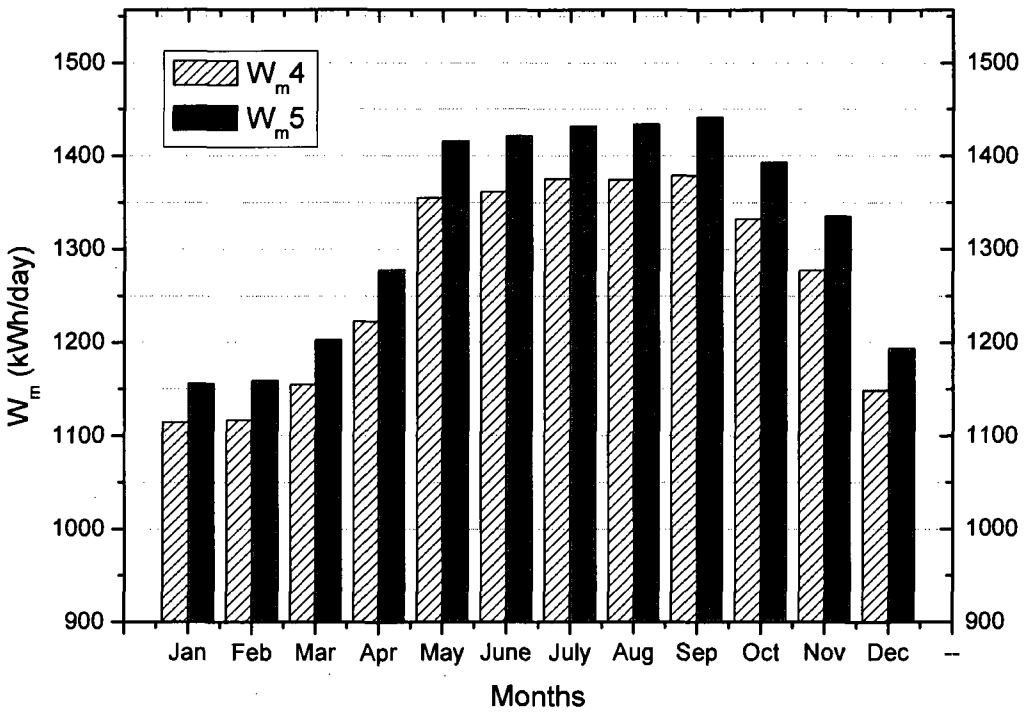

Figure 3.14 Average daily energy consumption by the compressors for two operating strategies

The heat rejected by each of the three regions of the condensers (desuperheating, phase change and subcooling) is presented in figures 3.15A and 3.15B for the two operating strategies under consideration while figure 3.15C compares the corresponding totals.

According to the results in figures 3.15A and 3.15B the heat rejected by the subcooling regions is insignificant for both operating strategies. This explains the fact that many studies do not take into account this effect. They also show that the heat rejected during phase changes is almost four times greater than for desuperheating. However, in most ice rinks only the heat rejected by the desuperheating region of the condensers is recovered and used for space heating, DHW heating or snow melting. The present results illustrate the considerable energy, and potentially economic, gains which can be achieved by recovering the heat rejected during the condensation of the refrigerant.

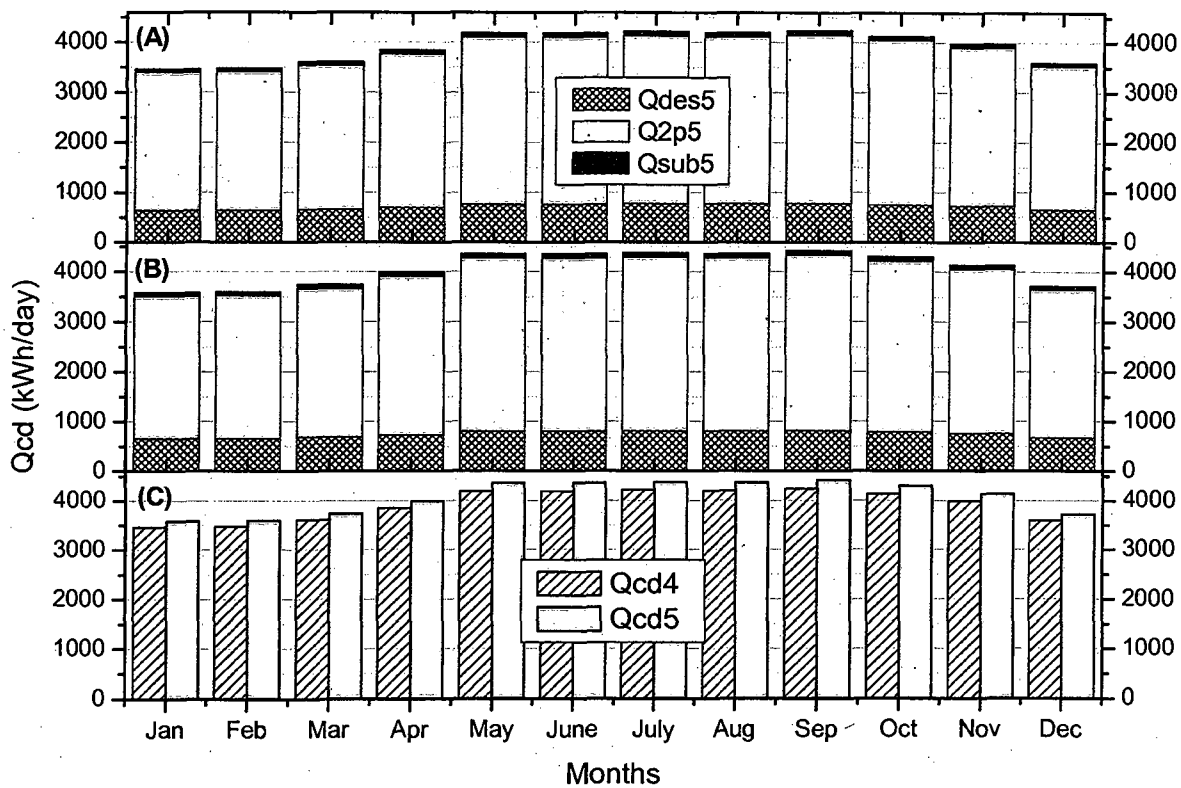

Figure 3.15 Average energy rejected by the condensers (A) maximum N_C=5, (B) maximum N_C=4, (C) comparison of total for maximum N_C=5 and maximum N_C=4

Figure 3.15C compares the average values of the total heat rejected at the condensers by the two operating strategies under consideration. When the maximum number of compressors in simultaneous operation is 5 the system rejects more heat than when that number is 4 because of the increase of both the heat absorbed in the evaporator (figure 3.13) and the compressor work (figure 3.14). Their difference is higher during the summer months, when it can reach almost 200 kWh/day, since the need of a fifth compressor is more frequent during warm days.

Also, during the summer, when the outside temperature and the refrigeration load are higher, the energy consumption by the condenser fans is significantly higher than in winter as shown in figure 3.16. This is due to the fact that more fans are operating during hot days to evacuate the heat rejected by the refrigerant in the condensers. However, their consumption represents only 5 to 10 % of the compressors consumption.

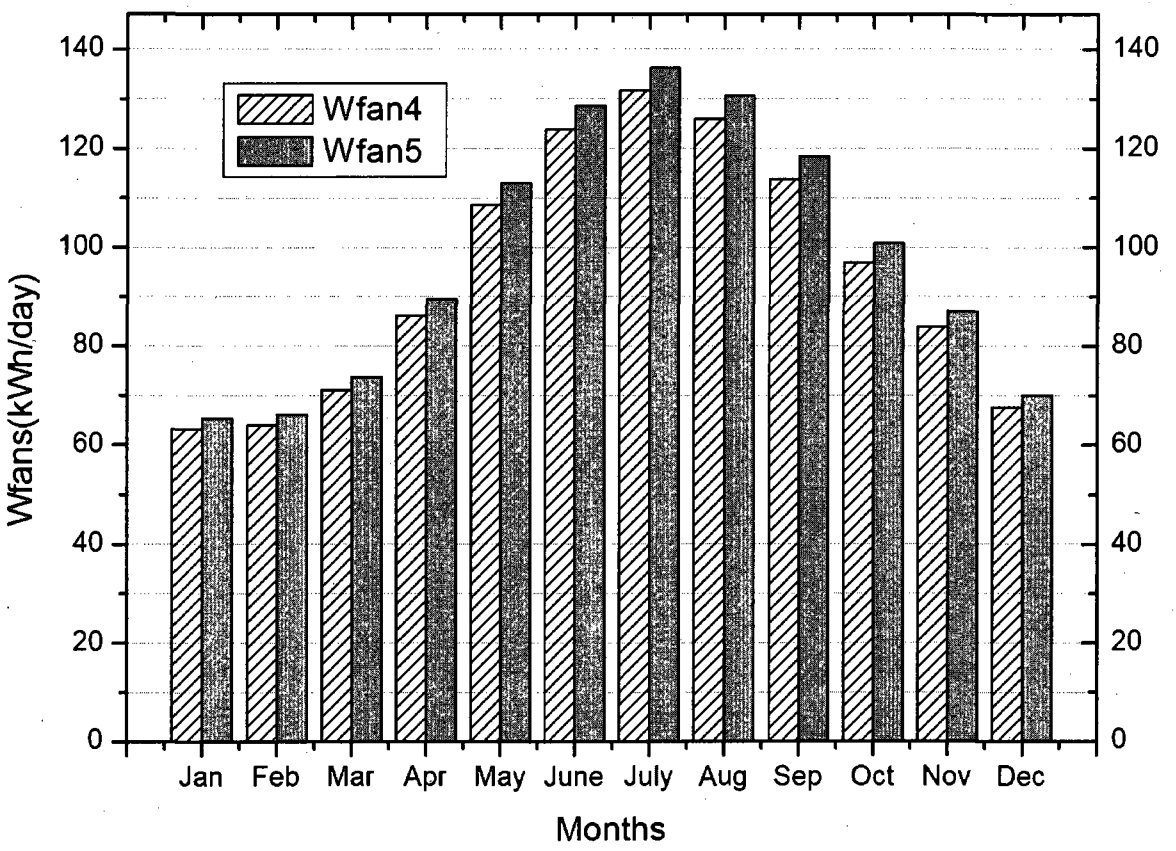

Figure 3.16 Average energy consumption by the condenser fans for two operating strategies

3.6 Conclusion

A computer program was developed to simulate the quasi-steady operation of the large refrigeration system of an indoor ice rink using R22 as the working fluid and brine for the secondary loop. The phase changes in both heat exchangers as well as the time dependent ambient conditions and refrigeration load were taken into account. The results are in good agreement with the experimental measurements and with the manufacturer's data.

The model was used to predict the number of compressors in operation, their energy consumption, the fans' energy consumption, etc. for a typical day and an entire typical year. The results show that the coefficients of performance of the thermodynamic cycle and the system increase during the resurfacing operations but decrease immediately afterwards. They also illustrate the considerable potential for heat recovery from the two phase region of the condensers which is almost 4 times higher than the heat rejected during desuperheating. The average daily energy consumption by the compressors and fans were calculated for each month of the year for two different control strategies: by reducing the maximum number of simultaneously operating compressors from 5 to 4 the peak electrical demand is reduced by 20% and the annual energy consumption of the motors driving the compressors is reduced by almost 10% while the temperature of the brine increases by approximately 0.5°C during short periods following the resurfacing operations.

In the future this model of the refrigeration system will be coupled to the models of the ice rink and the concrete slab with brine pipes described in previous articles (Daoud and Galanis, 2006; Daoud et al., 2008; Seghouani et al. 2009). Furthermore, other processes such as thermal storage and heat recovery, or changes such as replacing the air cooled condensers by water cooled condensers, will be included since the developed code is very flexible and allows such modifications.

CHAPITRE 4

SIMULATION OF THE DYNAMIC INTERACTION BETWEEN AN ICE RINK AND ITS REFRIGERATION SYSTEM

Auteurs et affiliation:

L. SEGHOUANI: étudiant au doctorat, Université de Sherbrooke, Faculté de génie, Département de génie mécanique.

A. DAOUD: Chercheur Scientifique, Institut de Recherche d'Hydro-Québec Laboratoire des Technologies de l'Énergie (LTE), Shawinigan, (Québec).

N. GALANIS: professeur, Université de Sherbrooke, Faculté de génie, Département de génie mécanique.

Date de soumission: 02 mai 2009

Revue: International Journal of Refrigeration

Référence: (Seghouani et coll. 2009)

Titre français: Simulation dynamique de l'interaction entre un aréna et son système de réfrigération.

Résumé:

Dans ce dernier chapitre de la présente thèse, le modèle complet de simulation en mode transitoire qui calcule le transfert de chaleur et la consommation d'énergie d'un aréna a été réalisé en couplant les différents modèles (AIM, BIM et REFSYS) décrits dans les deux précédents chapitres. Celui-ci permet donc d'analyser le couplage dynamique entre les phénomènes qui se produisent dans l'aréna (transfert de chaleur, condensation, mouvement de l'air) et le système de réfrigération en tenant compte des conditions météorologiques variables et de l'inertie thermique des composantes modélisées dans le BIM.

Le modèle ainsi développé est en mesure de prévoir le nombre de compresseurs en marche, la chaleur rejetée par les condenseurs, la charge de réfrigération, les pressions de condensation et d'évaporation et de nombreux autres détails tels que la température de la saumure, la température de la surface de la glace et cela sur une base d'une année typique pour les données météorologiques et la cédule d'exploitation de l'aréna.

Le modèle a été utilisé pour analyser les effets couplés de la réduction de l'émissivité du plafond et de l'augmentation de la température de la saumure à l'entrée de la dalle de béton de près de 1°C. Les résultats montrent que la température de la glace demeure essentiellement la même et que, par conséquent, sa qualité n'est pas affectée. D'autre part, ces changements résultent en une diminution substantielle de la consommation d'énergie du système de réfrigération allant de 16% à 22% au cours de l'année typique. Les résultats illustrent également le potentiel considérable pour la récupération de la chaleur à partir des condenseurs qui peut réduire l'énergie requise par le système de ventilation de la l'aréna.

Mots clés: aréna, charge de réfrigération, consommation d'énergie, performance annuelle

Abstract

A transient model of airflow and heat transfer in an indoor ice rink and a quasi-steady model of its refrigeration system have been coupled and used to simulate their response to the time dependent ambient conditions and operating schedule for a typical meteorological year. The results for two different cases show that it is possible to reduce significantly the time of operation of the compressors and the energy consumption of the refrigeration system by simultaneously reducing the ceiling emissivity and increasing the secondary coolant temperature without affecting the quality of the ice.

Keywords: ice rink (aréna), refrigeration load (charge de réfrigération), energy consumption (consommation d'énergie), yearly performance (performance annuelle)

Nomenclature

T_{a_out} Outlet air temperature from the condensers (°C)

T_{a_in} Inlet air temperature to the condensers (°C)

T_{ice} Ice surface temperature (°C)

T_{b_out} Outlet brine temperature from the refrigeration system (°C)

T_{b_in} Inlet brine temperature to the refrigeration system (°C)

T_{int} Temperature at the interface between ice and concrete slab (°C)

P_{cd} Condensation pressure (kPa)

P_{ev} Evaporation pressure (kPa)

Q_{ice} Heat flux from AIM to BIM (kW)

Q_R Refrigeration load (kW)

N_C Number of compressors in operation

Δt Timestep

Abbreviations

BIM	Below Ice Model
AIM	Above Ice Model
REFSYS	Refrigeration System

4.1 Introduction

Ice rinks are large buildings which consume a great amount of energy and generate considerable emissions contributing to the greenhouse effect. The thousands of such buildings in North America offer a big potential for improvement since most of them are old, oversized and were not designed for high energy efficiency. However, the available methods for the calculation of their annual energy consumption are not as developed as those for conventional buildings Bellache et al. (2006). The large dimensions of these building, the simultaneous need of refrigeration and heating, as well as time-dependent schedules for ventilation, lighting and resurfacing of the ice are some of the reasons for this situation.

Readily available large computers have prompted some researchers to use Computational Fluid Dynamics (CFD) for the calculation of the refrigeration load of ice rinks. Thus, Bellache et al. (2005) developed a steady state 2D CFD model which predicts velocity, temperature, absolute humidity distributions and calculates the fluxes toward the ice due to convection from the air, to condensation of vapor and to radiation from the walls and ceiling. It was improved by Bellache et al. (2006) by including transient phenomena, heat transfer through the ground and gains from lights as well as the effects of resurfacing and dissipation of pump work in the coolant pipes. This model was validated with experimental results by Ouzzane et al. (2006). The great disadvantage of these CFD based models is the considerable calculation time required to obtain results for even a typical 24-hr period. Shortly afterwards, Daoud & Galanis (2006) and Daoud et al. (2007) proposed an alternative method to CFD which requires considerably less calculation time and computer memory and provides good results for an entire year. This model (AIM) takes into account the transient phenomena and 3D geometry of the building as well as the resurfacing and occupation loads but assumes that the temperature of the brine entering the concrete slab under the ice is constant. Heat fluxes toward the ice surface were calculated and are in good agreement with measurements.

Following this work, Seghouani et al. (2009) developed a complementary model to AIM, called BIM, which calculates the transient heat fluxes to the brine pipes from the soil under and around the foundation of the ice rink. The two models AIM and BIM have been successfully coupled under TRNSYS software and permit a wide range of parametric studies (such as determining the effect on energy consumption of the climate, the ice sheet thickness, the emissivity of the ceiling, the brine temperature entering the concrete slab... etc.).

In parallel, Seghouani & Galanis (2009) developed a quasi-steady state model of the air cooled refrigeration system of the ice rink (REFSYS) based on a combination of thermodynamic relations, heat transfer correlations and data available in manufacturers' catalogues. Results such as the monthly energy consumption, the number of compressors in operation as well as the heat rejected by the condensers were shown among numerous other outputs. This model requires as an input the time-dependent refrigeration load and the corresponding brine temperature entering the evaporators. These were taken from a data file calculated by the AIM+BIM models. However, REFSYS did not take into account the complete interaction between the ice rink and its refrigeration system since the refrigeration load was not recalculated when the refrigeration system was unable to cool the brine to the assumed temperature of the brine used by the AIM and BIM models.

The purpose of the present paper is to integrate the previous works by coupling the refrigeration system (REFSYS) and the ice rink (AIM and BIM) models. The resulting model constitutes a complete simulation tool of an ice rink and its refrigeration system, able to predict the annual energy consumption by the compressors and the ventilation system, the ice surface temperature evolution as well as the potential for heat recovery.

4.2 Ice rink description

Figure 4.1 shows a schematic representation of the ice rink under study. A short description is presented here since more details are available in our previous publications Seghouani et al. (2009). The ice surface is 61 m long and 25.9 m wide. The spectator stand is heated by 8 radiant heaters which are controlled by an electronic thermostat with a set point equal to 15 °C; its hysteresis is ±0.2 °C and its nocturnal setback is 7 °C. Seven inlets supply a stream of ventilation air. Its flow rate is 4270 L/s except during resurfacing of the ice when it is increased to 10384 L/s to evacuate the combustion gases of the resurfacing vehicle. The air exits through 4 outlets on the walls. Heat gains from lighting are 10 W/m^2 above the ice and 5 W/ m^2 above the stands; those due to the presence of the audience are also taken into account while the number of spectators is specified according to a weekly schedule. The ice resurfacing is done several times per day, lasts 12 minutes and is modeled as a 1mm film of hot water at 60 °C. Its frequency, specified in the schedule mentioned above, is higher in the evenings and weekends. The ground structure beneath the ice rink comprises horizontal layers

of ice (2.5 cm), concrete (15 cm), thermal insulation (10 cm), sand (20 cm) and, finally, soil. The total depth included in the calculation domain is 4 m. The secondary coolant used to maintain the ice at the desired temperature is calcium chloride brine (concentration 20% by mass). It is supplied from a header located at the west end of the ice sheet and circulates in the concrete slab within 74 uniformly distributed, four-pass polyethylene tubes. An electrical heater of 8 kW is activated in the sand layer when the ground temperature at a depth of 4m is below 4°C to prevent freezing under the concrete slab which can cause damage to the underground structure and ice.

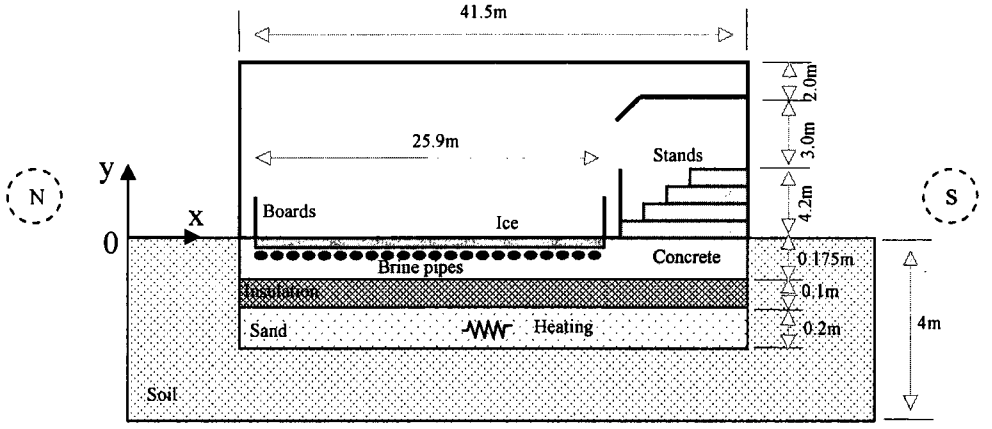

Figure 4.1 Schematic section of the ice rink and the different layers under the ice (not to scale)

The refrigeration system is constituted of two parallel shell and tubes evaporators, five open-drive four-cylinder compressors (Carrier 5H40 model), five air-cooled condensers (Larkin RC8, 0768 model) with four fans per condenser (the flow rate of each fan is 5.89 kg/s). The system also includes five thermostatic expansion valves (Parker) and one split-case brine pump (1200 rpm, 56.7 L/s, 18.7 kW). The primary refrigerant is R-22.

4.3 Models description

The complete model of the ice rink under study is constituted of three major parts: the AIM, the BIM, and the REFSYS. A short description of each of them and of their connection is presented below. More details about each of these three parts including their validation are available in our previous papers (Daoud & Galanis 2006, Daoud et al. 2007, Seghouani et al. 2009, Seghouani & Galanis 2009).

4.3.1 *Above ice model*, AIM (Daoud and Galanis, 2006, Daoud et al. 2007)

This model simulates the air movement inside the ice rink building and calculates the heat fluxes towards the ice by radiation, convection and phase changes using a 3D transient zonal model with 64 zones. It consists of six coupled submodels (Energy, Radiation, Zonal, Air Age, Ventilation System, Humidity and Condensation) solved simultaneously with the "onion" method. The data exchange between these six submodels takes place several times at every timestep until the outputs of each submodel vary by less than 10^{-3}. The ventilation system consists of two units. The first one is used for cooling, dehumidifying and reheating the external air when its temperature is above 23 °C while the second unit is for heating and humidifying it when its temperature is below 15 °C. When the temperature of the entering air is between 23 and 15 °C none of the units is in operation unless the humidity level is too high or too low. The humidity controls are such that the relative humidity of the air entering the ice rink is maintained between 20% and 33%.

4.3.2 *Below ice model*, BIM (Seghouani et al. 2009)

The BIM is based on the transient one-dimensional vertical conduction equation and the electrical circuit analogy but takes into account heat exchanges with the lateral soil around the foundations of the ice rink. It also includes the thermal inertia of the different layers which constitute the structure under the ice (ice, concrete slab with embedded brine pipes, insulation, sand with electrical heater and finally soil). For that, the ice surface is divided in 8 equal surfaces which correspond to those used by the zonal model of the AIM. Each of these surfaces is subdivided into two parts (A and B). The brine flows from west to east under part A of the eight surfaces and in the opposite direction under part B. The model calculates the heat fluxes to the brine from the soil below and around the ice sheet as well as those from above corresponding to the heat gains of the ice calculated by the AIM. It then evaluates the brine outlet temperature based on its inlet temperature, the ice surface temperature and the temperature at each interface between the layers under the ice for each timestep.

4.3.3 Refrigeration system model, REFSYS (Seghouani & Galanis 2009)

The third part simulates the refrigeration system which is the heart of the ice rink. Therefore its modeling is of a substantial nature since it has the responsibility to reject the heat

corresponding to the refrigeration load with a suitable control strategy which insures a good ice quality while limiting the energy consumption and peak electrical demand. For that, each component of the system is modeled separately. The evaporator is divided into two regions (phase change and superheating) and appropriate correlations are applied to model the heat transfer between refrigerant and brine. The compressor is modeled using thermodynamic relations, a polytropic compression and data from the manufacturer's catalogue (curve fitting). The air cooled condenser is modeled similarly to the evaporator but is divided into three regions (desuperheating, phase change, subcooling). The heat exchanges between the system components and the environment are neglected while the expansion of the refrigerant through the thermostatic valves is considered isenthalpic. The number of compressors in operation (N_C) is determined by dividing the refrigeration load (Q_R) by the capacity of each compressor (obtained from a correlation based on the manufacturer's data) and from the condition that the outside air temperature must be smaller than the condensation temperature.

This model is able to successfully predict the energy consumption of the compressors and fans, the brine temperature at the exit of the evaporator, the condensation and evaporation pressures, the heat rejected by the condensers and the performance coefficient of the system as well as many other operating parameters at each timestep.

4.4 Coupling the different models

The three previously described models are coupled in TRNSYS software using the "onion" method as illustrated in figure 4.2. The calculations proceed as follows after giving initial inputs to each model at t = 0. The model reads the corresponding values of the inputs (weather data, occupancy, lighting, etc.). AIM calculates the heat fluxes towards the ice and it provides them as inputs to BIM, in which they are used as boundary conditions. In its turn BIM calculates both the temperature of the brine leaving the slab and the interface temperature between the slab and ice and communicates them to REFSYS and AIM as their boundary conditions. Finally, REFSYS calculates the temperature of the brine leaving the evaporator and communicates it to the AIM and BIM. Several such data exchanges take place until outputs of each model vary by less than 10^{-3}. Then time is incremented (Δt = 6min) and this procedure is repeated.

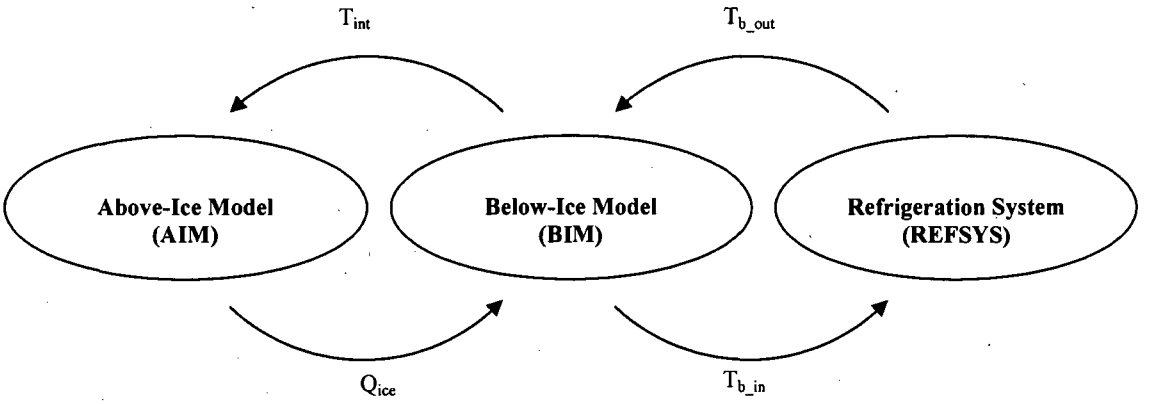

Figure 4.2 Schematic representation of the onion coupling between the different parts of the model

The simulations in the present project used hourly weather data for a typical meteorological year for the city of Montréal, Canada (ENERGYPLUS). In order to ensure the periodicity of the results (values at the end of the 365th day must be identical to those at the beginning of the first one) we carried out simulations over 17 months by repeating the meteorological data for January to May and did not consider the results of the initial five months to ensure that the effects of the arbitrary initial values are eliminated.

4.5 Results and discussion:

In this section the response of the modeled refrigeration system to the time-dependent input data (operating schedule and weather data) is analysed and discussed for two time periods. A short period of 240 timesteps corresponding to typical days (January 1st and July 1st) illustrates the variation of operating conditions (ice temperature, brine temperature, number of compressors in operation, etc.) due to the diurnal variations of the inputs. A long period of 87600 timesteps corresponding to a typical year is used to compare monthly energy consumption by the refrigeration and ventilation systems for two cases: case 1 which represents the base case has a ceiling emissivity of 0.9 and a setpoint of -9°C for the brine temperature at the outlet of the evaporators and ice thickness 2.5 cm while case 2 has a ceiling emissivity of 0.05 and a setpoint of -8.1°C for the brine outlet temperature.

Figure 4.3 shows the January 1st profiles of the ice surface temperature and of the brine temperature at the outlet from the evaporators for these two cases. During this day, from 0h00 to 12h00 the ice temperature decreases slightly for both cases due to the decrease of the refrigeration load while the brine outlet temperature stays constant at the setpoint since the refrigeration system is able to meet the load. At 12h00 the first resurfacing takes part and results in a significant increase of the mean ice temperature as well as a small increase of the brine outlet temperature because the refrigeration load is higher than the maximum capacity of the refrigeration system.

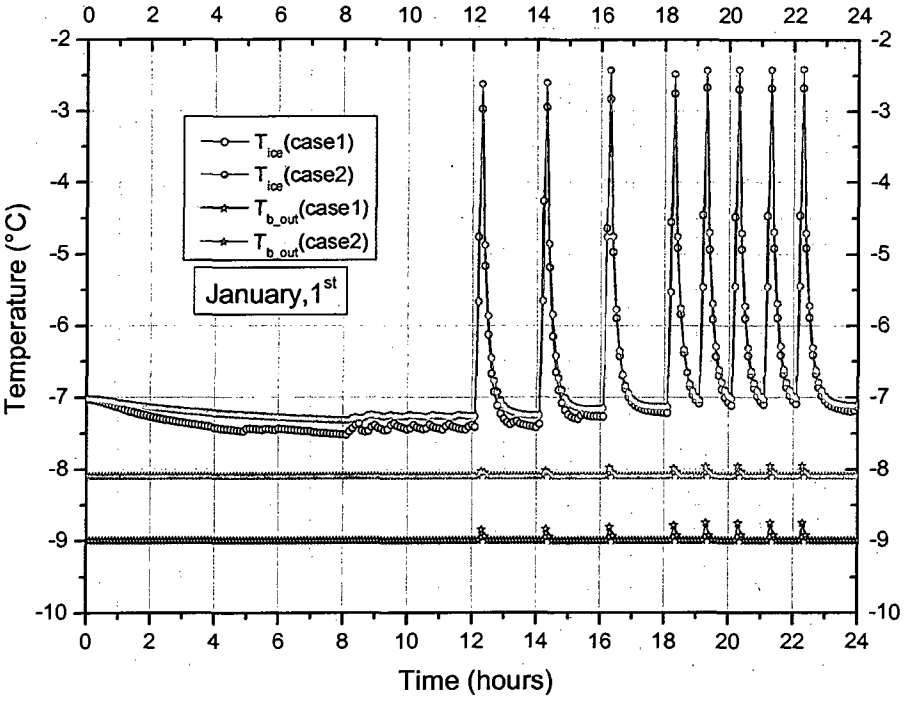

Figure 4.3 Evolution of the ice surface temperature and the brine temperature at the outlet of the refrigeration system for two cases on January 1st

Although the resurfacing lasts for 12 minutes (two timesteps) the increase of the ice temperature lasts longer due to the inertia of the ice sheet and the concrete slab. In the evening the resurfacing takes place at shorter intervals and the return of the brine outlet temperature to its setpoint takes longer while the ice temperature does not reach the low nightly values. A

qualitatively similar behaviour is obtained for July 1st when the number of resurfacings is increased to eleven.

However the ice temperature is slightly higher than in winter due to the fact that the refrigeration load increases during hot days as discussed by Seghouani et al. (2009). The increase of the brine outlet temperature due to resurfacing is also more important than in winter for both studied cases.

Finally, it is important to note that the increase of the brine temperature by 0.9°C (from -9°C to -8.1°C) causes a much smaller increase of the ice temperature (less than 0.3°C). This is due to the fact that in case 2 the heat flux towards the ice decreases principally because of the reduction of the ceiling emissivity.

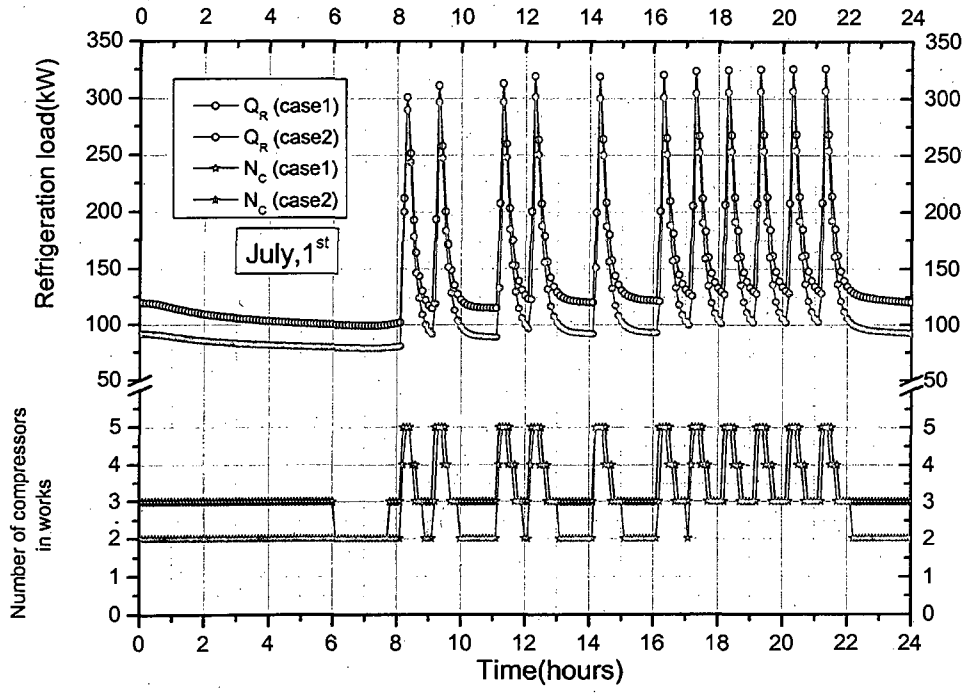

Figure 4.4 Refrigeration load and number of compressors in operation for two cases on July 1st

Figure 4.4 illustrates the diurnal variation of the refrigeration load (top 2 curves) on July 1st for both cases. It shows that in case 2 the load is reduced by almost 25 kW compared to case1, principally due to the decrease of the net radiation flux from the ceiling to the ice but also due to a reduction of the conductive heat fluxes through the soil because of the increase of the brine temperature from -9°C to -8.1°C.

The response of the refrigeration system to this variation is illustrated by the number of compressors in operation (bottom 2 curves). During the night and between resurfacings during the day only two compressors are in operation in case 2 while it takes three in case 1 to meet the load. However in the evening when the resurfacing operations are more frequent the number of compressors in operation is essentially the same for the two cases under consideration.

More detailed statistics on the number of compressors in operation for cases 1 and 2 are presented in table 4.1 for each month of the year. These results clearly show that the simultaneous reduction of the ceiling emissivity and the increase of the brine temperature result in a significant reduction of the time during which all five compressors are in operation. This observation is valid for each month of the year.

Table 4.1 Monthly and annual solicitation of compressors as a percentage of the number "m" of simulated operating conditions for the two cases under consideration

	Nc=1	Nc=2	Nc=3	Nc=4	Nc=5
January m=7440	1.4 (case 1) 6.2 (case 2)	60.7 72.6	20.6 9.9	8.7 3.9	8.0 7.3
February m=6720	1.5 7.4	60.2 71.2	20.7 9.9	8.9 4.1	8.2 7.4
March m=7440	0.7 5.6	53.5 72.0	27.7 10.2	8.4 4.7	9.4 7.5
April m=7200	0 0	42.0 75.8	38.5 11.5	7.4 5.4	12.0 7.3
May m=7440	0 0	23.5 71.7	55.4 14.1	7.6 6.8	13.4 7.3
June m=7200	0 0	12.6 68.4	65.5 14.9	7.9 9.0	13.9 7.6
July m=7440	0 0	10.3 67.4	67.6 15.8	8.1 9.1	13.9 7.8
August m=7440	0 0	7.9 67.9	70.5 15.6	7.8 8.9	13.7 7.5
September m=7200	0 0	8.5 68	68.7 15.2	8.4 9.3	14.3 7.5
October M=7440	0 0	19.2 70.8	59.3 14.3	7.7 7.5	13.7 7.3
November m=7200	0 0	31.2 73.2	48.4 13.8	7.6 5.6	12.7 7.3
December m=7440	0 0.4	55.9 77.5	26.1 9.1	8.9 5.5	8.8 7.5
Annual m=87600	0.3 1.6	32 71.4	47.6 12.9	8.1 6.7	11.9 (case 1) 7.4 (case 2)

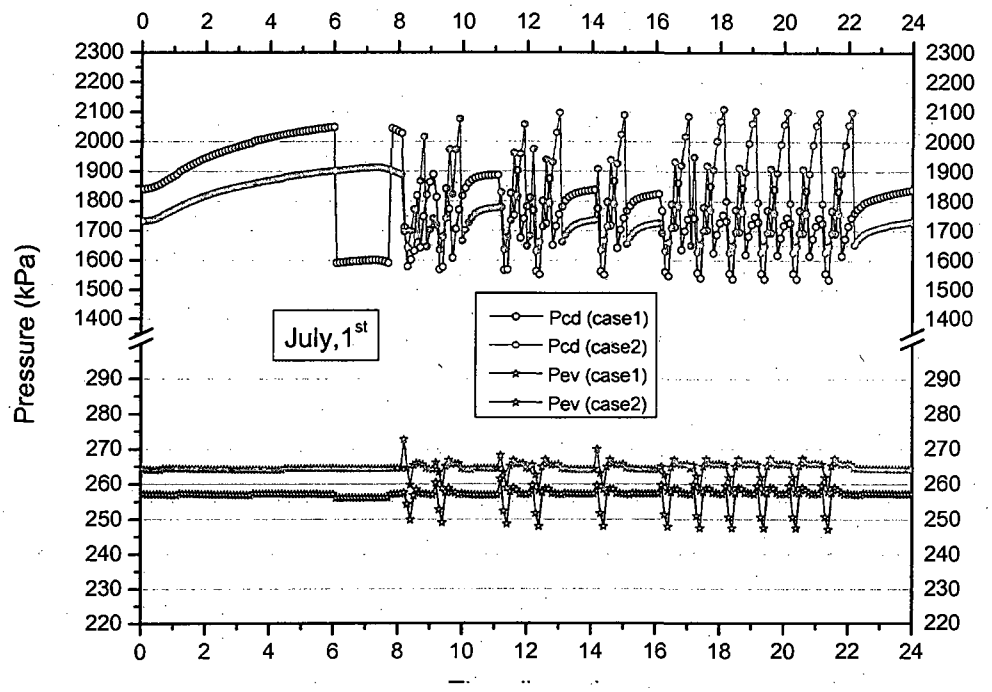

Figure 4.5 Condensation and evaporation pressures for two cases on July 1st

Pressures of condensation and evaporation for July 1st are presented in figure 4.5. The evaporation pressure is essentially constant at about 258kPa and 265kPa for cases 1 and 2 respectively since the temperature of the brine remains almost constant, except during resurfacings when the brine is warmer. On the other hand, the condensation pressure varies between 1550 and 2100 kPa due to the combined effect of the outside air temperature and the refrigeration load per unit. Between 0h00 and 6h00 this refrigeration load Q_R^* decreases for both cases, therefore P_{cd} rises as indicated by the manufacturer's data (Seghouani & Galanis 2009).

However, after 6h00 the P_{cd} decreases suddenly from 2050 to 1600 due to the change of the number of compressors in operation from three to two. The peak values of the condensation pressure occur shortly after the resurfacing operations. A second peak shortly afterwards is due to the increase of Q_R^* as the number of compressors in operation decreases gradually from 5 to 3 when the resurfacing finishes.

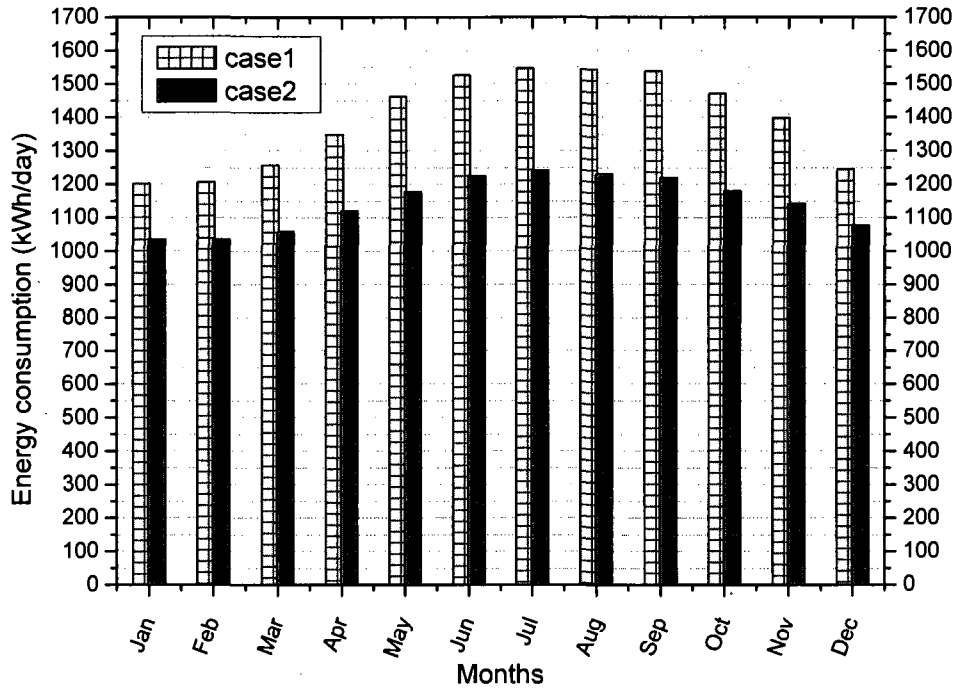

Figure 4.6 Monthly energy consumption by the refrigeration system for the cases under consideration

The predicted average daily energy consumption by the refrigeration system (compressors and fans) is shown in figure 4.6. During the winter months it is reduced by almost 200 kWh/day when the ceiling emissivity is reduced from 0.9 to 0.05 and the brine temperature is increased from -9°C to -8.1°C. During the summer months, when the refrigeration load is higher, the reduction of energy consumption is even more important and can reach almost 350 kWh/day. This is a consequence of the results in Table 1 which show that during the summer months the most probable number of compressors in operation is three for case 1 and two for case 2.

Figure 4.7 compares the annual energy rejected by the condensers with the corresponding energy consumption by the ventilation system (heating and reheating) and the radiant heating above the spectators' stands. It is noted that the latter is always much smaller than the energy needed to treat the ventilation air.

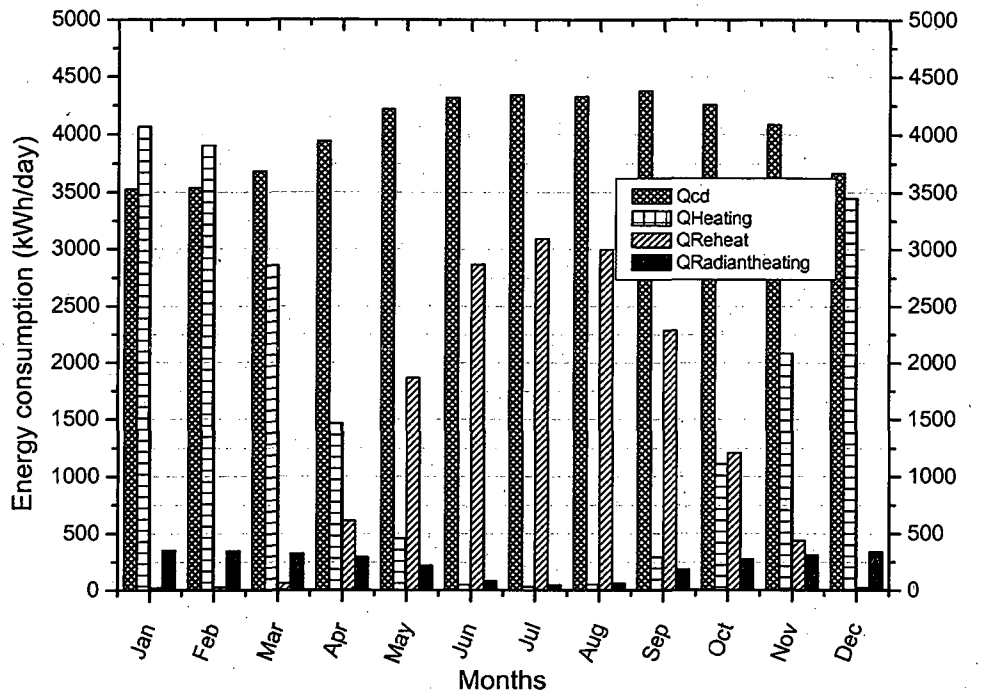

Figure 4.7 Monthly energy quantities (consumption by the ventilation system and the radiant heating as well as energy rejected by the condensers)

During the first two months of the year the energy needed to heat the outside air is greater than the heat rejected by the condensers. This is due to the very cold weather in Montreal during these months. However this heating energy decreases as the temperature of the outside air rises, is essentially zero in summer but starts rising again in autumn. On the other hand, the energy of reheating after dehumidification and/or cooling of the ventilation air is lowest in winter and highest in summer as expected.

At first glance, the results of figure 4.7 indicate that the heat rejected by the condensers can provide practically all the energy needed to treat the ventilation air. However, the energy rejected by the condensers cannot always be fully used to heat the ventilation air because the temperature of the air leaving the condensers is often well below the air temperature needed inside the ice rink. This is illustrated by figure 4.8 which shows the air temperature entering and leaving the condensers on January 1st. Despite the fact that it has increased by almost 12°C the air temperature leaving the condenser is still well below the 15°C required in the stands.

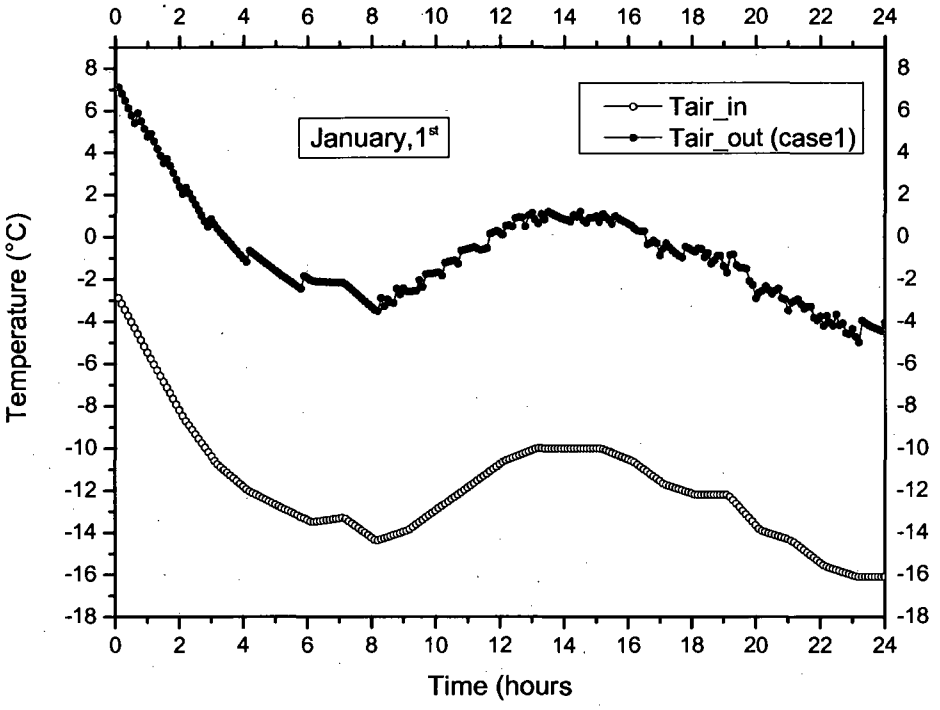

Figure 4.8 Air inlet temperature to condensers vs. air outlet temperature

4.6 Conclusion:

A complete transient simulation code which calculates heat transfer and energy consumption in an indoor ice rink has been successfully realized by coupling different models (AIM, BIM and REFSYS) described in our previous publications. The developed code is able to predict the number of compressors in operation, the heat rejected by the condensers, the refrigeration load, the condensation and evaporation pressures and many other details such as brine temperatures, ice surface temperature, etc. on a yearly basis for any meteorological data and different operating schedules supplied by the user.

The code was used to analyze the effects of simultaneously reducing the ceiling emissivity from 0.9 to 0.05 and increasing the brine temperature at the inlet of the concrete slab by almost 1°C. The results show that the temperature of the ice remains essentially the same and that therefore its quality is not influenced. On the other hand these changes result in a substantial decrease of the daily energy consumption of the refrigeration system varying from 16% to 22% during the typical year. The results also illustrate the considerable potential for heat recovery from the condensers to satisfy or reduce the energy needed by the ventilation system of the ice rink.

CHAPITRE 5

CONCLUSION GÉNÉRALE

Le principal objectif de la présente thèse de doctorat était de concevoir un outil de simulation numérique du fonctionnement complet d'un aréna en mode transitoire, capable d'estimer et d'optimiser la consommation énergétique de ce genre de bâtiment avec bonne précision et rapidité des calculs. Au terme du projet nous pouvons affirmer que cet objectif a été atteint.

Les différentes étapes qui ont permis de réaliser cet objectif étaient les suivantes :

- Dans un premier temps il a fallu créer un modèle numérique (BIM) de la structure sous la glace pour calculer les flux de chaleur conductifs transitoires absorbés par la saumure. Cette tâche était compliquée à cause des grandes dimensions de la patinoire et du fait que le sol en dessous de la glace est constitué de différentes couches (glace, dalle de béton, tuyaux de saumure, isolant thermique, sable, sol). Il fallait donc tenir compte de leurs dimensions et de leurs propriétés thermiques tout en considérant le mouvement de la saumure dans la dalle de béton, le chauffage électrique au niveau du sable ainsi que le sol au dessous et autour de l'aréna.
- Lors de la seconde étape il a fallu faire le couplage numérique entre le modèle développé (BIM) et le modèle thermo-aéraulique du bâtiment (AIM) développé par Daoud et coll. (2006, 2007). Cette tâche a été réalisée à l'aide du logiciel TRNSYS avec une méthode dite «Oignon». Selon celle-ci, et au cours d'un pas de temps, le BIM calcule la température d'interface entre la glace et le béton et la transmet à l'AIM. Ce dernier calcule alors le flux de chaleur vers la glace et l'envoi à titre d'input au BIM. Plusieurs de ces échanges de données ont lieu jusqu'à ce que les résultats de chaque modèle varient de moins de 10^{-3}. Ensuite, le temps est incrémenté et cette procédure est répétée. Des simulations annuelles ont été effectuées nécessitant des données horaires (température de l'air et du sol à 0 m et 4 m de profondeur ainsi que le rayonnement solaire) d'une année météorologique typique. Afin d'assurer la périodicité des résultats nous avons effectué des simulations sur 17 mois en répétant les données météorologiques de Janvier à Mai pour être sûr que les effets des valeurs initiales arbitraires soient éliminés.

- La troisième étape était de développer un modèle numérique du système de réfrigération de l'aréna étudié. Ce dernier est constitué principalement de cinq compresseurs à pistons, deux évaporateurs (tubes et calendre), cinq condenseurs à air et autant de vannes de détente. Le réfrigérant principal est le R-22 et le fluide secondaire est la saumure qui sort du système à une température de consigne s'établit à -9°C. Ainsi et en ayant analysé de nombreuses et très variées publications sur les systèmes de réfrigération, nous avons opté pour une modélisation se basant sur une combinaison de relations thermodynamiques, de corrélations de transfert de chaleur et de corrélations élaborées à partir de données disponibles dans le catalogue du manufacturier. Cette technique de modélisation est très pratique lorsque les données expérimentales des différentes composantes sont disponibles. Aussi, plusieurs hypothèses simplificatrices communes ont été utilisées dans le but d'alléger le calcul sans pour autant affecter les résultats de façon significative. Ensuite, une stratégie de contrôle appropriée à été mis au point pour la mise en marche des compresseurs en réponse à une charge variable.
- Enfin la dernière étape était de faire le couplage numérique entre le modèle du système de réfrigération (REFSYS) et l'ensemble (AIM+BIM). Encore une fois la même procédure (oignon) qu'à la deuxième étape a été reprise. L'ensemble couplé AIM+BIM calcule la température de la saumure à la sortie de la dalle de béton et la charge de réfrigération correspondante et les envois au modèle REFSYS qui calcule à son tour la température de retour de la saumure et la renvoi à l'AIM+BIM comme input, et ainsi de suite jusqu'à convergence.

La validation des différents modèles (AIM, BIM, REFSYS) à été effectuée à différentes étapes de leurs développements à l'aide de mesures expérimentales réalisées sur l'aréna et sur le système de réfrigération, mais aussi à l'aide des données du manufacturier. La concordance entre résultats simulés et mesurés était très acceptable.

Les inputs dynamiques du système (qui changent avec le temps) sont les conditions météorologiques (humidité et température de l'air extérieur, radiation..) et la cédule horaire d'utilisation de l'aréna (spectateurs, lumières, resurfaçage, etc.). Les autres inputs invariables avec le temps sont considérés comme étant des paramètres et incluent la géométrie et le type des composantes du système de réfrigération, les dimensions des différentes couches qui

constituent la structure sous la glace, leurs caractéristiques thermiques, le type de réfrigérant, la puissance du chauffage radiant, les propriétés du fluide secondaire,....etc.

Le modèle ainsi développé et validé est en mesure de prévoir (comme outputs) le nombre de compresseurs en marche à n'importe quel moment, la chaleur rejetée par les condenseurs, la charge de réfrigération, les pressions de condensation et d'évaporation, la consommation énergétique des système de ventilation, de réfrigération, des lumières, de la pompe à saumure, du chauffage radiant, du chauffage électrique dans le sable ainsi que de nombreux autres détails tels que la température de la saumure, la température de la surface de la glace, la température de l'air au dessus de la glace et au dessus des estrades,...etc.

Le modèle à été utilisé pour plusieurs études paramétriques telles que l'effet du climat sur la consommation d'énergie des différents systèmes (ventilation, chauffage électrique et chauffage radiant). Le choix de quatre villes Nord Américaines aux conditions météorologiques très différentes à été alors effectué (Edmonton, Houston, Montréal et Pittsburgh). Les effets de l'épaisseur de la glace, de l'épaisseur de l'isolant thermique sous la dalle de béton, de la température de consigne de la saumure, du type de thermostat qui contrôle la température de l'air au dessus des estrades et de son *set back* nocturne ont tous été simulés et les principaux résultats se résument ainsi :

- La consommation annuelle d'énergie par le système de ventilation est fortement influencée par les conditions météorologiques, elle est plus élevée dans les endroits chauds et humides et est toujours supérieure à la charge de réfrigération correspondante.
- L'utilisation d'un thermostat électronique avec une hystérésis de ±0,2°C plutôt que d'un thermostat bimétallique avec une hystérésis de ±1,5°C augmente la charge de réfrigération de plus de 10%. Ce résultat est dû au fait que les présents calculs ont été effectués avec la même température de consigne (+15°C). Dans le domaine résidentiel l'utilisation d'un thermostat électronique résulte à une économie d'énergie car les occupants ont tendance à fixer la même température minimale ce qui conduit à une température de consigne supérieure pour le thermostat bimétallique. Les économies d'énergie associées à l'utilisation d'un thermostat bimétallique dans les arénas sont au détriment du confort des spectateurs pour le scénario considéré.
- Une réduction de la température de la saumure entraine une augmentation de la charge de réfrigération et la réduction de la température de surface de la glace.

- Une augmentation de l'épaisseur de la glace entraîne une diminution de la charge de réfrigération de la glace et l'augmentation de la température de surface de la glace.
- Une augmentation de l'épaisseur de la couche d'isolant thermique sous la dalle entraîne une légère diminution de la charge de réfrigération et réduit sensiblement le risque de gel du sol.

À l'aide des résultats obtenus, quatre corrélations exprimant la consommation d'énergie du système de ventilation en fonction de la température sol-air on été formulées.

On a aussi remarqué que les résultats sur une année montrent que la chaleur rejetée lors du changement de phase dans les condenseurs est environ quatre fois plus grande que celle rejetée lors de la désurchauffe ; ils mettent en évidence l'intérêt considérable de la récupération de la chaleur de ces deux processus qui peut réduire l'énergie requise par le système de ventilation de la l'aréna.

Aussi, on a utilisé le modèle pour illustrer les avantages d'une stratégie de contrôle qui limite le nombre maximum de compresseurs fonctionnant simultanément à quatre, au lieu de cinq, lors des fréquentes opérations de resurfaçage de la glace. Cette stratégie se traduit par une diminution de 10% de l'énergie utilisée par les moteurs de compresseurs et de 20% de la demande de la puissance de pointe. Mais en contre partie durant ces courtes périodes, la température de la saumure augmente à la sortie des évaporateurs d'environ 0,5°C.

Le modèle a enfin été utilisé pour analyser les effets couplés de la réduction de l'émissivité du plafond et de l'augmentation de la température de la saumure à l'entrée de la dalle de béton de près de 1°C. Les résultats montrent que la température de la glace demeure essentiellement la même et que, par conséquent, sa qualité n'est pas affectée. D'autre part, ces changements résultent en une diminution substantielle de la consommation d'énergie du système de réfrigération allant de 16% à 22% au cours de l'année typique.

Enfin, le modèle numérique final de par sa forme modulaire sous l'interface de TRNSYS peut servir comme outil fiable et précis dans le but de tester d'autres techniques et stratégies d'amélioration de l'efficacité énergétique des arénas. Comme par exemple la réduction du nombre de compresseurs en opération pendant la nuit où même leur arrêt total, le stockage de froid et de chaleur, l'intégration de nouveaux condenseurs à eau pour la récupération d'énergie rejetée par les condenseurs, l'utilisation de compresseurs à vis ou à puissance ajustable, l'intégration d'un système de pompe à chaleur géothermique, etc.

BIBLIOGRAPHIE

Arias, J. and Lundqvist, P. (2006): Heat recovery and floating condensing in supermarkets, Energy and Buildings 38 p. 73–81

ASHRAE, (2001) Non-residential cooling and Heating load Calculations ASHRAE Handbook-fundamentals, p 29.14-29.17, Atlanta: American Society of Heating, Refrigeration, and Air-Conditioning Engineers, Inc.

ASHRAE, (2002) Ice Rinks, ASHRAE Handbook-Refrigeration, Atlanta: American Society of Heating, Refrigeration, and Air-Conditioning Engineers, Inc.

ASHRAE, (2005) Residential cooling and Heating load Calculations ASHRAE Handbook-fundamentals, p 29.11-29.12, Atlanta: American Society of Heating, Refrigeration, and Air-Conditioning Engineers, Inc.

Bechtler, H., Browne, M. W., Bansal, P. K. and Kecman, V. (2001) New approach to dynamic modelling of vapour-compression liquid chillers: artificial neural networks, Applied Thermal Engineering 21 (9), p. 941-953

Bellache, O., Ouzzane, M. and Galanis, N. (2005) Coupled conduction, convection, radiation heat transfer with simultaneous mass transfer in ice rinks, Numerical Heat Transfer part A 48 p. 219-238.

Bellache, O., Ouzzane, M. and Galanis, N. (2005) Numerical prediction of ventilation and thermal processes in ice rinks, Building and Environment 40 (3) p. 417-426.

Bellache, O., Galanis, N., Ouzzane, M., Sunyé, R. and Giguère, D. (2006) Two-Dimensional Transient Model of Airflow and Heat Transfer in Ice Rinks (1289-RP), ASHRAE Transactions 112 (2) p. 706-716.

Bendapudi, S. and Braun, J.E. (2002) A review of literature on dynamic models of vapor compression equipment. ASHRAE Report #4036-5

Bourdouxhe, J.P., Grodent, M., Lebrun, J.J. and Saavedra, C. (1994). A toolkit for primary HVAC system energy calculation—Part 1: BoilerModel. ASHRAE Transactions 100(2): p. 759-773.

Bourdouxhe, J.P., Grodent, M., Lebrun, J.J., Saavedra, C. and Silva, K.L. (1994) A toolkit for primary HVAC system energy calculation—Part 2 Reciprocating chiller models, ASHRAE Transactions, 100(2), p. 774-786.

Bourdouxhe, J.P., Grodent M. and Lebrun J.J. (1997) HVAC1 Toolkit: Algorithms and subroutines for primary HVAC system energy calculations, The American Society of Heating, Refrigerating and Air Conditioning Engineers.

Browne, M.W. and Bansal, P.K. (2002) Transient simulation of vapour-compression packaged liquid chillers, International journal of refrigeration 25 p.597-610

Cavallini, A., Zecchin, R. (1974) A dimensionless correlation for heat and mass transfer in forced convection condensation, Proceedings of the 5th Int. Heat Transfer Conf, p. 309-313.

Cecchini, C., Marchal, D. (1991) A simulation model of refrigerant and air-conditioning equipment based on experimental data. ASHRAE Transactions 97(2), p. 388-393.

Chan, K.T., Yu, F.W. (2006) Thermodynamic-behaviour model for screw chillers with a variable set-condensing temperature, Applied Energy 83 p. 265–279.

Daoud, A. and Galanis, N. (2006) Calculation of the thermal loads of an ice rink using zonal model and building energy simulation software, ASHRAE Transactions, 112(2), p. 526-537.

Daoud, A., (2007) Analyse des transferts de chaleur et de masse transitoires dans un aréna à l'aide de la méthode zonale, Thèse de doctorat en sciences appliquée, Université de Sherbrooke (Québec), Canada.

Daoud, A., Galanis, N. and Bellache, O., (2008) Calculation of refrigeration loads by convection, radiation and condensation in ice rinks using a transient 3D zonal model. Applied Thermal Engineering, Volume 28, Issues 14-15 p. 1782-1790.

El Biyaali, A., Roux, J.J., Inard, C. (1996), Sous-structuration et couplage de modèles réduits appliqués aux transferts thermiques dans le sol, Int. Comm. Heat Mass Transfer, Vol 23 No. 4, p. 575-586.

ENERGYPLUS, http://www.eere.energy.gov/buildings/energyplus/.

Fisher, S.K. and Rice, C.K. (1983) The Oak Ridge heat pump design models: 1. a steady-state computer design model for air-to-air heat pumps. Report No. ORNL/CON-80/R1., Oak Ridge, Tenn., Oak Ridge National Laboratory.

Fu, L., Ding, G., Su, Z. and Zhao (2002) Steady-state simulation of screw liquid chillers, Applied Thermal Engineering 22, p. 1731–1748

Garcıa-Valladares, O., Perez-Segarra, C.D. and Rigola, J. (2004) Numerical simulation of double-pipe condensers and evaporators, International Journal of Refrigeration 27 p. 656–670.

Ge, Y.T. and Tassou, S.A. (2000) Mathematical modelling of supermarket refrigeration system for design, energy prediction and control, Proc. Inst. Mech. Eng. Part A **214**

Gebhart, B. (1971) Heat Transfer, McGraw-Hill, Second edition.

Gnielinski, V. (1976) New equations for heat and mass transfer in turbulent pipe and channel flow, Int. Chem. Eng., 16, p. 359.

Jian, Z. and Chen, Q. (1995) Airflow and air quality in a large enclosure, ASME Journal of Solar Energy Engineering 117 (2) p. 114-122.

Jin, H. and Spitler, J.D. (2002) A parameter estimation based model of water-to-water heat pumps for use in energy calculation programs. ASHRAE Transactions 108 (1), p. 3-17.

Jones, P.J. and Whittle, G.E. (1992) Computational Fluid Dynamics for Building Air Flow Prediction-Current Status and Capabilities, Building and Environment 27 (3) p. 321-338.

Kakaç, S. and Liu, H., (2002) Heat exchangers selection, rating and thermal design. Second Edition CRC PRESS, Washington, D.C.

Krarti, M., Claridge, D.E. and Kreider, J.F. (1988) ITPE technique applications to time varying twodimensionalground-coupling problems Int. J. HeatMass Transfer, Vol.31(9), p. 1899-1911.

Krarti, M., Claridge, D.E. and Kreider, J.F. (1990) The ITPE Method Applied to Time-Varying threedimensional Ground-coupling Problems ASME J. of Heat Transfer, Vol. 112, No. 4, p. 849-856.

Krarti, M., Claridge, D.E. and Kreider, J.F. (1993) Energy Calculations for Basements, Slabs, and Crawl Space, ASHRAE TC 4.7 Project 666-RP, p. 69-97.

Krarti, M. (1994) Steady-state heat transfer from horizontally insulated slabs, Int. J. Heat Mass Transfer, Vol. 36 (8), p. 2135-2145.

Laouadi, A., (2004) Development of a radiant heating and cooling model for building energy simulation software Building and Environment, Volume 39, Issue 4, p. 421-431

Le, C.V., Bansal P.K. and Tedford, J.D. (2004) One-zone simulation model of an oil-injected screw chiller, Int. J. Energy Res 28 p. 1343–1359.

Lavoie, M., Sunyé, R. and Giguère D. (2000) Potentiel d'économies d'énergie en réfrigération dans les arénas du Québec. Report prepared by the CANMET Energy Technology Center, Varennes, Quebec.

Madani, (2008) Étude d'un système de réfrigération fonctionnant avec une pression de condensation variable : Élaboration d'un programme de simulation appliqué aux arénas. Mémoire de maîtrise Sherbrooke, Quebec.

Nyers J., Stoyan G., 1994. A dynamical model adequate for controlling the evaporator of a heat pump, International Journal of Refrigeration, 17 (2) p. 101-108.

Ouzzane, M., Sunyé, R., Zmeureanu, R., Giguère, D., Scott, J. and Bellache, O., (2006) Cooling load and environmental measurements in a Canadian indoor ice rink (RP-1289), ASHRAE Transactions, 112 (2) p. 538-545.

Petukhov, B.S., (1970) Heat transfer and friction in turbulent pipe flow with variable physical properties, in Advances in Heat transfer, vol. 6, Academic Press, New York.

Popovic, P., Shapiro, H.N., (1995) A semi-empirical method for modeling a reciprocating compressor in refrigeration system, ASHRAE Transactions, 101(2) p. 367-382.

Reference Fluid Thermodynamic and Transport Properties Database (REFPROP): Version 8.0

Roux, J.J., Colda, I. and Brau, (1997) Model reduction applied to heating floor coupled with a building Clima 2000 http://www.inive.org/Ibase_Search/airbase-search-formulaire-bibinf-clima2000-001.asp

Sami, S.M. and Dahmani, A., (1996) Numerical prediction of dynamic performance of vapor compression heat pump using new HFC alternatives to HCFC-22, Journal of Applied Thermal Engineering 16, p. 691-705.

Seghouani, L., Daoud, A. and Galanis, N., (2009) Prediction of yearly energy requirements of indoor ice rink, Energy and Buildings. 41 (5), p. 500-511.

Seghouani, L. and Galanis, N., (2009) Quasi-steady state model of an ice rink refrigeration system», Building simulation: an international journal. (2), p. 119–132.

Seghouani, L., Daoud, A. and Galanis, N., (2009) Simulation of the dynamic interactions between an ice rink and its refrigeration system, International journal of refrigeration (Submitted)

Shah, M.M., (1982) Chart correlation for saturated boiling heat transfer: equation and further study, ASHRAE Transactions, 88, p. 185.

Solati, Zmeureanu, R. and Haghighat, F. (2003) Correlation based models for the simulation of energy performance of screw chillers, Energy Conversion and Management 44 p. 1903-1920.

Somrani, R., Mun J. and Krarti, M., (2007) Heat Transfer Beneath Ice Rink Floors, Building and Environment 43 (10), p. 1687-1698

Sreedharan, P., Haves, P., (2001) Comparison of chiller models for use in model-based fault detection. Proceedings International Conference for Enhanced Building Operation, Austin TX (http://www.osti.gov/bridge/servlets/purl/829977-eNbJEo/native/829977.pdf)

Stefanuk, N.B.M., Aplevich, J.D. and Renksizbulut, M. (1992) Modeling and simulation of a superheat-controlled water-to-water heat pump. ASHRAE Transactions 98(2), p. 172-184.

Svenssen M.C. (1999) Non-steady-state modelling of a water-to-water heat pump unit, Proceedings of the 20th International Congress of Refrigeration, Sydney, Paper No. p. 263

Swider, D.J., Browne, M.W., Bansal, P.K. and Kecman,V. (2001) Modelling of vapour-compression liquid chillers with neural networks, Applied Thermal Engineering 21 p. 311-329

Teyssedou, G., Zmeureanu, R. and Giguère, D. (2009) Thermal Response of the Concrete Slab of an indoor Ice Rink (RP-1289), HVAC & R Research 15 (3) p.509-520.

TRNSYS, (2000) A transient system simulation program, Software manual, Solar Energy Laboratory, University of Wisconsin-Madison.

Webb, R.L. (1990) Airside heat transfer correlations for flat and wavy plate fin-and- tube geometries, ASHRAE Transactions, 96(2), p. 445-449.

Williatzen, M., Pettit, N.B.O.L. and Ploug-Sorensen, L. (1998) A general dynamic simulation model for evaporators and condensers in refrigeration. Part I: moving-boundary formulation of two-phase flows with heat exchange, Int. J. of Refrigeration, 21(5), p. 398-403.

Xiandong, H., Liu, S., and Asada, H. (1997) Modeling of vapor compression cycles for multivariable feedback control of HVAC systems, ASME Journal of Dynamic Systems, Measurement and Control, 119 (2).

Xuejun, S., Liu, W., Que, X. and Chen, Z., (1999) Researches on dynamic simulation and optimization of automobile air-conditioning system, part1: mathematical model and dynamic simulation of automobile air-conditioning system, Proceedings of the 20th International congress of refrigeration, Sydney, Paper No. 577.

Yang, C., Demokritou, P., Chen, Q., Spengler, J.D. and Parsons, A. (2000) Ventilation and air quality in indoor ice skating arenas, ASHRAE Transactions 106 (2) p. 338-346.